

**Reaction-Induced Phase Separation of PPG/PEO/HDI based
bi-Soft Segment Polyurethanes**

Inaugural-Dissertation

zur

Erlangung des Doktorgrades

der Mathematisch-Naturwissenschaftlichen Fakultät

der Universität zu Köln

vorgelegt von

Christian Wenning

aus Emsbüren

Köln, 2018

Berichtersteller/in: Prof. Dr. Annette M. Schmidt

Prof. Dr. Marc C. Leimenstoll

Tag der letzten mündlichen Prüfung: 24. Mai 2017

Danksagung

An dieser Stelle möchte ich mich besonders bei Prof. Dr. Marc C. Leimenstoll für das Vertrauen mir gegenüber in der Bearbeitung des Themas bedanken. Besonderen Dank möchte ich aussprechen für die gebotene Offenheit in der Gestaltung der Arbeit, für die dies betreffenden konstruktiven Diskussionen und für die immerwährende Hilfsbereitschaft.

Mein besonderer Dank gilt außerdem Prof. Dr. Annette M. Schmidt für die Betreuung meiner Arbeit als Erstgutachterin seitens der Universität zu Köln. Vielen Dank für die Aufnahme in die freundliche Arbeitsgruppe und für die stetige, konstruktive Beratung in jedweden Belangen.

Der Covestro Deutschland AG danke für die Bereitstellung der verwendeten Polyurethanrohstoffe. Hier geht außerdem mein herzlicher Dank an Dr. Dirk Achten, Dr. Dick Dijkstra und Dr. Hans Grablowitz für die fachlichen Diskussionen im Laufe des Projektes.

Prof. Dr. Stéphan Barbe möchte ich zum einen für seine Hilfestellung im Rahmen der Berechnung der Phasendiagramme und zum anderen für die intensiven Diskussionen über die daraus entstandenen Ergebnisse danken.

Außerdem danke ich Jens Noe für die Unterstützung dieser Arbeit durch die Erstellung seiner Masterarbeit unter meiner Leitung. Weiterhin bedanke ich mich bei meinen Kolleginnen und Kollegen für das freundliche Arbeitsklima und die konstruktiven Diskussionen.

Zu guter Letzt möchte ich mich herzlich bei meiner Familie, insbesondere meinen Eltern Agnes und Werner für die fortwährende Unterstützung danken. Besonderer Dank gilt meiner Freundin Jessica für ihren unermüdlichen Rückhalt und ihre Geduld.

Table of Contents

I	Abstract.....	i
II	Kurzzusammenfassung.....	ii
III	Abbreviations and symbols	iii
1	Introduction	1
2	Scope of this study and objectives.....	3
3	Theory.....	5
3.1	Polyurethane chemistry	5
3.1.1	Isocyanate chemistry.....	5
3.1.2	Catalysis	8
3.1.3	Polyether polyols	9
3.1.4	Isocyanate-terminated polyurethanes.....	10
3.1.5	Morphology of polyurethanes.....	12
3.2	Solubility parameters	14
3.2.1	Definition	14
3.2.2	Determination of solubility parameters	15
3.3	Flory-Huggins lattice theory.....	20
3.3.1	Definition and function	20
3.3.2	Estimation of phase diagrams	21
4	Results and discussion.....	23
4.1	Ternary phase diagram of PPG/PEO/HDI mixtures.....	23
4.1.1	The binary mixture of PPG/PEO	23
4.1.2	Phase diagram of the ternary mixture PPG2k/PEO600/HDI.....	29
4.1.3	Summary on PPG/PEO/HDI phase diagrams	36
4.2	Reaction kinetics, phase behaviour and properties of PPG/PEO bi-soft segment polyurethanes.....	38
4.2.1	Kinetics of the reaction in ternary PPG/PEO/HDI mixtures	39
4.2.2	Onset of phase separation	49
4.2.3	Thermal properties and glass transitions of the ITPUs.....	60
4.2.4	Molecular weight distribution of the ITPUs	64
4.2.5	Phase behaviour of the ITPU	66
4.2.6	Summary on the reaction-induced phase separation in PPG2k/PEO600/HDI reaction mixtures.....	78
5	Conclusion and outlook.....	79
6	Experimental part	83
6.1	Materials	83
6.2	Analytical methods	85
6.3	Synthesis of isocyanate-terminated polyurethanes.....	88

6.4	Phase isolation and composition analysis	89
6.5	Determination of the solubility parameters	90
6.6	Determination of cloud points.....	93
6.7	Binodal composition analysis by size exclusion chromatography	93
6.8	Computational determination of phase diagrams.....	94
7	References.....	98
IV	Appendix.....	107
V	Figures.....	129
VI	Tables.....	131

I Abstract

The presented thesis explores the physicochemical background of reaction-induced phase separation (RIPS) in bi-soft segment isocyanate-terminated polyurethanes (ITPUs). ITPUs are a preliminary product in the synthesis of various PU products like foams, dispersions or elastomers. Typically, only one soft segment is used but it was shown in the literature that the application of two different soft segments can lead to an improvement of morphological properties. In this work, it is hypothesized that the combination of two soft segments can lead to RIPS during the ITPU formation process. It is suggested that the occurrence and the extent of phase separation is closely related to the initial phase diagram of the reactants.

In order to study the proposed relationship, the initial ternary phase diagram of the reaction mixture, consisting of poly (ethylene oxide) (PEO), poly (propylene oxide) (PPG) and 1,6-hexamethylene diisocyanate (HDI) is determined at first. Secondly, detailed experimental observation of the RIPS is conducted to identify critical parameters. Furthermore, the composition and morphology of the phase separated products are studied briefly.

The ternary phase diagram is determined by theoretical and experimental methods. Flory-Huggins theory and solubility parameters are applied in order to calculate equilibrium compositions of demixed phases in the binary (PEO/PPG) and ternary (PEO/PPG/HDI) mixtures. The obtained data is in qualitative agreement with experimental cloud points and equilibrium compositions. The results demonstrate that HDI acts as a solvent for PEO and PPG.

Reaction monitoring by NCO%-content titration, FTIR- and UV-Vis spectroscopy revealed a dependency between the onset of phase separation and the reaction conversion. It is found that an increase of the initial HDI content leads to a delayed onset of phase separation. The competing second order kinetic of the reaction is studied by ¹H-NMR analysis. DSC analysis reveals that the phase separation is a consequence of the incompatibility of the soft segment structures. The composition and molar weight distribution found in isolated phases of the ITPUs indicate that the phase separation is controlled thermodynamically.

Overall, the findings support the hypothesis that mechanism and extent of the phase separation are closely related to the ternary phase diagram of the reactants. This work comprises a comprehensive description of the phase behaviour during the reaction towards bi-soft segment ITPUs and provides a basis for future studies on this topic.

II *Kurzzusammenfassung*

Die vorliegende Arbeit beleuchtet den physikochemischen Hintergrund der reaktionsbedingten Phasenseparation in bi-Weichsegment Polyurethan-Präpolymeren. Präpolymere werden in Klebstoffen und Lacken angewendet und sind ein wirtschaftlich wichtiges Zwischenprodukt in der Herstellung von verschiedensten Polyurethanprodukten, wie z. B. Schäumen sowie thermoplastischen Materialien. In der Literatur wurde gezeigt, dass die Anwendung von zwei unterschiedlichen Weichsegmenten eine gezielte Beeinflussung der Morphologie zulässt und damit zu einer Verbesserung der mechanischen Eigenschaften führen kann.

In dieser Arbeit wurden Präpolymere auf Basis von Polypropylenglykol/Polyethylenglykol Mischungen und Hexamethylendiisocyanat hergestellt. Die Eingangshypothese war, dass die Anwendung von zwei unterschiedlichen Weichsegmenten bereits zu einer reaktionsbedingten Phasenseparation während der Herstellung des Präpolymers führen kann. Hauptaufgabe war die Untersuchung des Zusammenhangs zwischen dem initialen Mischungsverhalten der drei Reaktionskomponenten und dem Auftreten und dem Ausmaß der Phasentrennung.

Das ternäre Phasendiagramm der Reaktionsmischung wurde durch experimentelle und theoretische Methoden bestimmt. Auf Grundlage der Flory-Huggins-Theorie wurden Gleichgewichtszusammensetzungen der entmischten Phasen numerisch berechnet. Es zeigte sich, dass die Mischungslücke der binären Polyolmischung entscheidenden Einfluss auf das ternäre Phasendiagramm besitzt. Das Diisocyanat agierte als Lösevermittler. Die berechneten Daten sind in Übereinstimmung mit experimentellen Trübungspunkten.

Die Verfolgung der reaktionsbedingten Phasenseparation zeigte, dass der Zeitpunkt des Eintrübens in direktem Zusammenhang mit dem Umsatz der Reaktion steht. Eine Erhöhung des initialen Diisocyanatgehaltes führt zu einer verspäteten Trübung. Darüber hinaus wurde mittels $^1\text{H-NMR}$ Analyse die kompetitive Kinetik zweiter Ordnung der Polymerisation aufgezeigt. Die thermische Analyse der Produkte demonstrierte, dass die Phasenseparation auf der Inkompatibilität der Weichsegmente beruht. Ergebnisse aus der Analyse der getrennten Phasen deuten auf einen Gleichgewichtsprozess hin.

Zusammenfassend zeigen die Ergebnisse engen Zusammenhang zwischen dem Phasendiagramm der Edukte und der reaktionsbedingten Phasenseparation. Diese Arbeit liefert umfassende Beschreibung des Phasenverhaltens während der Reaktion und stellt damit ein Fundament für weitere Forschungsarbeiten auf diesem Gebiet.

III *Abbreviations and symbols*

<u>Abbreviation</u>	<u>Meaning</u>
$[NCO]$	molar concentration of isocyanate groups
$[NCO]_0$	initial concentration of isocyanate groups
μ_i	chemical potential
$^1\text{H-NMR}$	proton nuclear magnetic resonance
α	molar aggregation number in Hoy's group contribution theory
<i>Abs</i>	absorption
A_{NCO}	area of NCO band in the FTIR spectrum
ATR	attenuated total reflectance
<i>B</i>	base value in Hoy's group contribution theory
BIP	binary interaction parameter
<i>c</i>	concentration
CED	cohesive energy density
<i>d</i>	optical path length
DBTDL	dibutyltin dilaurate
ΔG_{Mix}	free energy of mixing
DoC	Degree of conversion
d_P	particle diameter
DSC	differential scanning calorimetry
ΔT	temperature molar function in Hoy's group contribution theory
$\Delta T^{(P)}$	temperature molar function in Hoy's group contribution theory
$\delta_{D,i}$	dispersion partial Hansen solubility parameter of compound <i>i</i>
$\delta_{H,i}$	H-bonding partial Hansen solubility parameter of compound <i>i</i>
$\delta_{i,j}$	solubility parameter of compound <i>i</i> based on method <i>j</i>
$\delta_{P,i}$	polar partial Hansen solubility parameter of compound <i>i</i>
$\delta_{t,i}$	total solubility parameter of compound <i>i</i>
EO	ethylene oxide
E_V	energy of vaporization
ε	molar attenuation coefficient

f	functionality of polyols
FH	Flory-Huggins
F_i	molar attraction constant in Fedors group contribution theory
ϕ_i	volume fraction of compound i
Φ_i	initial volume fraction of compound i in polyether polyol mixture
$\Phi_{PEO600,obs}$	exp. found volume fraction of PEO600 with respect to total soft segments
F_P	polar additive molar function in Hoy's group contribution theory
f_P	third order polynomial function
F_t	total additive molar function in Hoy's group contribution theory
FTIR	Fourier-transformation infrared spectroscopy
GCT	group contribution theory
HDI	1,6-hexamethylene diisocyanate
HMBC	Heteronuclear multi bond correlation
HSQC	Heteronuclear single quantum correlation
I	intensity of emitted light
I_0	intensity of transmitted light
I_{Sca}	Intensity of scattering
I_{Abs}	Intensity of absorbance
ITPU	isocyanate-terminated polyurethane
k	rate constant
λ	wavelength of electromagnetic radiation
m	number of repeating units
m_{EO}	number of ethylene oxide units
MeOH	methanol
M_n	number-average molecular weight
m_{PO}	number of propylene oxide units
M_w	weight average molar mass
MWD	molar weight distribution
N	number of lattice sites in Flory–Huggins theory
n	refractive index
NCO	isocyanate group

NCO%	weight percentage of NCO groups in compound
NG	nucleation and growth
ν_i	IR vibration of group i
OBJ	objective function for the numerical solver
OH	hydroxyl group
OH#	hydroxyl number of polyols
p	conversion in Carothers's equation
PEO	poly (ethylene oxide)
PEO600	Desmophen L300 (86.6 % EO, $M_n=590.5$ g/mol, $f=2$, OH#=190)
PO	propylene oxide
PPG	poly (propylene oxide)
PPG1k	Desmophen 1111BD (PPG, $M_n=1007.2$ g/mol, $f=2$, OH#=111.4)
PPG2k	Acclaim 2200 (PPG, $M_n=2000$ g/mol, $f=2$, OH#=56.1)
PPG400	Desmophen 1262BD (PPG, $M_n=431.5$ g/mol, $f=2$, OH#=260)
PPG4k	Acclaim 4200 (PPG, $M_n=4007.1$ g/mol, $f=2$, OH#=28)
ppm	parts per million
PU	polyurethane
P_x	molar probability of x -mer
θ	angle of incidence
r	molar fraction of isocyanate to hydroxyl groups
R	gas constant
ρ	specific gravity
RIPS	reaction-induced phase separation
RPM	rounds per minute
SD	spinodal decomposition
SEC	size exclusion chromatography
SP	solubility parameter
T	absolute temperature
t	time in sec.
T_{CP}	cloud point temperature
T_g	glass temperature

TPU	thermoplastic polyurethane
UCST	upper critical solution temperature
UV-Vis	ultraviolet and visible electromagnetic radiation
v_i	Fedors group contribution to V_m
$V_{m,i}$	molar volume of compound i
V_{ref}	reference volume in Flory-Huggins theory
x_i	molar fraction of i
$x_{PEO600,obs}$	exp. found molar fraction of PEO600 with respect to total soft segments
ω_i	weight fraction of compound i
\bar{X}_n	polymerisation degree
$\chi_{i,j}$	Flory-Huggins interaction parameter

1 Introduction

The formation of polyurethanes (PU) was first described by Otto Bayer in 1937.^[1] His discovery of the reaction of diisocyanates with macromolecular diols opened a new branch in the synthesis of polymers, namely the polyaddition reaction.^[2] Nowadays PU has found its way in practically all fields of application, e. g. foams, thermoplastics, adhesives, elastomers and coatings.^[3–8] This results particularly from the great variance in the morphology^[4,9–11] obtained by using different reactants, for example aliphatic/aromatic polyisocyanates, different macrodiols (polyether, polyester, polycarbonate, polysiloxanes,...) or short polyols (1,4-butane diol, glycerol,...) just to name of few of it. By appropriate choice of the educts, the manufacturer has the possibility to tailor the properties of the PU material.^[12]

It is well known that in PU chemistry disparate polarity and the consequential miscibility of reactants can lead to heterogeneous reaction mixtures.^[4] In this context, reaction-induced phase separation (RIPS) is discussed as a promising process to result in unique morphologies like co-continuous or spherical domain structures in the products.^[13,14] In such cases, the reaction starts in an initially homogeneous mixture until the occurring reaction causes the system to enter metastable/unstable regions leading to phase separation. The properties of the resulting product can strongly benefit from the occurring morphologies like in segmented PUs.^[11]

In the case of these materials, incompatibility is purposely induced in order to obtain domained morphologies by phase separation of hard and soft segments.^[15,16] Most commonly this is accomplished by conversion of a short polar polyol (e. g. 1,4-butanediol), often referred to as the chain extender, and a less polar macromolecular or oligomeric polyol (soft segment forming components) with diisocyanates.^[11] In this concern, it is often spoken of compatibility and incompatibility in PU science.^[17–19]

To avoid misleading interpretation of results, it shall be noted that throughout this thesis the expression (in)compatibility will be relevant to phase separated segments in polymers, while it is referred to the term miscibility speaking of mixtures of educts/reactants.

It was shown that the mechanical properties of thermoplastic PUs (TPU) can be improved by addition of a second soft segment polyol.^[20] Commonly these PUs are referred to as bi-soft segment^[21] or mixed soft segment^[22] PUs. Gunatillake et al. investigated mixtures of different soft segment structures and showed that the tensile strength of the resulting chain extended TPU improves in comparison to single soft segment TPUs.^[20] Yildirim et al. recently supported these findings by a coarse-grained simulation.^[22] The results indicate that the

beneficial effect relies on an enhanced control over microphase separation by application of soft segments with altered polarity. In this regard, the tuneable interaction of the two unlike soft segments with the hard segments allows for tailored morphologies.^[22] The possible fields of application of these materials ranges from shape-memory polymers^[23] to membranes^[24,25]. Particularly regarding membranes, Zhao et al. demonstrated that not only the interaction between hard/soft segments but primarily the interaction between the two soft segments plays a crucial role in the development of the morphology.^[24] Those membranes consisted of crosslinked PPG and polybutadiene soft segments and incorporated low hard segment content.^[21,24,26,27]

In order to control the development of the morphology, it needs to be ensured that the RIPS is properly understood.^[14] Despite the vast number of investigations in the field of single soft segment PUs,^[11,28,29] the kinetics and thermodynamics of the phase separation in bi-soft segment PUs remained mostly unexplored.

Typically the synthesis of polyurethanes is a two-step process.^[11] In the first stage, the soft segments are reacted with the diisocyanate towards a so-called isocyanate terminated polyurethane (ITPU) prepolymer, followed by chain extension with low-molecular weight polyols in the second stage. This study focuses on the first stage, the ITPU formation. Blending of different soft segment forming polyols allows for tailoring the properties of the final product but creates further complexity in concern of miscibility. In order to control the process, detailed knowledge about miscibility and consequentially the phase diagram of the reaction mixture is required. This is of particular importance in the view of a conceivable future utilisation of RIPS.^[14]

In the following study, the RIPS in bi-soft segment ITPUs is investigated in order to understand the relationship between initial miscibility of the reactants and the phase behaviour during the reaction process. Therefore, the thesis is divided into two main parts: (1) theoretical and experimental description of the initial miscibility and (2) characterisation of the RIPS process and the resulting product. In this regard, Flory-Huggins^[30] (FH) theory is applied in order to predict the phase diagrams of typical bi-soft segment ITPU reactant mixtures. The obtained theoretical data is then compared with experimental findings. For the second part, the phase separation is monitored during the reaction progress. In addition to this, it is displayed how the phase separation process affects the morphology of the resulting product. The understanding of the phase behaviour in these reactions may be of great interest in order to allow tailored design towards co-continuous or spherical domain structures.

2 Scope of this study and objectives

This work focuses on ternary bi-soft segment reaction mixtures comprising poly (ethylene oxide) (PEO), poly (propylene oxide) (PPG) and 1,6-hexamethylene diisocyanate (HDI). This composition is considered as a potential system for reaction induced phase separation, due to the difference in polarity between PEO and PPG. A requirement for RIPS is that the reactant mixture exhibits a partially miscible phase diagram.

It is presumed that the molecular weight of PPG affects the miscibility with a given PEO soft segment. To find a partially miscible PPG/PEO/HDI combination a molecular weight series of PPG in the range of 400 to 4 000 g·mol⁻¹ is investigated in combination with a fixed PEO macrodiol possessing a molecular weight of $M_n = 590$ g·mol⁻¹ (referred to as PEO600). The EO content in PEO600 amounts to 86.6 wt.% while the rest consists of PO and starter molecule content (i. e. 1,2-propylene glycol) of 0.6 wt.% and 12.8 wt.%, respectively.^[31] It was chosen on the basis of its lower tendency for crystallisation compared with pure PEOs.

One goal of this study was to show the potential of FH theory^[30] in combination with solubility parameters (SPs)^[32] to estimate the miscibility in the initial reactant mixture. For the sake of practicability a simple approach was preferred excluding sophisticated mathematical models like composition-dependent interaction parameters^[33] or polydispersity effects^[34,35].

In general, the critical factor for the estimation of phase diagrams via FH theory is the application of suitable binary interaction parameters (BIP). In this work, the BIPs should be calculated on basis of SPs. In this regard, it is essential that the required SPs of the reactants are determined properly. In this concern, the potential of group contribution theories (GCTs) for the estimation of the SPs should be demonstrated. GCTs allow for the prediction of the SPs solely based on the information about the chemical structure of the compounds without experimental analysis.

In the following, the obtained SPs should be used in FH calculations to predict the miscibility/phase diagrams of the different PPGs with PEO600 to identify a partially miscible soft segment pair. The effect of the molecular weight increase of PPG on the miscibility with PEO600 should be discussed on basis of the computational results from FH theory and SPs. Phase diagrams should be computed and compared to experimental findings. For this purpose, cloud point curves and binodal compositions of the partially miscible binary polyol mixtures should be determined.

The main part of this work is subsequently dealing with the identified partially miscible ternary mixture PPG/PEO600 and HDI as potential system for reaction-induced phase

separation. Once more, the phase diagrams should be computed and compared to experimental cloud point data. For proper estimation of the phase diagram of the ternary mixture it will be focused on the BIP of the remaining binary pairs in the mixture again, i. e. PEO600/HDI and PPG/HDI. Once the experimentally found miscibility of the binary pairs are successfully reflected by the SPs, the ternary phase diagram will be assessed.

The comprehensive scope of the work until here is to illustrate the potential of the FH theory in predicting qualitatively and quantitatively the phase behaviour of PU reaction mixtures based on sole information of their chemical structure.

After the identification and description of the partially miscible ternary reactant mixture it is focused on the RIPS. ITPUs should be prepared at various compositions. The reactions should be monitored in conversion and in turbidity for analytical determination of the onset of phase separation. The resulting ITPU emulsions should be characterised on behalf of their molar weight distribution and their thermal properties. Major goal of this work is the comprehensive description of the phase separation process. For this purpose, the phase behaviour and composition of the separate phases in the ITPU emulsions should be investigated in detail. The results from this analysis should be discussed in regard of the preliminary determined phase diagram of the initial ternary reactant mixture.

3 Theory

3.1 Polyurethane chemistry

Polyurethanes are characterised by their name giving urethane group (see Figure 3-1). Chemically seen, urethanes are esters of the carbamic acid, therefore also known as carbamates.^[12]

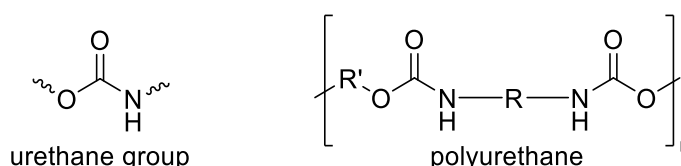


Figure 3-1. Structural unit of polyurethanes.

Polyurethanes are mostly formed by the reaction of diisocyanates with hydroxy-containing compounds^[2] but may also be formed by different reactions^[36]. As already mentioned in the introduction, the variety of available reactants in PU chemistry makes it a very adaptable material. The following sections are about to show the essential fundamentals regarding the presented work.

3.1.1 Isocyanate chemistry

Isocyanate (NCO) groups are highly reactive with hydrogen active compounds. This results from the resonance structures displayed in Figure 3-2.^[37]

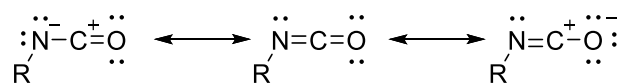


Figure 3-2. Resonance structures of the isocyanate group.

Due to the higher electronegativity of oxygen with regard to the carbon and nitrogen atom, the carbon is partially negatively charged. The exothermic addition of an alcohol to a NCO group is illustrated in Figure 3-3. The free electron pair of the alcohol oxygen attacks the electrophilic carbon atom. Subsequently the hydrogen is cleaved from the oxygen and binds via intramolecular rearrangements to the nitrogen.

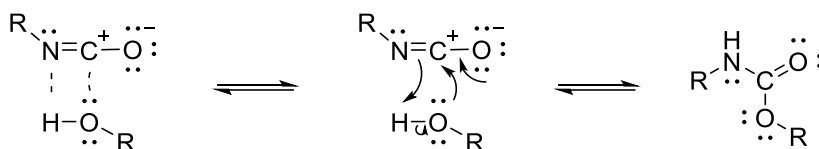


Figure 3-3. Addition of an alcohol to an isocyanate group.^[37]

The reactivity of isocyanates is strongly dependent in the rest of the molecule. In general aliphatic isocyanates are less reactive than aromatic, for example like between 4,4'-diphenylmethane diisocyanate and 4,4'-dicyclohexyl diisocyanate.^[8,36] For the reason of the lower reactivity of aliphatic isocyanates often catalysts are used.^[4,8] Symmetric diisocyanates like HDI do not exhibit differences in reactivity between the NCO groups (see Figure 3-4). In contrast, steric hindrance leads to different reactivities of the two NCO groups in the asymmetric isophorone diisocyanate.

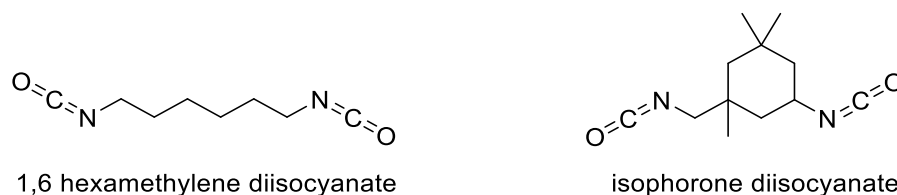


Figure 3-4. Structures of 1,6 hexamethylene diisocyanate (HDI) and isophorone diisocyanate.

Ideally, only the reaction between hydroxy groups and diisocyanates occurs to produce PUs. Nevertheless, due to the high reactivity of the NCO groups several other reactions might arise. Table 3-1 shows the differences in the reactivities of isocyanates with different nucleophiles for an uncatalysed reaction.

Table 3-1. Relative reactivities of isocyanates with hydrogen active compounds.^[12]

Hydrogen active compound	relative reaction rate (25 °C, without catalyst)
primary aliphatic amine	2 500
primary hydroxyl	2.5
water	2.5
secondary hydroxyl	0.75
urethane	0.0025

The reaction of NCO groups with water results eventually in urea groups and carbon dioxide (cf. Figure 3-5). At first, the water reacts with one NCO group towards the unstable carbamic acid which immediately cleaves towards a primary amine and carbon dioxide. Due to the high nucleophilicity of the primary amine an urea group is formed by the reaction with another NCO moiety.

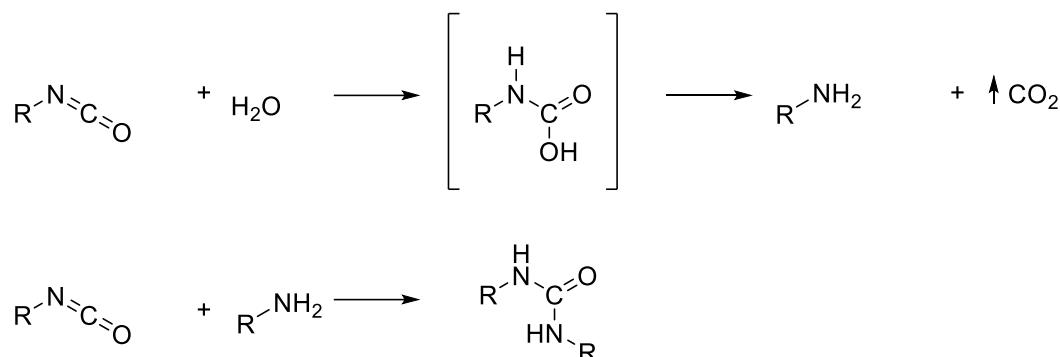


Figure 3-5. The reaction of isocyanates with water molecules towards carbon dioxide and urea.

In addition to this, the NCO group can react with urethane groups in a subsequent reaction to form allophanate groups (cf. Figure 3-6). The reaction is reversible and typically only accessible in high extents at temperatures above 110 °C.^[12,38] The lower nucleophilicity of the urethane group results from the electron withdrawing character of the carbonyl group. Allophanates act as crosslinking sites in the material. The analogue reaction between urea groups and NCO leads to biuret groups.^[4]

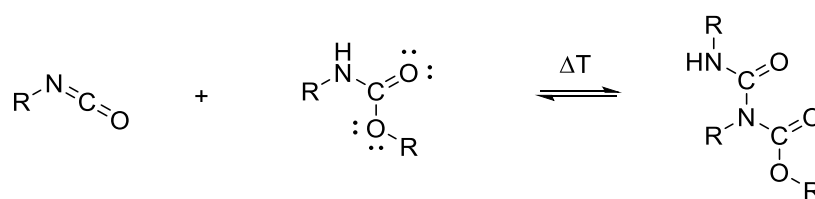


Figure 3-6. Addition of an isocyanate and an urethane group to an allophanate.

Isocyanates undergo numerous additional reactions with nearly any imaginable compound that contains active hydrogen. Additionally to the addition reactions, polyisocyanates are able to dimerize or even trimerize to form uretidinediones or isocyanurates when special catalysts are applied.^[36] Such systems are frequently applied in coatings where crosslinked structures are needed.^[5]

3.1.2 Catalysis

Catalysis plays a big role in PU chemistry not only due to its accelerating effect on the kinetics of the reaction but also because of their potential to enhance the selectivity of the isocyanate reaction.^[39] The choice of a suitable catalyst offers the possibility for selective formation of urethanes or urea or isocyanurates.^[39,40] For the reaction between isocyanates and compounds containing active hydrogens, there are generally two types of catalysts available: (a) amines and (b) organotin substances. Figure 3-7 shows the most commonly used ones of both types, which are 1,4 diazobicyclo-[2,2,2]-octane (DABCO) and dibutyltin dilaurate (DBTDL).

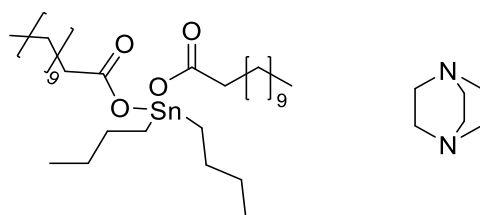


Figure 3-7. Chemical structure of DBTDL (left) and DABCO (right).

The catalytic effect of DBTDL is based on its Lewis acidic character and the consequential complexation with isocyanate groups.^[40] On the other hand Lewis basic amine catalysts are known to complex alcohol groups.^[41] For this reason, a combined application of organotin substances and amines leads to synergistic effects.^[37,40] The relative catalytic effect^[40] on isocyanate/hydroxyl reactions is shown in Table 3-2.

Table 3-2. Relative catalytic reactivity of DBTDL and DABCO.^[40]

Catalyst formulation	rel. reactivity
None	1
DABCO (0.1%)	130
DBTDL (0.1%)	210
DABCO (0.1%) + DBTDL (0.2%)	1 000

For the selective reaction of isocyanates with water, so-called “blowing” catalysts have been tailored.^[39] Tertiary amines are most commonly referred to in this context.^[42] In contrast, organotin catalysts are known to effectively catalyse the isocyanate/alcohol reaction.^[39]

3.1.3 Polyether polyols

Polyether polyols are the most prominent soft segment type used in PU representing approx. 80% of the overall macrodiols production.^[12] Common monomers for the synthesis of polyether polyols are alkylene oxides like ethylene oxide (EO), propylene oxide (PO) or butylene oxide (BO) (see Figure 3-8). Aside from that, other special monomers like tetrahydrofuran are applied occasionally in the synthesis of polyether polyols.

For the polymerisation of such products, a so-called starter molecule is needed. Typically these are low-molecular polyfunctional alcohols ($f \geq 2$), for example ethylene or propylene glycol ($f=2$) or trimethylol propane ($f=3$). The resulting functionality of the polyether polyol is dependent on the f -value of the starter molecule. The polymerisation follows the principle illustrated in Figure 3-8. Common catalyst used in the polymerisation are potassium hydroxide and, in the special case of polypropylene oxides, so-called dimetallic catalysts (DMC, also known as double metal cyanide). Latter, for example zinc hexacyanocobaltate, are the most efficient catalysts and allow for high purity and very low polydispersity in the product.^[39] Furthermore, DMC catalyst based polyether polyols contain significantly lower terminal double bonds - so-called monools - which are formed by KOH catalysed isomerisation of propylene oxide towards allyl alcohol.^[39] These monools lead to lower f -values in the polyether polyol and results in chain termination.^[12]

In general, the formation of co-polyether structures is conceivable via anionic polymerisation. Step-wise addition of different monomers leads to block structures, while the simultaneous addition of two monomers results in a more or less random distribution.^[4,12,43]

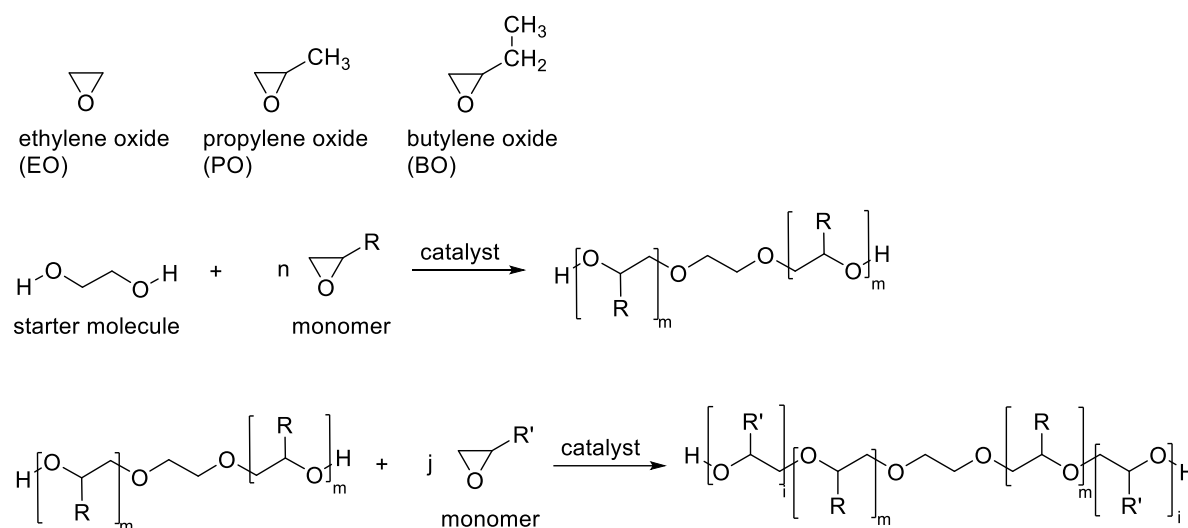


Figure 3-8. Monomers and general synthesis route for common polyether polyols.

Due to the difference in reactivity of secondary and primary OH groups with isocyanates, the type of the hydroxy group at the end of the polyether chain is of particular importance regarding their application in polyurethane building reactions. The anionic polymerisation of EO always results in primary OH groups. The type of OH groups in PPGs is dependent on the carbon atom which is attacked during the process.^[12] Due to the steric hindrance by the methyl group, the reaction is regiospecificly resulting in mostly secondary hydroxyls.^[12]

The quantitative amount of hydroxy groups is given by the hydroxyl number (OH#). It is expressed in the unit of milligram potassium hydroxide per gram polyol (mg KOH·g⁻¹). This originates from the titrational determination method by organic anhydrides and potassium hydroxide. The hydroxyl number is proportional to the functionality f and to the inverse average molar weight M_n (Eq.(3-1)).^[12,44]

$$OH\# = \frac{f \cdot 1000 \frac{mg}{g} \cdot 56.1 \text{ g/mol}}{M_n} \quad \text{Eq.(3-1)}$$

3.1.4 Isocyanate-terminated polyurethanes

In the fabrication of PU materials, for example in TPUs^[11] or PU dispersions^[45], it is often favoured to employ a multi-step process. Generally, the first step of the procedure is the synthesis of the isocyanate-terminated polyurethane (ITPU), also known as the prepolymer.^[38,46-48] In order to obtain thermoplastics or elastomers the prepolymer is chain-extended by addition of short polyols, polyamines or in case of PU dispersions by ionic compounds.^[11]

However, prepolymers itself are applied in one-component adhesives and sealants as they cure under atmospheric moisture.^[46,48-50] Moreover, reactive hot melt adhesives are of great interest.^[51-55] These typically consist of a blend of polyether and polyester based ITPUs with polyacrylates. Their adhesive effect relies on a combination of crystallisation, vitrification, phase separation and curing of NCO groups with moisture.^[54] Duffy et al. highlighted the importance of the phase behaviour concerning their performance.^[52-54]

In general, the ITPU formation is carried out in bulk by the reaction of the macromolecular polyol (mostly diols) with an excess of diisocyanate. This step polymerisation results in a mixture of oligomers.^[56] For linear (i. e. difunctional) reactants the molar weight distribution (MWD) in these oligomeric mixtures follows the Schulz-Flory distribution. Based on this fact, Singh and Weissbein^[57] stated that the molar fraction of each x -mer species P_x is given

by Eq.(3-2), where r is the molar ratio of the two reactive groups ($r = n_{\text{OH}}/n_{\text{NCO}}$) and x is an odd, total number of diisocyanate and soft segment units in the chain.

$$P_x = r^{(x-1)/2} \cdot (1 - r) \quad \text{Eq.(3-2)}$$

Correspondingly the polymerisation degree \bar{X}_n in dependence of the conversion p and r is described by Carothers equation (Eq.(3-3)).^[58]

$$\bar{X}_n = \frac{1 + r}{1 + r - 2 \cdot p \cdot r} \quad \text{Eq.(3-3)}$$

In polyurethane research, it is common to define the so-called “index” as the inverted ratio r according to the excess of NCO groups. The index is then defined $n_{\text{NCO}}/n_{\text{OH}}$. In this work, an index of 1.5 was applied, which leads to the theoretical MWD illustrated in Figure 3-9.

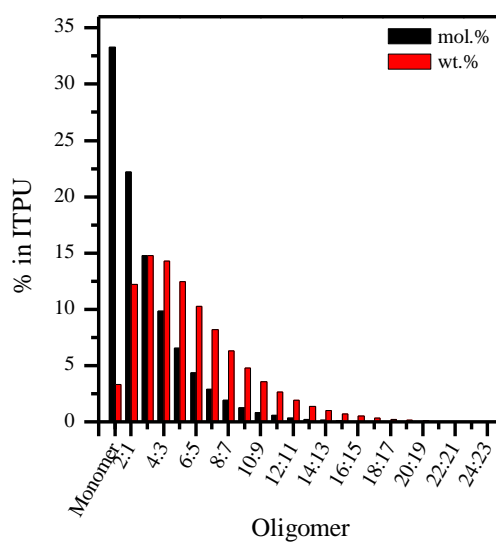


Figure 3-9. Schulz-Flory distribution at an index of 1.5.

3.1.5 Morphology of polyurethanes

Polyurethanes appear in a large variety of different morphologies. The proper choice of the reactants allows for tailoring PUs properties to fit the requirements for various applications like elastic/rigid foams, thermoplastics, elastomers, coatings.^[4] In general, the morphology results from the alignment of so-called soft and hard segments.^[11] The soft segments are formed by macromolecular polyols, like polyether polyols, polyester polyols, polycarbonate polyols etc. On the other hand, hard segments comprise the urethane groups themselves, which by the use of low-molecular polyols can occur in high concentrations. Figure 3-10 illustrates a typical PU chain based on a PEO soft segment chain extended with ethylene glycol.

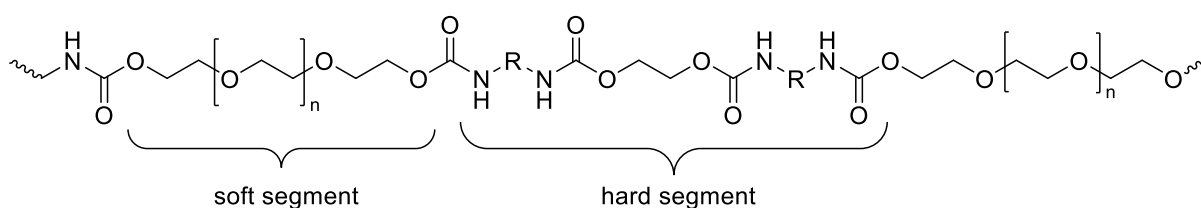


Figure 3-10. Schematically illustration of the structure of a linear PU chain containing hard and soft segments.

It was shown in various studies that the morphology of the PU is greatly dependent on the chemical structures of the soft/hard segment and on the content of hard segments.^[59,60] In addition to this, several other influencing factors were identified like the polymerisation procedure, segment flexibility/symmetry and the extent of interaction between the soft and hard segments.^[61-70] In dependence on all these factors, microphase separation can occur in the way that the soft and hard segments organize into soft and hard domains. This is the typical morphology of segmented PUs exhibiting the characteristic properties of thermoplastics or elastomers.^[11] Bras et al. demonstrated that the major driving force for this microphase separation is the free energy of mixing, which causes the phase separation thermodynamically.^[28] By simultaneous FTIR and small-angle x-ray scattering reaction monitoring, they found out that extensive hydrogen bonding (H-bonding) between the hard segments occurred four minutes later than microphase separation.

Nevertheless, it was shown that H-bonding is one of the most important influence defining the resulting morphology.^[10,11,71,72] These so-called specific interactions can be formed by the partially positive charged hydrogen atoms of the urethane group in combination with an electron donating group. Typically, numerous electron donating groups appear in PU

structures for example the carboxyl group of the urethane or the ether oxygens in polyether polyols. This leads to the situation that H-bonds can either be formed between the hard segments themselves or between hard and soft segments (cf. Figure 3-11).^[10] Yilgör et al. demonstrated that the value of the urethane/urethane H-bond energy is twice the size compared to the urethane/ether H-bond energy, which indicates that the urethane/urethane interaction is thermodynamically favoured.^[10] However, the soft segment structure is strongly affecting the extent of H-bonding between hard and soft segments.^[60] For instance, PEO based soft segments are known to interact more intensively with hard segments than polydimethylsiloxanes (PDMS).^[60] The extent of hard-soft segment H-bonding is known to affect the degree of hard/soft segment phase mixing.^[11] It has been demonstrated that the extent and type of H-bonding occurring in PUs can be detected by FTIR spectroscopy.^[11,71,73,74]

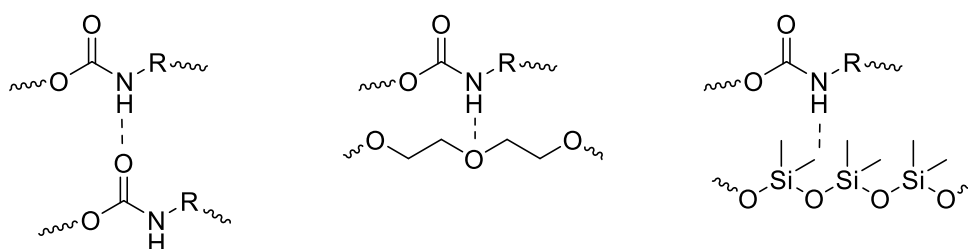


Figure 3-11. H-bonding between hard segment and (left) hard segment, (middle) PEO and (right) PDMS.

The behaviour of single molecule hard segments in non-chain-extended PUs has been studied quite recently.^[70,75,76] It was demonstrated that the use of symmetric diisocyanates (e. g. HDI) resulted in aggregation into hard domains, while asymmetric hard segments were mostly dispersed in the soft segment matrix. Urška and Krajnc demonstrated how the dispersed hard segments in the soft segment matrix affect the thermal properties of the PU prepolymers.^[47] According to them, only one glass transition temperature (T_g), lying between those of the pure segments, is observed when the hard segments are located in the soft segments. On the other hand dispersed hard domains result in an additional T_g or melting transition. Typically, soft segments exhibit glass transition temperatures around $-50\text{ }^\circ\text{C}$ whereas hard domains show melting transitions or T_g s at temperatures greater than $100\text{ }^\circ\text{C}$.^[11,47]

3.2 Solubility parameters

3.2.1 Definition

Solubility parameters δ (SP) were first introduced by Hildebrand and Scott in 1949.^[32] Hildebrand defined the SP as the square root of the cohesive energy density (CED) according to Eq.(3-4).

$$\delta = \sqrt{CED} = \left(E_V / V_m \right)^{\frac{1}{2}} \quad \text{Eq.(3-4)}$$

The CED is the fraction of the molar energy of vaporization E_V divided by the molar volume V_m of a substance. E_V can be quantified by calorimetric analysis but in case of polymers this method is not applicable.^[77] By this definition, the SP can be seen as a measure for the strength of interaction between the molecules in a substance. Originally, the unit of the SP was $(\text{cal}\cdot\text{cm}^{-3})^{1/2}$ but nowadays its numerical value is mostly given in $\text{MPa}^{1/2}$. In accordance to its name the SP is an important numerical value to estimate solubility in mixtures.^[78]

Patterson and Delmas stated that the non-combinatorial free energy of mixing $\Delta G_{Mix}^{noncomb}$ of two substances is proportional to the squared difference in their individual SPs following Eq.(3-5).^[79]

$$\Delta G_{Mix}^{noncomb} = \phi_S \cdot \phi_P \cdot V_{Mix} \cdot (\delta_S - \delta_P)^2 \quad \text{Eq.(3-5)}$$

ϕ_S and ϕ_P are the volume fractions of the solvent S and the polymer P and V_{Mix} is the volume of the mixture. Combinatorial effects on the free energy of mixing are not reflected by SPs. This will be further described in section 3.3 when the Flory-Huggins lattice theory is introduced. Anyway, based on this definition two substances are predicted to be miscible with one another if their SPs are similar in their numerical values.

In the original postulation of Hildebrand's SPs, specific interactions like polar interactions or H-bonds were omitted.^[32] To overcome this major drawback, Hansen introduced a more complex multidimensional SP known as the Hansen solubility parameter (HSP).^[80-84] Hansen stated that the CED and with it the heat of vaporization is based on three individual interactions, i. e. dispersion forces, polar forces and hydrogen-bonding forces. From definition, these forces are the mutual interactions between two identical molecules.

Therefore, the HSP comprises three partial SPs, i. e. δ_D , δ_P and δ_H . The London dispersion force contribution δ_D to the HSP arises from the van-der-Waals interactions of the atoms due to the fluctuations in their electron shell. These are relatively weak interactions in comparison to dipole-dipole interactions between the molecules or between particular segments of the molecules, which are included in the polar contribution δ_P . The H-bonding contribution δ_H encompasses the strongest interactions in this theory as it comprises the specific interaction of positively polarised hydrogens with negatively polarised atoms, mainly oxygen.^[78,85] Considering all these contributions the total SP can be calculated according to Eq.(3-6). This value is comparable to the one-dimensional Hildebrand SP.^[78]

$$\delta_t^2 = \delta_D^2 + \delta_P^2 + \delta_H^2 \quad \text{Eq.(3-6)}$$

3.2.2 *Determination of solubility parameters*

In general, SPs can be determined by several different theoretical or practical approaches utilizing their relationship to physical properties like the boiling point, the surface tension or the internal pressure.^[86,87]

The most obvious method of determination would be the quantification of the heat of vaporization. Unfortunately, this is not applicable on macromolecular substances as they typically tend to decompose before evaporation. Given this fact, several approaches to determine the SP of polymers have been published, comprising the measurement of the internal pressure or the intrinsic viscosity, the collection of swelling data in different solvents and many more.^[86]

To estimate the partial HSP, it is convenient to investigate the solubility of the polymer in a series of diverse solvents.^[78] Using established HSPs of the solvents, a three dimensional solubility sphere can be derived from the solubility data. The centre of the solubility sphere is regarded as the HSP of the respective polymer.

In addition to these experimental approaches, so called group contribution theories (GCT) allow for the determination of SPs without any physical experiments. To this point several GCTs have been published.^[88-92] In general, all of these theories state that the CED of a molecule consisting of several functional groups can be derived from the sum of the contributions of the individual groups. The original methods by Small,^[89] Fedors,^[90] Hoy^[88] and van Krevelen^[91] introduced the molar attraction constant F_i (see Eq.(3-7)) that is given by the fraction of the energy of vaporisation E_i divided by its molar volume V_i . The dataset of the

values of F_i has been analytically derived from the investigation on typical low-molecular weight compounds such as solvents.

$$F_i = \left(\frac{E_i}{V_i} \right)^{1/2} \quad \text{Eq.(3-7)}$$

In contrast to these methods, Stefanis^[92,93] GCT is related to the Universal Quasichemical Functional Group Activity Coefficients^[94,95] (UNIFAC) model. Originally, the UNIFAC GCT allows for the determination of vapour-liquid equilibria by prediction of the combinatorial and residual parts of the activity coefficients γ .

In the following, only Fedors', Hoy's and Stefanis' GCTs are described in further detail as they are used in this study.

Fedors' group contribution theory

Fedors^[90] GCT proposed that the heat of vaporization E_i and molar volume V_m are given by Eq.(3-8) and Eq.(3-9), where e_i and v_i represent the contributions of the individual groups.

$$E_i = \sum_i e_i \quad \text{Eq.(3-8)}$$

$$V_m = \sum_i v_i \quad \text{Eq.(3-9)}$$

The group contributions used in this study are listed in Table 3-3. By combining Eq.(3-7), Eq.(3-8) and Eq.(3-9) δ can be derived according to Eq.(3-10).

$$\delta = \left(\frac{E_i}{V_m} \right)^{1/2} = \left(\frac{\sum_i e_i}{\sum_i v_i} \right)^{1/2} \quad \text{Eq.(3-10)}$$

Table 3-3. Group contributions from Fedors' theory.^[90]

Atom or group	e_i [cal·mol ⁻¹]	v_i [cm ³ ·mol ⁻¹]
CH ₃	1 125	33.5
CH ₂	1 180	16.1
CH	820	-1.0
C	350	-19.2
COO	4 300	18.0
CO	4 150	10.8
OH	7 120	10.0
O	800	3.8
NCO	6 900	35.0

Hoy's group contribution theory

The GCT of Hoy^[88,96,97] is more complex than the one of Fedors owing to the fact that it permits not only the calculation of the total SP but also the partial HSPs. In his set of equations, (see Table 3-5) he discriminates between low-molecular liquids and amorphous polymers. Four additive molar functions are defined, i. e. F_t , F_P , V and Δ_T . F_t is the total molar attraction and F_P its polar contribution. V again is the molar volume and Δ_T stems from the Lydersen^[98,99] GCT for the estimation of critical properties like the critical temperature T_c . Lydersen stated a relationship between T_c and the boiling point T_b . In these supplementary equations, α and m are defined as the molar aggregation number and the quantity of repeating units per effective chain segment respectively.^[91,96]

The Lydersen group contributions are different for low-molecular liquids (Δ_T) and polymers ($\Delta_T^{(P)}$) (cf. Table 3-4). α is relevant concerning the estimation of the polar and H-bonding partial SP and is a measure for the association of molecules. Moreover, Hoy implemented a base value $B = 277$ in the calculation of the total SP. Table 3-4 lists all group contributions needed in this study.

Table 3-4. Hoy's group contributions used in this thesis.^[91]

Atom or group	$F_{t,i}$ [(MJ·cm ⁻³) ^{1/2} ·mol ⁻¹]	V_i [cm ³ ·mol ⁻¹]	Δ_T	$\Delta_T^{(P)}$
CH ₃	303.5	21.55		0.022
CH ₂	269.0	15.55	0.138	0.020
CH	176.0	9.56		0.013
C	65.5	3.56		0.040
COO	640.0	23.70		0.050
CO	538.0	17.30		0.040
OH primary	675.0	12.45		0.049
OH secondary	591.0	12.45		0.049
O	235.0	6.45		0.018
NCO	736.0	25.90	0.046	0.054

Table 3-5. Set of formulae in Hoy's GCT for the calculation of the SP of low-molecular compounds and amorphous polymers.^[91]

	Low-molecular liquids	Amorphous polymers
Additive molar functions	$F_t = \sum N_i \cdot F_{t,i}$	$F_t = \sum N_i \cdot F_{t,i}$
	$F_p = \sum N_i \cdot F_{p,i}$	$F_p = \sum N_i \cdot F_{p,i}$
	$V = \sum N_i \cdot V_i$	$V = \sum N_i \cdot V_i$
	$\Delta_T = \sum N_i \cdot \Delta_{T,i}$	$\Delta_T^{(P)} = \sum N_i \cdot \Delta_{T,i}^{(P)}$
Supplementary equations	$\text{Log } \alpha = 3.39 \cdot \text{Log}(T_b/T_{cr}) - 0.1585 - \text{Log } V$	$\alpha^{(P)} = 777 \cdot \Delta_T^{(P)} / V$
Lydersen equation	$T_b/T_{cr} = 0.567 + \Delta_T - (\Delta_T)^2$	$m = 0.5/\Delta_T^{(P)}$
Solubility parameter equations^a	$\delta_t = (F_t + B)/V$	$\delta_t = (F_t + B/m)/V$
	$\delta_p = \delta_t \cdot \left(\frac{1}{\alpha} \cdot \frac{F_p}{(F_t + B)} \right)^{1/2}$	$\delta_p = \delta_t \cdot \left(\frac{1}{\alpha^{(P)}} \cdot \frac{F_p}{(F_t + B/m)} \right)^{1/2}$
	$\delta_H = \delta_t \cdot [(\alpha - 1)/\alpha]^{1/2}$	$\delta_H = \delta_t \cdot [(\alpha^{(P)} - 1)/\alpha^{(P)}]^{1/2}$
	$\delta_d = (\delta_t^2 - \delta_p^2 - \delta_H^2)^{1/2}$	$\delta_d = (\delta_t^2 - \delta_p^2 - \delta_H^2)^{1/2}$

^a B is a base value defined as B = 277

Stefanis' group contribution theory

Stefanis^[93] published method makes the estimation of the Hildebrand SP for pure organic compounds possible. In contrast to the approaches of Fedors and Hoy, Stefanis discriminates between so called first order and second order groups. The first order groups are derived from UNIFAC and describe the molecular structure of the investigated substance. Secondary order groups are based on the ABC approach^[100] that presumes that the structure of a compound is an average of its conjugate forms. This second order is meant to improve the predictions substantially.^[92,93]

The equation for the calculation of the total SP (in MPa^{1/2}) is given in Eq.(3-11). n_i is the number of appearances of the group and F_i the respective first-order contribution. The second-order contribution is given similarly by m_j and S_j . For compounds containing no second-order groups, the second sum term equals 0.^[93]

$$\delta_t = \left(\sum_i n_i (F_i/\text{MPa}) + \sum_j m_j (S_j/\text{MPa}) + 75954.1 \right)^{0.383837} \text{MPa}^{1/2} - 56.14 \text{MPa}^{1/2} \quad \text{Eq.(3-11)}$$

Table 3-6 lists an extract of the first order group contributions relevant in this thesis. No second order contributions were published for these groups.

Table 3-6. Extract of first-order contributions of Stefanis' GCT.^[93]

First order groups	F_i
CH ₂	-277.1
NCO	2 694.6

3.3 Flory-Huggins lattice theory

3.3.1 Definition and function

Flory-Huggins (FH) theory was published and developed independently by Flory^[30] and Huggins^[101]. The lattice theory allows for the interpretation and prediction of the behaviour in mixtures of small molecules as well as polymer blends.^[102]

The statistical approach divides the volume of the mixture into N equally sized lattice sites that can either be populated by a segment of a polymeric chain or by a solvent molecule (see Figure 3-12). Conceptionally, each lattice site exhibits the volume of a solvent molecule V_s .

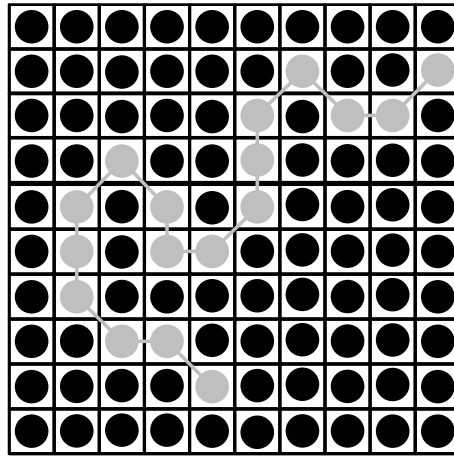


Figure 3-12. Illustration of a polymeric chain (grey) arranged in a lattice of solvent molecules (black).

Furthermore, the following assumptions are made:

- the polymer molecules are equal in chain length and are not distinguishable.
- the polymeric chain is divided into n segments, each comprising the volume V_s .
- all orientations of the polymeric chain are of equal probability

This description of the binary solution of a polymer P in a solvent S can be analogously expanded to a ternary or even higher order system. For a binary system, the FH theory allows for the estimation of the Gibbs free energy of mixing ΔG_{Mix} according to Eq.(3-12).^[102]

$$\frac{\Delta G_{Mix}}{RT} = \frac{\phi_S}{V_S} * \ln(\phi_S) + \frac{\phi_P}{V_P} * \ln(\phi_P) + \chi'_{S,P} * \phi_S * \phi_P \quad \text{with } \chi'_{S,P} = \frac{\chi_{S,P}}{V_{ref}} \quad \text{Eq.(3-12)}$$

ϕ_i is the volume fraction and V_i the molar volumes of the solvent and the polymer. χ_{ij} is the binary Flory-Huggins interaction parameter, T is the absolute temperature in Kelvin and R is the molar gas constant. V_{ref} is an arbitrarily chosen reference volume mostly set according to the molar volume of the solvent molecule or the repeating unit of the polymer.

The first two summands of the equation represent the combinatorial entropy that is gained by the system if the molecules are in entropic maximum. The term is always negative but with increased chain length and the implemented high molar volume V_P the entropic contribution to ΔG_{Mix} becomes negligible. The last term is the enthalpic contribution based on the binary interaction parameter, which is a measure for the material specific interactions between the different segments.^[91]

There are several different theories for the estimation of binary interaction parameters. The original FH theory was based on the simple approximation that χ_{ij} is only depending on inverse temperature and on two mixture specific constants A and B , mostly described by $\chi_{ij} = A + B/T$.^[102] Following this equation, the favoured attraction of two identical molecules compared to two different molecules in the mixture is reduced at increased temperatures. Therefore, only upper critical solution temperature (UCST) behaviour can be reflected by this basic approach. In this regard, Hildebrand SP can be used to estimate χ_{ij} according to Eq.(3-13), with $\delta_{i,j}$ as the SPs of the substances.^[102,103]

$$\chi_{i,j} = V_{ref} \cdot \frac{(\delta_i - \delta_j)^2}{RT} \quad \text{Eq.(3-13)}$$

For the description of solutions comprising specific interactions that lead to complex phase diagrams, numerous modifications in the equations for χ_{ij} have been published.^[104–106] Here it shall only be noted, that most of them deal with composition dependency of the interaction parameter or the implementation of quadratic terms.^[102]

3.3.2 Estimation of phase diagrams

Based on the presented equation for ΔG_{Mix} , phase diagrams or being more precise, binodal and spinodal curves can be predicted.^[102,107] A schematically phase diagram of a partially miscible blend consisting of two polymers A and B is shown in Figure 3-13. The binodal compositions are defined by the condition that the chemical potentials μ_i in the phases P and Q are equal. μ is given by the first derivative of ΔG_{Mix} with respect to the number of moles.

The binodal curve is the border between miscible and metastable region. Furthermore, the spinodal is defined by the condition that the second derivative equals zero.^[107] It represents the border between metastable and instable region.

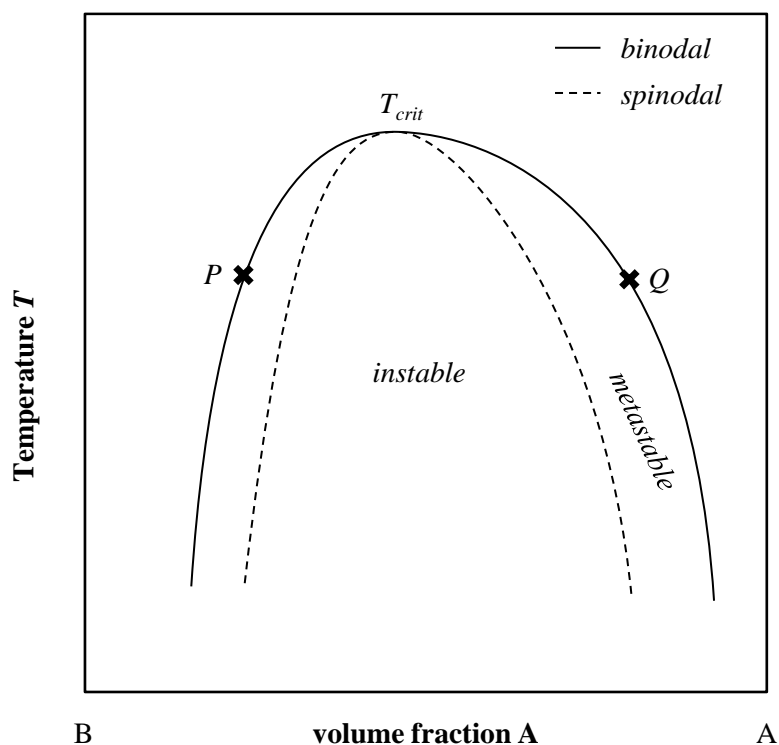


Figure 3-13. Schematically illustration of a phase diagram of a binary polymer blend of A and B.

Given these dependencies, critical conditions for phase separation can be derived by rather simple methods. For example the critical composition in a binary polymer blend is only dependent on the polymerisation degree of the two polymers.^[107,108]

For the estimation of phase diagrams, typically numerical methods are used, due to the existence of various unknown variables. In a binary mixture, four volume fractions are unknown, while in ternary mixtures even six variables need to be numerically solved. For the solving procedure the definition of an objective function is needed, which is minimized by the numerical algorithm. The mathematical procedure and the proper definition of the objective function was discussed in detail by Hsu and Prausnitz.^[109]

4 Results and discussion

4.1 Ternary phase diagram of PPG/PEO/HDI mixtures

The reaction yielding the bi-soft segment ITPU is starting in a ternary mixture. It contains the two soft segment forming polyols and the diisocyanate. In this study, a PPG/PEO combination was reacted with HDI. Prior to the investigation on the reaction-induced phase separation, a partially miscible soft segment combination had to be identified.

The concept to find this partially miscible mixture was to study the combination of PPG/PEO comprising a fixed molar weight PEO (PEO600, $M_n = 590 \text{ g}\cdot\text{mol}^{-1}$) and varying PPGs ($M_n = 400, 1\,000, 2\,000$ and $4\,000 \text{ g}\cdot\text{mol}^{-1}$). It is presumed that at some point the increased M_n of the PPG leads to poor miscibility due to the increasing lipophilicity at higher chain length. The SPs of the polyether polyols were estimated by means of group contribution theories to assess the miscibility via FH theory. Subsequent to the proper description of the partially miscible PPG/PEO mixture, the ternary system PPG/PEO/HDI is investigated via the same approach.

This section presents the findings in a step-by-step fashion starting from the binary polyether polyol mixtures and closing with the ternary reaction mixture.

4.1.1 *The binary mixture of PPG/PEO*

The first step in the theoretical estimation of the miscibility in the binary soft segment mixture is the determination of the SPs of the compounds. In order to determine the Hildebrand solubility parameters of the polyether polyols the group contribution theories (GCTs) of Fedors and Hoy were applied. The complete structure of the polyols, i. e. the starter content, the number of repeating units m_i in the polymeric EO/PO block(s) and the end-functional hydroxyl groups, was considered in the calculations. Cooper and Booth have been studying the miscibility behaviour of oligomeric EO and PO oligomers.^[110–112] They demonstrated by comparison of α - ω hydroxy oligomers with α - ω methoxy oligomers, that the end-functionality has a huge impact on the miscibility behaviour.^[110,111]

The applied methods led to the results shown in Table 4-1. Regarding the PPG series, the decrease in molecular weight led to an increase in the SP in both GCTs. This was due to the weakening statistical impact of the terminal, polar OH-group on the SP at higher chain length of the oligomer. Both methods yielded comparable results for PPG2k ($\Delta\delta = 0.13 \text{ MPa}^{1/2}$) and

Results and discussion

PPG4k ($\Delta\delta = 0.05 \text{ MPa}^{1/2}$) whereas the dissimilarity between the results increased for PPG1k ($\Delta\delta = 0.44 \text{ MPa}^{1/2}$) and PPG400 ($\Delta\delta = 1.00 \text{ MPa}^{1/2}$). The SPs of PEO600 were at a variance even larger than $1 \text{ MPa}^{1/2}$.

Table 4-1. Resulting SPs of the polyether polyols based on Fedors' and Hoy' GCT.

	PPG400	PPG1k	PPG2k	PPG4k	PEO600	
m_{PO}	4.12	14.03	31.13	65.68	0.05	
m_{EO}	-	-	-	-	9.61	
Starter	PO	PO	PO	PO	PO	
HO unit	PO-OH	PO-OH	PO-OH	PO-OH	EO-OH	
Fedors	E_i [cal·mol ⁻¹]	41 383	80 288	147 382	283 025	54 254
	V_i [cm ³ ·mol ⁻¹]	389	909	1 804	3 615	489
	δ_{Fedors} [MPa ^{1/2}]	21.09	19.23	18.49	18.1	21.54
Hoy	F_t [cal·mol ⁻¹]	9 367	22 123	44 124	88 601	11 137
	V [cm ³ ·mol ⁻¹]	485.3	1 225.3	2 502	5 082	511.2
	$\Delta_T^{(P)}$ [MPa ^{1/2}]	0.6903	1.6320	3.2560	6.539	0.8311
	m	0.7243	0.3063	0.1536	0.0765	0.6016
	$\delta_{t,\text{Hoy}}$ [MPa ^{1/2}]	20.09	18.79	18.36	18.15	22.69
$\Delta\delta$ [MPa ^{1/2}]	1.00	0.44	0.13	0.05	1.15	

The presented results were in the range of typical SPs of polyether polyols.^[86] However, published SP values are inconsistent, depending on the method that was used to determine it. Yilgör et al. listed the SP of PPG and PEO $\delta_{PPG} = 18.9 \text{ MPa}^{1/2}$ and $\delta_{PEO} = 20.2 \text{ MPa}^{1/2}$.^[11,16] In contrast to this Utracki published both as $\delta_{PPG} = 23.514 \text{ MPa}^{1/2}$ and $\delta_{PEO} = 24.444 \text{ MPa}^{1/2}$.^[113]

Nevertheless, the determined SPs were subsequently used in FH theory based calculations in order to estimate the miscibility of each compound of the PPG series with PEO600 at 298.3 K. The prediction of miscibility was here achieved by calculating the free energy of mixing ΔG_{Mix} for mixtures comprising volume fractions ϕ_{PPG} from zero to one. A negative ΔG_{Mix} without points of inflection over the entirety of volume fractions predicts full miscibility.

Figure 4-1 shows ΔG_{Mix} when using the SPs from Fedors' (left) and Hoy's (right) GCTs. Applying the SPs based on Fedors, the curve of ΔG_{Mix} was found to be negative for all compositions without any points of inflection for PPG400/PEO600 and PPG1k/PEO600 mixtures. Consequently, the model predicted complete miscibility for these mixtures. For

mixtures PPG2k/PEO600 and PPG4k/PEO600, points of inflection in ΔG_{Mix} were found and thus partial miscibility was predicted in these cases.

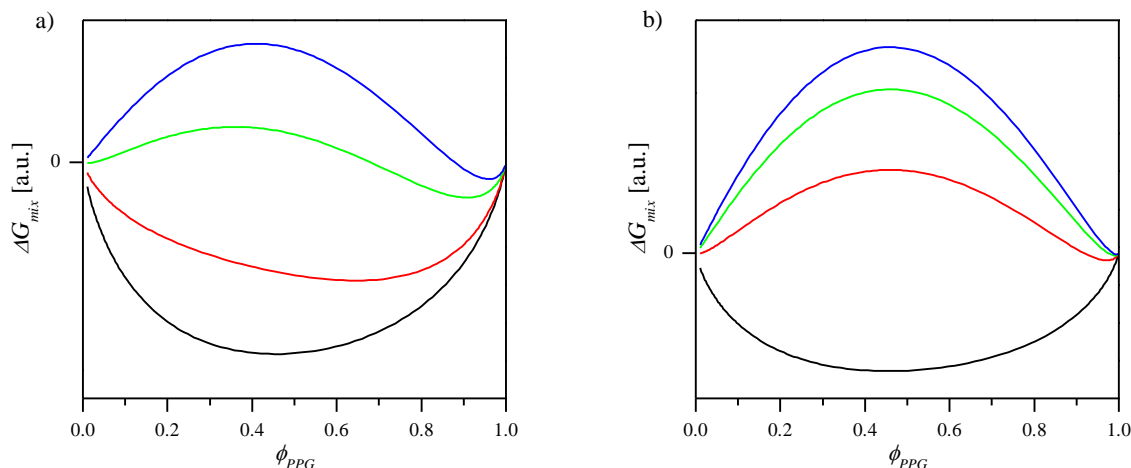


Figure 4-1. Free energy of mixing of the PPG series with PEO600 derived from the SPs based on Fedors' (a) and Hoy's GCT (b). (- PPG400; - PPG1k; - PPG2k; - PPG4k)

The curves of ΔG_{Mix} based on the SPs derived from Hoy's GCT predict very poor miscibility for the PPGs with PEO600, except for PPG400. This was mostly due to the higher SP of PEO600 ($\delta_{PEO600,Hoy} = 22.69 \text{ MPa}^{1/2}$) compared with the one based on Fedors' data ($\delta_{PEO600,Fedors} = 21.54 \text{ MPa}^{1/2}$). Consequently, the binary interaction parameter becomes a higher value, favouring immiscibility.

Experimental miscibility tests confirmed that the SPs series based on Fedors's data excellently reflected the real behaviour since PPG400 and PPG1k were completely miscible with PEO600 at 25 °C. On the other side the PPGs with molecular weight $\geq 2\,000 \text{ g}\cdot\text{mol}^{-1}$ exhibited limited miscibility. This confirmed that the presented method based on Fedors GCT matches qualitatively the real miscibility behaviour. Based on these results, the SPs based on Fedors' GCT were applied in the following calculations of the quantitative phase diagrams of the partially miscible PPG/PEO600 mixtures.

For the polyols with limited miscibility with PEO600, i. e. PPG2k and PPG4k, binodal curves were calculated using a numerical approach based on MATLAB. The resulting phase diagrams are shown in Figure 4-4. PPG2k/PEO600 (Figure 4-4 a) and PPG4k/PEO600 (Figure 4-4 b) exhibited the typical upper critical solution temperature (UCST) behaviour that results from the basic FH theory.

Both PPGs were predicted to have low miscibility with PEO600 at room temperature, approximately 10 vol.% for PPG2k and 5 vol.% for PPG4k. The binodal curves had an

asymmetrical shape suggesting that miscibility at high contents of PEO600 is poorer than at high contents of PPG.

The calculated phase diagrams of the PPG/PEO600 mixtures were compared with experimentally determined cloud points and binodal compositions. Figure 4-2 illustrates the typical resulting turbidity vs. temperature plot for the example of a 50:50 vol.% PPG2k/PEO600 mixture.

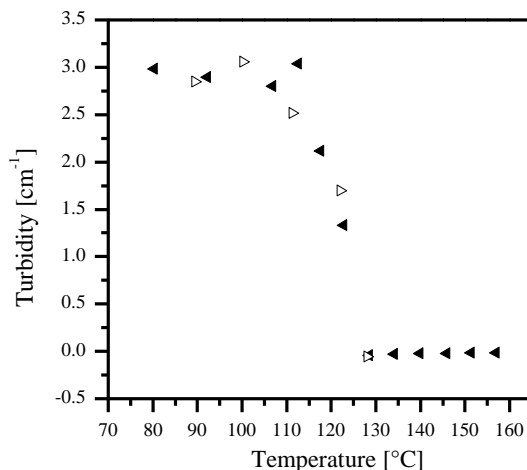


Figure 4-2. Temperature dependent turbidity analysis performed on a 50:50 vol.% PPG2k/PEO600 polyol mixture. ◀: Cooling ▷: Heating

Coming from the transparent mixture at high temperatures, there was a sharp increase of turbidity at 122 °C. This is defined as the cloud point temperature T_{CP} . Increasing the temperature again led to clearance of the mixtures. No hysteresis was observed. The respective turbidity vs. temperature plots of the remaining mixtures can be found in the appendix.

As illustrated in Figure 4-4, the cloud point curve was in qualitative accordance to the UCST dependency from the predicted binodal. However, the experimentally found UCST T_{crit} at 130 °C is far below the prediction. Nevertheless, the limits of miscibility at high and low contents of PEO600 were in good agreement in the temperature range up to 100 °C.

The cloud point curve points to a critical composition $\phi_{crit} = 0.30$ vol.% PPG2k. According to Bates ϕ_{crit} is solely dependent on the amount of occupied lattice sites N_i of the two polymers A and B as given by Eq.(4-1).^[108]

$$\phi_{crit, theo} = \frac{\sqrt{N_B}}{(\sqrt{N_A} + \sqrt{N_B})} \quad \text{Eq.(4-1)}$$

N_i is given by the fraction of the molar volume of compound i divided by V_{ref} ($V_{ref} = 52.4 \cdot \text{cm}^3 \cdot \text{mol}^{-1}$). For the system PPG2k/PEO600 with $N_{\text{PPG2k}} = 34.48$ and $N_{\text{PEO600}} = 10.34$ this results in $\phi_{\text{crit,theo}} = 0.35$ vol.% PPG2k, which is in good accordance to the observed critical composition.^a

Generally speaking it is questionable that determined cloud points resemble the binodal curve due to the existence of a metastable range between the binodal curve and the spinodal curve.^[107] Phase separation does not necessarily appear instantaneously in this metastable region due to the underlying process of nucleation and growth (NG). Hypothetically it is conceivable that the system might have already crossed the binodal and entered the metastable region without the occurrence of spontaneous phase separation. This can be kinetically favoured by fast cooling rates.^[114] In this case, the measured cloud point curve does not reflect the thermodynamical binodal curve. However, in the case that the spinodal curve is crossed, phase separation is inevitable.

Nevertheless, here it should be mentioned that in general the spinodal and binodal curve meet at T_{crit} .^[107] Considering this, the discrepancy between predicted and experimentally found T_{crit} is not readily explained by the possibility of kinetically belated phase separation. A possible explanation might be that the applied analytical method (optical turbidity) does not account for inhomogeneities at nanometre scale. Here, light scattering techniques are much more sensitive and could lead to more responsive detection of submicron phase separation. Anyway, as in the further progress of this work the phase separation during the polyurethane reaction was monitored by UV-Vis technique, for the sake of comparability it is advantageous to apply the same method.

However, on behalf of this discussed uncertainty of the cloud points, the definite binodal compositions were additionally analysed by SEC analysis. The phase separating PPG/PEO600 mixtures were equilibrated at distinct temperatures and samples were taken from the two separate transparent phases. Figure 4-3 shows exemplarily the MWDs of the samples taken from PPG2k/PEO600. The respective results from the PPG4k/PEO600 mixtures can be found in the appendix. The peaks of the respective macrodiols were well resolved. The weight fractions of PPG and PEO600 in the phases were derived from the peak areas and converted to the volume fractions under consideration of their specific volume.

^a See Table 6-2 for V_m of PPG2k and PEO600

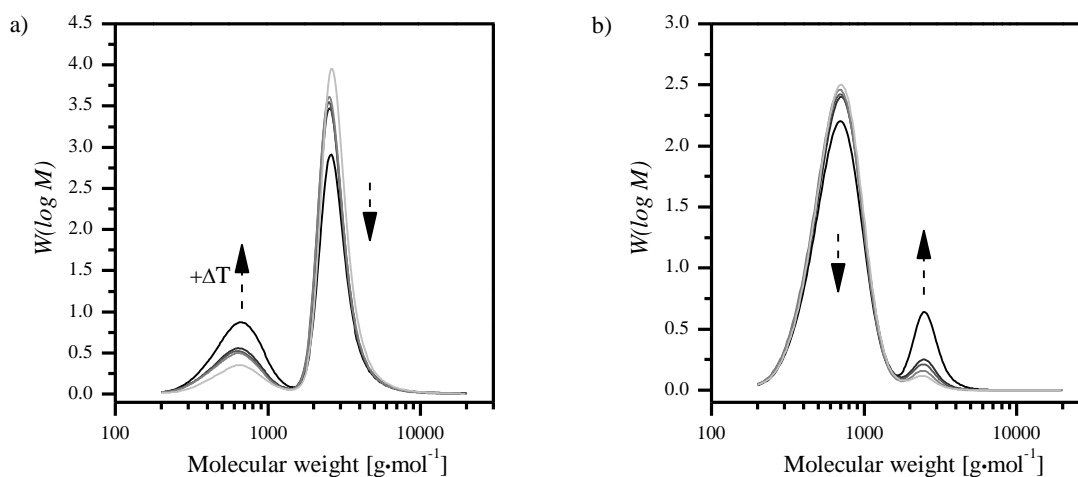


Figure 4-3. Temperature dependent MWDs of the two phases in PPG2k/PEO600 mixtures. ($T = 50\text{ }^{\circ}\text{C}; 80\text{ }^{\circ}\text{C}; 100\text{ }^{\circ}\text{C}; 120\text{ }^{\circ}\text{C}; 130\text{ }^{\circ}\text{C}$) a) PPG2k-rich phase and b) PEO600-rich phase.

Rising the temperature led to increased solubility of the minority compound in the mixtures. The derived binodal compositions were in excellent agreement to the predicted phase limits up to $120\text{ }^{\circ}\text{C}$ (see Figure 4-4). However, in accordance to the cloud point temperatures, above $130\text{ }^{\circ}\text{C}$ a single phase was observed.

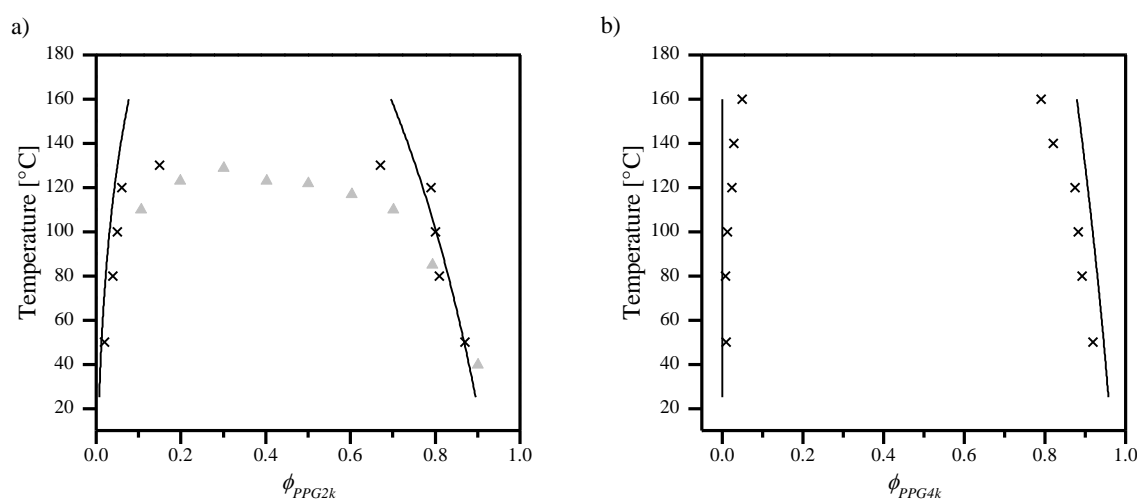


Figure 4-4. Theoretical and experimental phase diagram of PPG2k/PEO600 (a) and PPG4k/PEO600 (b) mixtures. Computational binodal curve (-), cloud points (\blacktriangle) and binodal compositions analysed via SEC (\times).

The predicted binodal curves for the partially miscible systems PPG2k/PEO600 and PPG4k/PEO600 were in excellent agreement to the experimentally observed binodal compositions. However, at elevated temperatures ($> 120\text{ }^{\circ}\text{C}$) the discrepancy between prediction and observation is increased.

To sum it up, for PPG2k/PEO600 it can be seen that the cloud point curve and the determined binodal compositions revealed a lower UCST than the computed binodal. Nevertheless, the predicted phase diagram reflected the experimentally found miscibility limits in the temperature range up to 120 °C.

These results demonstrated that the employed methods for the estimation of SPs and the FH theory are applicable to estimate the miscibility in polyether polyol mixtures at temperatures typical for polyurethane reactions. It was found that the GCT data provided by Fedors was best suitable for the determination of the SPs of the polyols. On basis of the derived SPs, the resulting value for the BIP per lattice site in PPG2k/PEO600 mixtures is $\chi_{\text{PPG2k,PEO600}} = 0.1966$ at $T = 298$ K.

Friday et al. published a similar BIP $\chi(30\text{ °C})$ of 0.17 for a mixture comprising PEO ($M_n = 600\text{ g}\cdot\text{mol}^{-1}$) and PPG ($M_n = 2\,025\text{ g}\cdot\text{mol}^{-1}$).^[111] In the same study they showed that the interaction $\chi(30\text{ °C})$ between the equivalent methoxylated oligomers only amounted 0.09. This emphasizes the significance of the hydroxy groups regarding the interactions in the mixture. It appears likely that the hydroxy groups are forming hydrogen bonds with one another or with the ether oxygen in the oligomer backbone. These specific interactions are known to play a crucial role regarding the free energy of mixing.^[85]

It is presumed that theories that are more sophisticated are required to explain the deviation at high temperatures. To this day it is not yet fully understood but it is assumed that, in addition to specific interactions, molecular weight distribution effects^[35] and composition-dependency of the interaction parameter^[33] could play an essential role. Fortunately, for the mixtures evaluated in this work this is not necessary as high temperature ($> 120\text{ °C}$) behaviour can be neglected.

4.1.2 Phase diagram of the ternary mixture PPG2k/PEO600/HDI

The miscibility of two polyols with the isocyanate is of particular interest to ensure homogeneous reaction conditions. This part is focusing on the ternary situation and elaborates on the ability to predict limited miscibility of polyols with polyisocyanates on basis of SPs. In analogy to the methodology applied in the binary polyol mixtures, the SP of HDI is needed to be addressed first.

Table 4-2 shows the respective SP calculation for HDI based on Fedors and Hoy. Both results were calculated to be $22.79\text{ MPa}^{1/2}$ for $\delta_{\text{HDI,Fedors}}$ and $23.18\text{ MPa}^{1/2}$ for $\delta_{\text{HDI,Hoy}}$.

Unfortunately, there was no reference value found in the literature for HDI to compare the results to.

Table 4-2. Calculation of the SP of HDI based on Fedors and Hoy.

	n	e_i	v_i	$\delta_{HDI, Fedors}$	$F_{t,i}$	v_i	$\delta_{HDI, Hoy}$
		[cal·mol ⁻¹]	[cm ³ ·mol ⁻¹]	[MPa ^{1/2}]	[(MJ·cm ⁻³) ^{1/2} ·mol ⁻¹]	[cal·mol ⁻¹]	[MPa ^{1/2}]
		<i>Fedors</i>			<i>Hoy</i>		
CH₂	6	1 180	16.1		269	15.55	
NCO	2	6 800	35		736	25.9	
HDI		20 680	166.6	22.79	3 086	145.1	23.18

For the binary mixtures of each polyol with HDI ΔG_{Mix} was calculated to investigate the predicted miscibility behaviour by FH theory. Figure 4-5 demonstrates the resulting curves of ΔG_{Mix} of PEO600/HDI and PPG2k/HDI mixtures, applying $\delta_{HDI, Fedors}$ (Figure 4-5a) and $\delta_{HDI, Hoy}$ (Figure 4-5b), respectively. The results indicate that using both values complete miscibility between PEO600 and HDI was predicted. On the other hand, limited miscibility was forecast for mixtures of PPG2k/HDI (grey lines in Figure 4-5). This results from the large difference between $\delta_{HDI} \approx 23 \text{ MPa}^{1/2}$ and $\delta_{PPG2k} \approx 18.5 \text{ MPa}^{1/2}$.

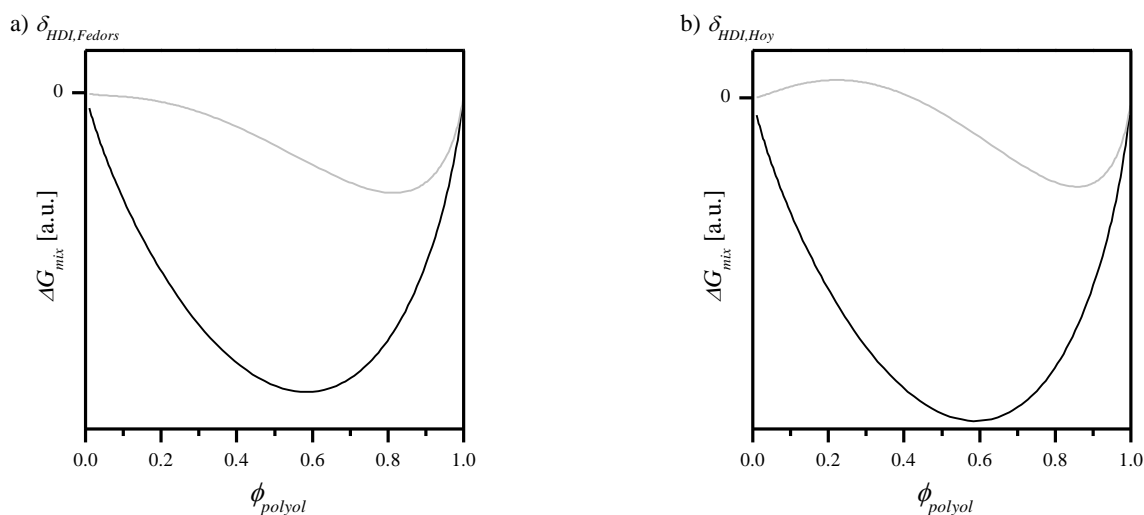


Figure 4-5. Predicted free energies of mixing using the SPs of HDI based on Fedors and Hoy. PEO600 (-)/HDI and PPG2k (-)/HDI. For the polyols their respective SP based on Fedors' GCT was used in the calculations.

In contrast to these predictions, solubility tests demonstrated that HDI is completely miscible with both, PEO600 and PPG2k. Against this background it was needed to further

evaluate the SP of HDI by additional methods of determination. Therefore an additional GCT published by Stefanis^[93] and experimental Hansen parameter determination were applied.

Interestingly, the results were quite different from the previous ones. Stefanis' GCT led to the value 19.95 MPa^{1/2} for $\delta_{HDI,Stefanis}$ as illustrated in Table 4-3.

Table 4-3. Calculation of the SP of HDI based on Stefanis.

	n_i	F_i	$\sum n_i \cdot F_i$	δ_i [MPa ^{1/2}]
CH₂	6	-277.1	-1 662.6	
NCO	2	2694.6	5 389.2	
HDI			3 726.6	19.95

This compares with 18.09 MPa^{1/2} for $\delta_{HDI,exp}$, which is based on the experimental Hansen SP determination as given in Table 4-4. The detailed experimentally found solubility of HDI is illustrated in Figure 4-6. It shows the typical solubility plots suggested by Hansen^[83], where the partial SPs δ_D , δ_P and δ_H are plotted against each other. For the sake of clarity, the two-dimensional plots are preferred in comparison with a three-dimensional depiction. Conventionally the units along the δ_D -axis are twice the size compared with the δ_P and δ_H units.^[81] It can be seen that HDI is soluble in the majority of polar as well as apolar solvents but becomes insoluble in protic compounds containing very high δ_H -values (e. g. ethylene glycol, glycerol and 1,3 propylene glycol). The experimental solubility of HDI definitely points to the conclusion that HDI is not as polar as the high values of $\delta_{HDI,Fedors}$ and $\delta_{HDI,Hoy}$ indicated.

Table 4-4. Hansen SP of HDI determined by solubility tests.

	$\delta_{D,exp}$ [MPa ^{1/2}]	$\delta_{P,exp}$ [MPa ^{1/2}]	$\delta_{H,exp}$ [MPa ^{1/2}]	solubility radius	$\delta_{t,exp}$ [MPa ^{1/2}]
HDI	13.3	8.0	9.3	14.0	18.09

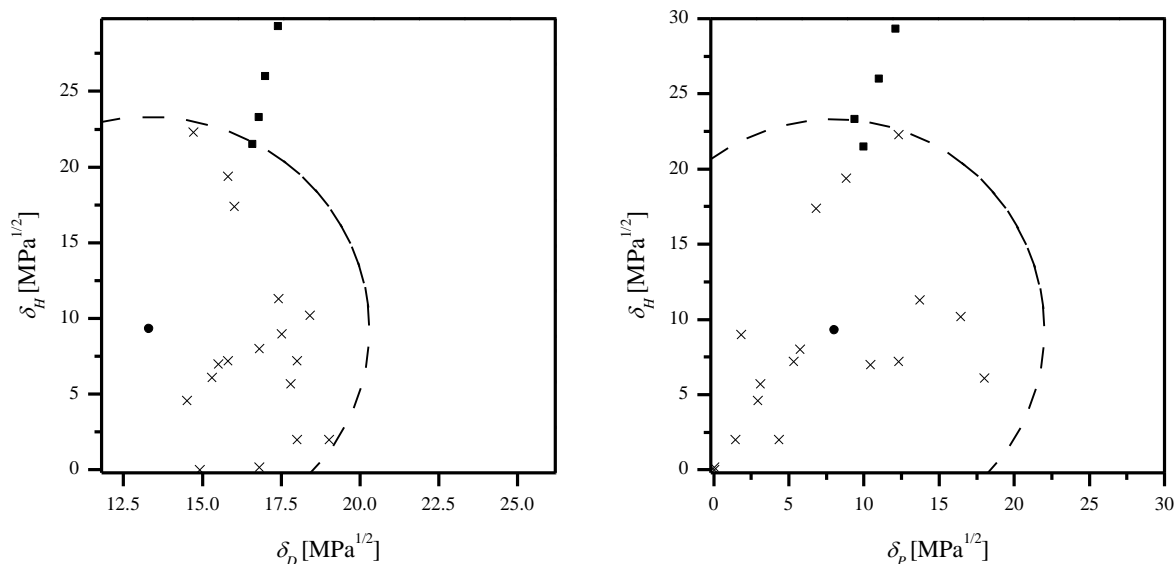


Figure 4-6. Results from the HSP determination by experimental solubility test of HDI. (\times : soluble in solvent; \blacksquare : insoluble in solvent; \bullet : resulting HSP; - - solubility radius)

Based on these results, $\delta_{HDI,exp}$ and $\delta_{HDI,Stefanis}$ were further used in FH theory based calculations in order to obtain predicted ΔG_{Mix} . As illustrated in Figure 4-7, in all cases ΔG_{Mix} was predicted to be negative over the complete range of volume fractions ϕ . There are no points of inflection in the curve, consequentially complete miscibility has to be assumed. Interestingly, in the case of $\delta_{HDI,Stefanis}$, HDI was predicted to be better soluble in PEO600 (black line in Figure 4-7) than in PPG2k (grey line in Figure 4-7) whereas $\delta_{HDI,exp}$ leads the contrary conclusion.

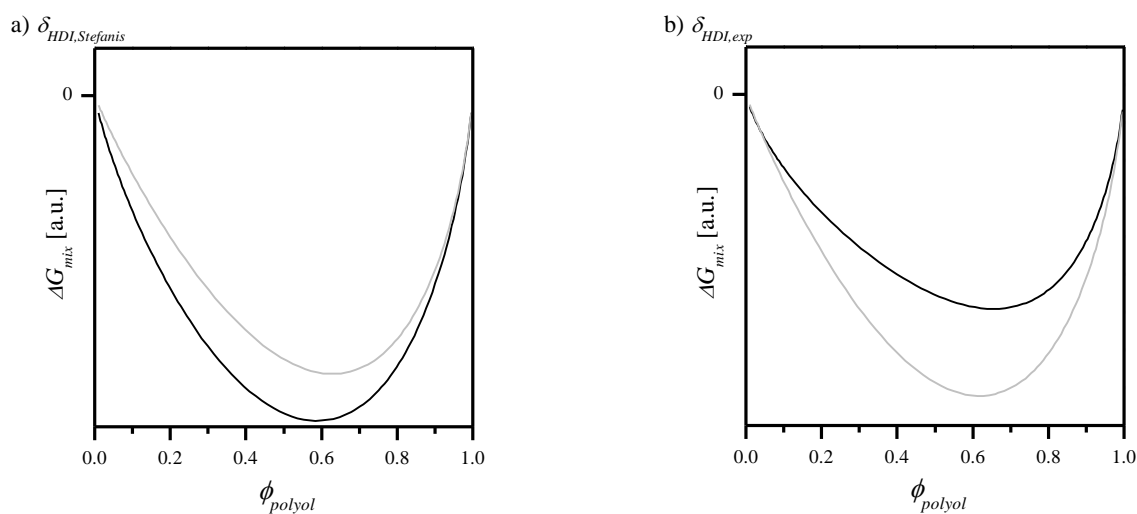


Figure 4-7. Predicted free energies of mixing using the SPs of HDI based on Stefanis and solubility tests. PEO600 (-)/HDI and PPG2k (-)/HDI. For the polyols their respective SP based on Fedors' GCT was used in the calculations.

In this regard, it should be noted that poorer miscibility of HDI in one of the two polyols would lead to non-uniform distribution of HDI in case of a phase separated ternary mixture. This is discussed later in further detail.

These results demonstrate that especially the value of δ_{HDI} is strongly dependent on which method of determination is applied. This leads to the situation that the predicted solubility of PPG2k in HDI is differing to a large extent. Based on the experimental observation that HDI is indeed miscible with PPG2k and PEO600 it is concluded that only $\delta_{HDI,exp}$ and $\delta_{HDI,Stefanis}$ might lead to a proper phase diagram of the ternary mixture PPG2k/PEO600/HDI. For the sake of comprehensive comparability, the impact of each of the individual δ_{HDI} -values on the phase diagram of the ternary mixtures is presented in the following. Each of the different δ_{HDI} s was employed in the numerical estimation of the ternary phase diagram. PPG2k and PEO600 are represented by $\delta_{PPG2k,Fedors} = 18.49 \text{ MPa}^{1/2}$ and $\delta_{PEO600,Fedors} = 21.54 \text{ MPa}^{1/2}$.

The applied numerical approach results in pairs of binodal compositions at which the chemical potentials are in equilibrium. These resulting binodal compositions are illustrated as the respective tie lines in Figure 4-8. It can be seen that all derived phase diagrams indicate a miscibility gap at low contents of HDI. In other words, a homogeneous mixture can only be expected if a sufficient amount of HDI is present.

However, the detailed outline of the binodal compositions is strongly dependent on the different δ_{HDI} s. For $\delta_{HDI,Fedors}$ (b) and $\delta_{HDI,Hoy}$ (c) the phase diagrams are similar as the SPs are only differing to a little extent of $0.40 \text{ MPa}^{1/2}$. In the phase separated region both predict two highly dissimilar binodal compositions. On the one hand phase separation results in a PEO-rich phase, which consists of comparable fractions of HDI and PEO600 without portions of PPG2k and on the other hand a PPG2k-rich phase, that contains mainly PPG2k (> 75 vol.%) and little HDI and PEO600. This results from the dissimilarity of the difference in the SPs $\Delta\delta = (\delta_i - \delta_{HDI})$ of both polyols i with respect to HDI, as already discussed on the respective ΔG_{MixS} .

The very opposite was found in the instance of the experimentally determined $\delta_{HDI,exp}$ (Figure 4-8 a). Here, $\Delta\delta_{PPG2k,HDI}$ is smaller than $\Delta\delta_{PEO600,HDI}$ leading to higher expected HDI contents in the PPG2k-rich phase in comparison with the PEO600-rich phase.

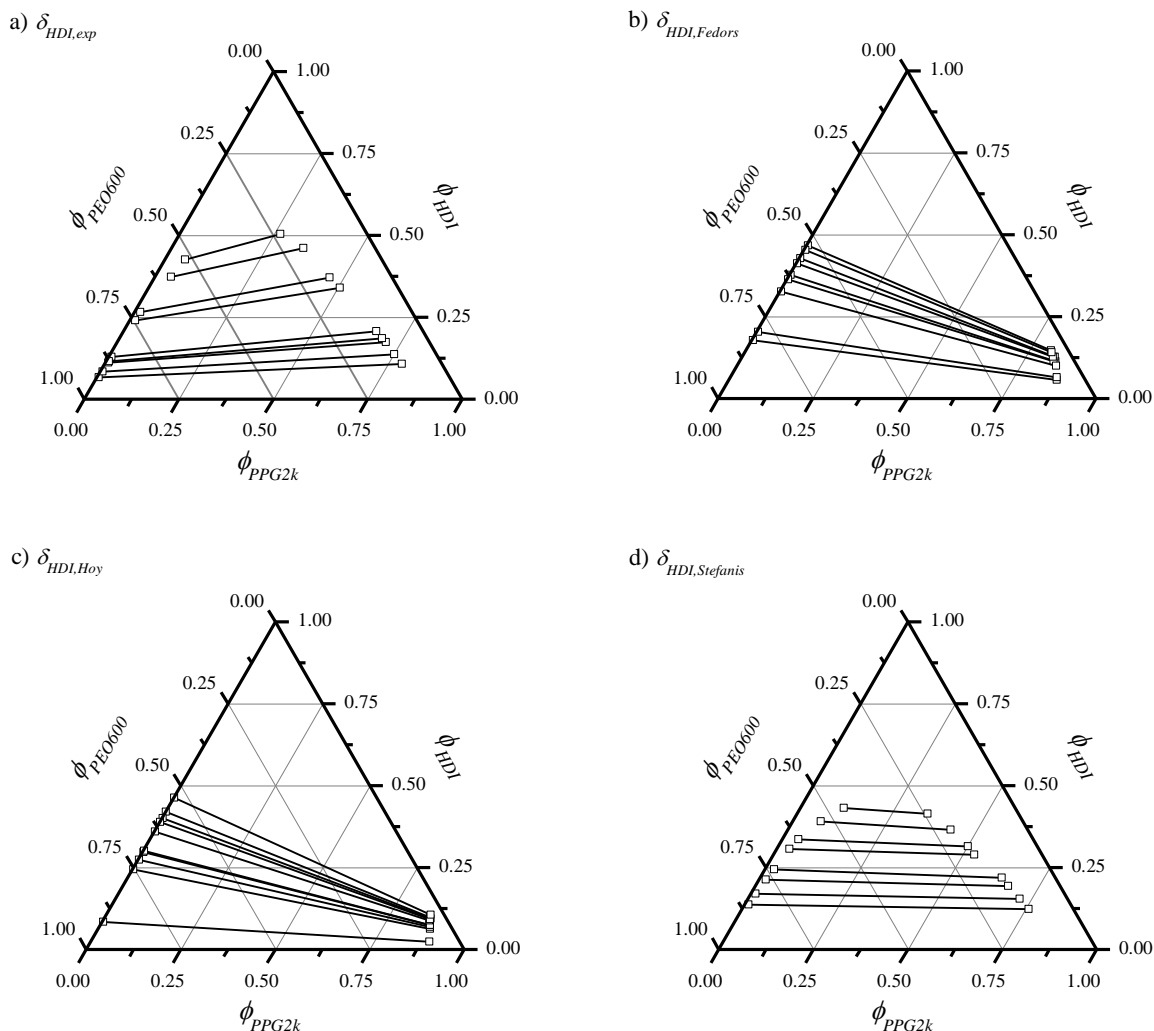


Figure 4-8. Predicted ternary phase diagrams based on the different solubility parameters for HDI. For PPG2k and PEO600, $\delta_{PPG2k} = 18.49 \text{ MPa}^{1/2}$ and $\delta_{PEO600} = 21.54 \text{ MPa}^{1/2}$ were applied. The resulting pairs of binodal compositions (\square) are displayed as the corresponding tie lines.

In contrast to this, the phase diagram in considering $\delta_{HDI,Stefanis}$ (Figure 4-8 d) demonstrates how the behaviour changes when the predicted miscibility of both polyols with HDI is nearly identical (see Figure 4-7a). The flat tie lines are indicating that the predicted HDI contents in the separate PEO600- and PPG2k-rich phases are almost identical.

Concerning the impact of the molar fraction of NCO/OH moieties on the MWD of polyurethanes,^[57] the presented cases can be of particular interest regarding the understanding and the control of polyurethane formation reactions in inhomogeneous mixtures. The thermodynamic equilibrium can hypothetically lead to the situation that in one phase there is a high excess or shortage of NCO groups with respect to OH groups. Owing to the step-growth

nature of the polyaddition reaction, this would affect the resulting MWD. This is discussed in detail regarding the presented polymerisations in section 4.2.5.

Aside from these qualitative discussions on the possible phase behaviour, the resulting phase diagrams were compared to experimental cloud points at a temperature of 25 °C. The cloud point curve shown in Figure 4-9 confirmed indeed the existence of an immiscible region at low contents of HDI.

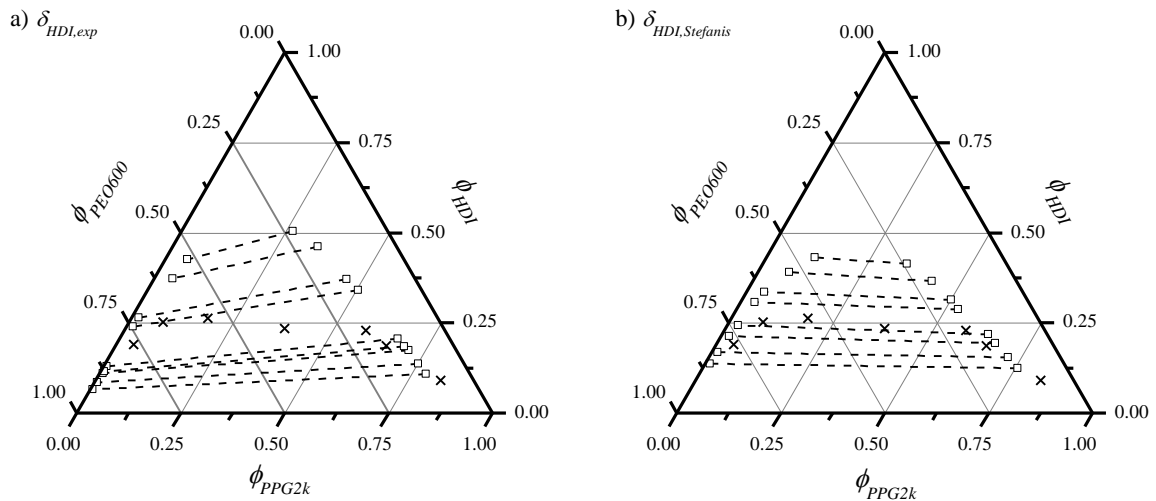


Figure 4-9. Theoretical and experimental ternary phase diagram of PPG2k/PEO600/HDI. Predicted binodal compositions (\square) using $\delta_{PPG2k,Fedors}$, $\delta_{PEO600,Fedors}$ and $\delta_{HDI,Stefanis}/\delta_{HDI,exp}$ in comparison with experimental cloud points (\times).

The cloud points demonstrated that the addition of HDI (> 25 vol.%) led to absence of turbidity in all cases. The resulting transparent liquid was interpreted as a homogeneous mixture, aware of the possible occurrence of submicron inhomogeneities, which might not have led to optical turbidity. The cloud point curve exhibited a slight asymmetry in the way that at high PPG2k volume fractions lower amounts of HDI were needed for clearance. This resembles the behaviour which was shown in Figure 4-8 b+c) indicating that in comparison with PPG2k, PEO600 might have indeed a better solubility in HDI. However, the effect was not as pronounced as seen in the theoretical approaches.

In general, the presented predicted phase diagrams did not reflect the experimental findings quantitatively as any of them showed a critical HDI-content $\phi_{HDI,crit}$ of approximately 50 vol.%. However, the phase diagram based on $\delta_{HDI,Stefanis}$ resulted in the best agreement to the cloud points. At high and low PPG2k volume fractions the resulting binodal curve was in very good accordance to the cloud point curve but prediction quality becomes less accurate near the critical point.

Here again it should be noted, that despite the absence of turbidity there might be inhomogeneities present, which would have been only detected by more sophisticated methods like dynamical light scattering. In this concern it should be stressed, that the studied mixture is reactive even at room temperature. Due to this, the quick method of cloud point titration was favoured compared to the SEC analysis used above. In the case of SEC analysis, two equilibrium phases are obligatory but to reach this condition time is needed even if centrifugation is used to accelerate phase separation.

Nevertheless, in regard of the deviation near the critical point between the cloud point curve and the theoretical binodal it has to be highlighted that the applied basic FH theory is simplified by many means as it did not consider specific interactions like H-bonding,^[52,85] composition-dependent interaction parameters^[33,106,115] or polydispersity effects^[35,116]. By the consideration of these effects, the FH theory is able to explain even complex phase diagrams like closed-loop or hourglass types.^[33] Presumably, the application of a more sophisticated approach would even lead to better description of the real behaviour. This study can be understood as a pioneering fundamental approach to the proper description of the phase behaviour in bi-soft segment polyurethane reaction mixtures. The result highlights the complexity and delivers a basis to develop cutting edge tools to predict the phase diagrams quantitatively.

4.1.3 Summary on PPG/PEO/HDI phase diagrams

Theoretical and experimental approaches were applied to assess the initial miscibility of typical polyurethane reactants, i. e. PPG- and PEO-based polyether polyols and HDI. The theoretical approach was based on FH theory. SPs were determined to estimate the binary interaction parameters of the reactants.

The miscibility of PPGs with PEO600 was studied in order to identify a partially miscible polyol mixture, which potentially exhibits reaction-induced phase separation. Group contribution theories were applied to estimate the SP of the macrodiols. The free energies of mixing for binary mixtures comprising PPGs and PEO600 were calculated on basis of FH theory. The calculation showed that the SPs based on Fedors method reflected the experimental observation that PPGs with average molecular weight $M_n > 1\,000\text{ g}\cdot\text{mol}^{-1}$ were partially miscible with PEO600.

Cloud point temperatures and binodal compositions of the partially miscible PPG2k/PE600 and PPG4k/PEO600 mixtures demonstrated UCST behaviour. The experimentally determined binodal compositions were in excellent agreement with the numerically calculated phase

diagram up to temperatures of 120 °C. At higher temperatures, the theoretical binodal deviated significantly from the experimental results. In fact, unexpected miscibility was experimentally found above 140 °C concerning PPG2k/PEO600 mixtures. Nevertheless, for the most part excellent agreement of theoretical and experimental phase diagrams confirmed the plausibility of the FH theory to reflect binary mixtures of polyether polyols.

To study the effect of the addition of HDI to mixtures of PPG2k/PEO600, the binary interaction parameters with respect to the polyether polyols were addressed. In this concern it was found that the SPs of HDI based on Fedors' and Hoy's methods ($\delta_{HDI} \approx 23 \text{ MPa}^{1/2}$) led to misleading prediction of immiscibility with PPG2k. Detailed experimental solubility tests confirmed that HDI was miscible with polar solvents (e. g. ethanol $\delta = 26.2 \text{ MPa}^{1/2}$) as well as with non-polar solvents (e. g. n-hexane $\delta = 14.9 \text{ MPa}^{1/2}$). This solubility assessment led to an alternative δ_{HDI} of about $18 \text{ MPa}^{1/2}$. A third independent group contribution theory supported the lower SP of HDI.

The implementation of the different SPs of HDI in the prediction of the ternary phase diagram revealed a drastic effect on the resulting binodal compositions. Experimentally determined cloud points demonstrated a miscibility gap at low concentrations of HDI (< 25 vol.%). The best agreement between theoretical and experimental miscibility limits was achieved using the lower SPs of HDI, i. e. $\delta_{HDI,exp} = 18.09 \text{ MPa}^{1/2}$ and $\delta_{HDI,Stephanis} = 19.95 \text{ MPa}^{1/2}$.

Overall, the objective to estimate the initial miscibility of the ternary polyurethane reactant mixture by theoretical and experimental techniques was successfully.

4.2 Reaction kinetics, phase behaviour and properties of PPG/PEO bi-soft segment polyurethanes

This section focuses on the experimental findings about the phase behaviour during the reaction towards the bi-soft segment ITPU. The composition of the reaction mixtures is systematically varied throughout the different experiments by means of the volume fraction of PPG2k/PEO600 in the polyol component. The initial volume fractions of PPG2k and PEO600 in the polyether polyol mixture are represented by the capitol letter Φ_i in the following. The individual experiments ITPU 1 to 9 are termed “ITPU X” with X representing the volume fraction 0.X of PPG2k in the polyol mixture. The molar fraction of NCO/OH was constant in all reaction mixtures. The scope of this section is a comprehensive description of the phase behaviour shown by the reaction mixture in the course of the formation of the ITPU.

At first, it is focused on the kinetics of the polymerisation on basis of in-line FTIR analysis and NCO%-content titration results. In order to get a more detailed insight into the kinetic a model reaction was performed and analysed by $^1\text{H-NMR}$.

Subsequently the onset of phase separation is investigated with particular focus on the influence of the composition of the initial reaction mixtures. This is discussed on basis of the previously estimated phase diagram of PPG2k/PEO600/HDI.

In order to get a comprehensive understanding of the phase behaviour, the synthesised ITPU emulsions were analysed regarding their molecular weight distribution (MWD) and their thermal properties. In this concern, special emphasis is placed on the characterisation of the composition of the separate phases of the emulsions. This aimed at identifying correlations between the thermodynamic phase diagram of the initial reactant mixture and the resulting properties of the ITPU.

4.2.1 Kinetics of the reaction in ternary PPG/PEO/HDI mixtures

In this study, the isocyanate concentration is monitored by in-line FTIR spectroscopy and by NCO%-content titration. Here it is shown by describing the procedure on the examples of the single soft segment polyurethanes (ITPU 10 and ITPU 11) how the reaction progress is evaluated on basis of these datasets.

Figure 4-10 shows the typical infrared spectrum of an ITPU reaction mixture containing only PPG2k as soft segment. The spectra at the start (grey line in Figure 4-10) and at the end (black line in Figure 4-10) of the reaction are shown. An overview about the important FTIR vibrations that are evaluated in this study is given in Table 4-5. The kinetic evaluation is based on the stretching band of the NCO group at a wavelength of $2\,270\text{ cm}^{-1}$.

In regard of the transmission-type measurement applied, the transmission at the NCO stretching band (νNCO) is increasing in course of the reaction. In the same instant the transmission at the carbonyl stretching band ($\nu\text{CO} = 1\,750\text{ cm}^{-1}$) is decreasing due to the formation of urethane groups, respectively. The same applies for the amide II region at $1\,550\text{ cm}^{-1}$ that is representing the N-H vibration of the formed urethane groups.

The spectrum shows increased signal noise in the regions above $2\,800\text{ cm}^{-1}$. This results from the relatively low intensity of the incident radiation that is reaching the detector in this region (see background spectrum in Appendix IV-4). This excludes the possibility to analyse the hydroxyl region of the spectrum (wavenumber $> 3\,000\text{ cm}^{-1}$).

Following Lambert-Beer's law (Eq.(4-2)), where I_0 is the intensity of the emitted light, I is the intensity of transmitted light, ϵ is the molar attenuation coefficient, c the concentration and d is the optical path length, $[NCO]$ is directly proportional to the absorbance Abs .

$$Abs = \ln\left(\frac{I_0}{I}\right) = \epsilon \cdot c \cdot d \quad \text{Eq.(4-2)}$$

Table 4-5. List of characteristic IR vibrations in the prepared polyurethanes.^[9,117]

Notation	Vibrational Mode	Wavenumber [cm ⁻¹]	Relating to:
$\nu_{As}COC$	Asymmetric C-O-C stretching	1 244	PEO600 ^a
$\nu_{sy}CH_3$	Symmetric bending of CH ₃	1 375	PPG2k ^a
νNH	Amide II of C(=O)-N-H	1 540 - 1 560	Urethane
νCO_{free}	Stretching of C=O (free)	1 730 - 1 740	Urethane
νNCO	Stretching of N=C=O	2 270	HDI ^a , ITPU
$\nu_{As}CH_2$	Asymmetric Bending of CH ₂	2 920	HDI ^a , PEO600 ^a
$\nu_{As}CH_3$	Asymmetric Bending of CH ₃	2 960	PPG2k ^a

^aReference spectra of the raw materials (HDI, PPG2k and PEO600) are given in Appendix IV-3.

In this respect, A_{NCO} is defined as the area under the absorption signal of νNCO . Following Lambert-Beer, A_{NCO} is proportional to the concentration $[NCO]$ and is therefore used for the calculation of the NCO conversion. The rectangle in Figure 4-10 illustrates the borders of the integration procedure to obtain A_{NCO} .

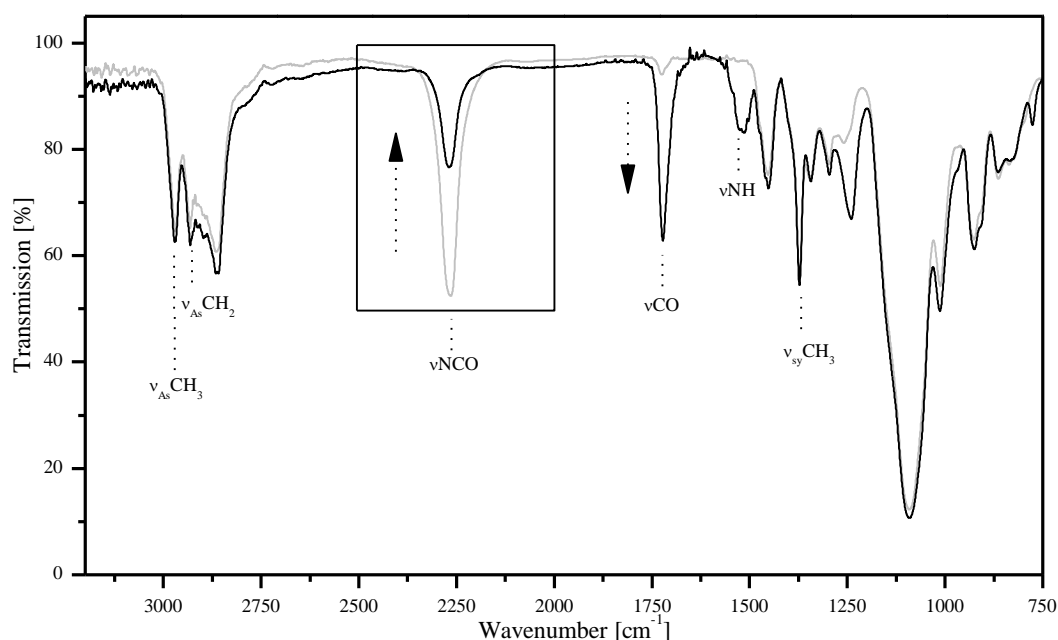


Figure 4-10. FTIR spectrum of the reaction mixture ITPU 10. Start (-) and at the end (-) of the polymerisation. Arrows indicate the decrease/increase of the NCO/CO stretching bands. The rectangle illustrates the integration range of the NCO-band.

Integration of the individual recorded spectra led to the time resolved dataset of A_{NCO} as shown in Figure 4-11 (grey squares). It can be seen that A_{NCO} is steadily decreasing throughout the reaction. With progress of the reaction, the gradient of the decrease diminishes until A_{NCO} reaches its final value. The data was compared to titrimetrically determined

NCO%-contents (black triangles in Figure 4-11), which represents the typically most trusted method for isocyanate quantification. The trend of both, titration and FTIR results, agree over the full reaction time. However, the FTIR dataset has much higher resolution (1 data point per minute) and allows additionally for detailed interpretation of the individual spectra.

The NCO conversion was calculated according to the procedure described in section 6.2. Here it shall be mentioned that 100 percent NCO conversion does imply that there are still isocyanate groups in the product due to the excess of NCO groups compared to the reaction partner OH. The NCO conversion derived from the FTIR spectroscopy (crosses in Figure 4-11) was in excellent agreement with the conversion calculated on basis of the NCO%-content titration (hollow squares in Figure 4-11).

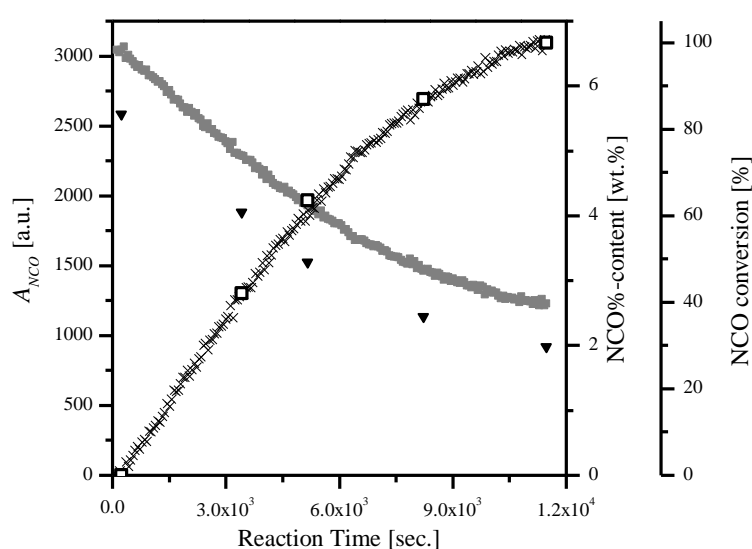


Figure 4-11. Comparison of FTIR measurement and NCO%-content titration in ITPU 10 formation. Integrals of the NCO stretching band (■), the titrated NCO%-contents (▼) and the NCO conversion (FTIR: ×; Titration: □) during the polymerisation of ITPU 10 over reaction time.

In the following, second order plots are used to illustrate the recorded reaction progresses. This approach is based on the fact that the reaction between hydroxyl and isocyanate groups is typically considered as a second order kinetic type.^[118–121] According to this, the rate equation is given by Eq.(4-3), where $[NCO]$ and $[OH]$ are the concentrations of isocyanate and hydroxyl groups and k is the rate constant.

$$\frac{d[NCO]}{dt} = -k \cdot [NCO] \cdot [OH] \quad \text{Eq.(4-3)}$$

Under the prerequisite that $[OH]$ equals $[NCO]$ Eq.(4-3) simplifies to Eq.(4-4). Integration of Eq.(4-4) leads then to Eq.(4-5), which is the basis of the typical linear second order plot where $1/[NCO]$ is depicted versus the reaction time t in seconds. The inverted initial NCO concentration $1/[NCO]_0$ presents the y-intercept.

$$\frac{d[NCO]}{dt} = -k \cdot [NCO]^2 \quad \text{Eq.(4-4)}$$

$$\frac{1}{[NCO]} = k \cdot t + \frac{1}{[NCO]_0} \quad \text{Eq.(4-5)}$$

It should be mentioned, that the application of second order plots in this context is based on the following simplifications that (1) the application of DBTDL as a catalyst does not lead to deviations from second order kinetics and (2) that the $[NCO]/[OH]$ fraction of 1.5 has no significant impact neither. The first assumption is regarded to be justified as it has been shown that the application of metal catalysts still results in second order kinetic type of reaction.^[122–124]

Against this background, it should be stressed that in this work the second order plots are only applied to illustrate the similarities and dissimilarities in the reaction kinetics throughout the series of experiments performed in this thesis. Due to the simplifications made, only qualitative interpretation of the reaction kinetics was performed waiving the calculation of absolute rate constants k .

However, the derived values of NCO conversion were used in order to calculate $[NCO]$ by consideration of the initial concentration of NCO-groups. The resulting datasets comprising $[NCO]$ vs. reaction time during the formation of the single soft segment ITPUs 10 and 11 have been illustrated in the second order plots shown in Figure 4-12.

The data obtained by the different methods of FTIR spectroscopy and NCO%-content titration showed again excellent agreement. The reaction of PPG2k showed slight deviation from the linearity ($R^2 = 0.987$) especially in the starting period of the polymerisation. Nevertheless, the small deviation from linearity demonstrated that the assumptions made above were applicable. The observed slope k_{obs} of the linear fit was $k_{obs,ITPU10} = 2.6011 \text{ L} \cdot \text{mol}^{-1} \cdot \text{s}^{-1}$. Likewise, the kinetics of PEO600 revealed a deviation from second order kinetics at the end of the reaction ($R^2 = 0.973$). In the case of PEO600, the digression is most likely explained on behalf of the existence of secondary hydroxy groups in

the polyol, which were evidenced by $^1\text{H-NMR}$ analysis (see section 4.2.5). Here, the slope of the linear fit was $k_{obs,ITPU11} = 1.4244 \text{ L}\cdot\text{mol}^{-1}\cdot\text{s}^{-1}$. It is well known that secondary hydroxyl groups do react more slowly with isocyanates than primary hydroxyl groups.^[37,40,123,125] The observed lower slope in the reaction of PEO600 with HDI results from the lower amount of catalyst that was used ($c_{DBTDL} = 10 \text{ ppm}$) in comparison to the polymerization of PPG2k ($c_{DBTDL} = 70 \text{ ppm}$).

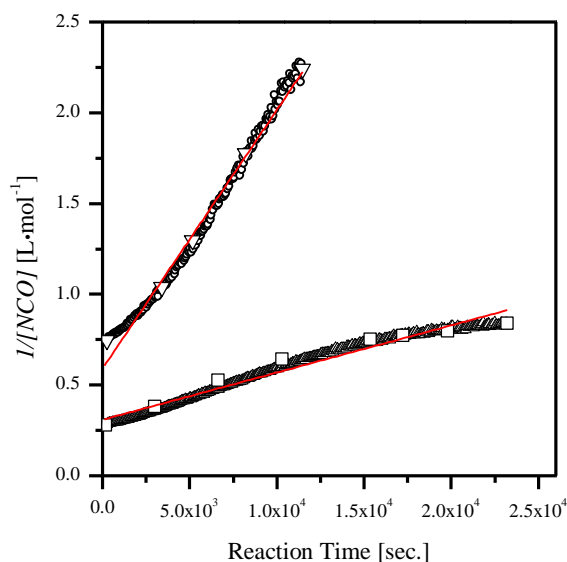


Figure 4-12. Second-order plot of the polymerisation kinetics. PPG2k (FTIR: \circ ; Titration: ∇) and PEO600 (FTIR: \triangle ; Titration: \square) with HDI at $T = 80 \text{ }^\circ\text{C}$ in the presence of 70 ppm and 10 ppm DBTDL respectively.

The difference in the kinetic between secondary and primary alcohols with isocyanates had to be investigated in more detail as in the case of the bi-soft segment ITPUs both types are concurrently reacted with HDI. To gain in depth information about the kinetics of the reaction in the mixture of secondary (PPG) and primary (PEO) hydroxyl groups with HDI, a model reaction (50:50 mol% PEO600:PPG2k) was performed in smaller scale (ITPU 12). To be comparable in reaction kinetics with regard to the other reactions, the dosed amount of DBTDL solution was properly adjusted. Samples for $^1\text{H-NMR}$ analysis and NCO%-content titration were taken in regular intervals.

Figure 4-13 shows the $^1\text{H-NMR}$ spectra of the corresponding final product of the reaction. The peak assignment is based on Heteronuclear Multiple Bond Correlation (HMBC)- and Heteronuclear Single Quantum Coherence (HSQC) NMR spectra (see Appendix IV-5). Fortunately, the $^1\text{H-NMR}$ spectrum allows for the discrimination between secondary

α -CH(CH₃)- ($d_{sec} = 4.8$ ppm) and primary α -CH₂- ($d_{prim} = 4.15$ ppm) groups bonded to the urethane group. Integration of these signals permits the evaluation of the conversion of the total hydroxy groups and in addition to that for the determination of the conversion of the individual primary and secondary alcohols.

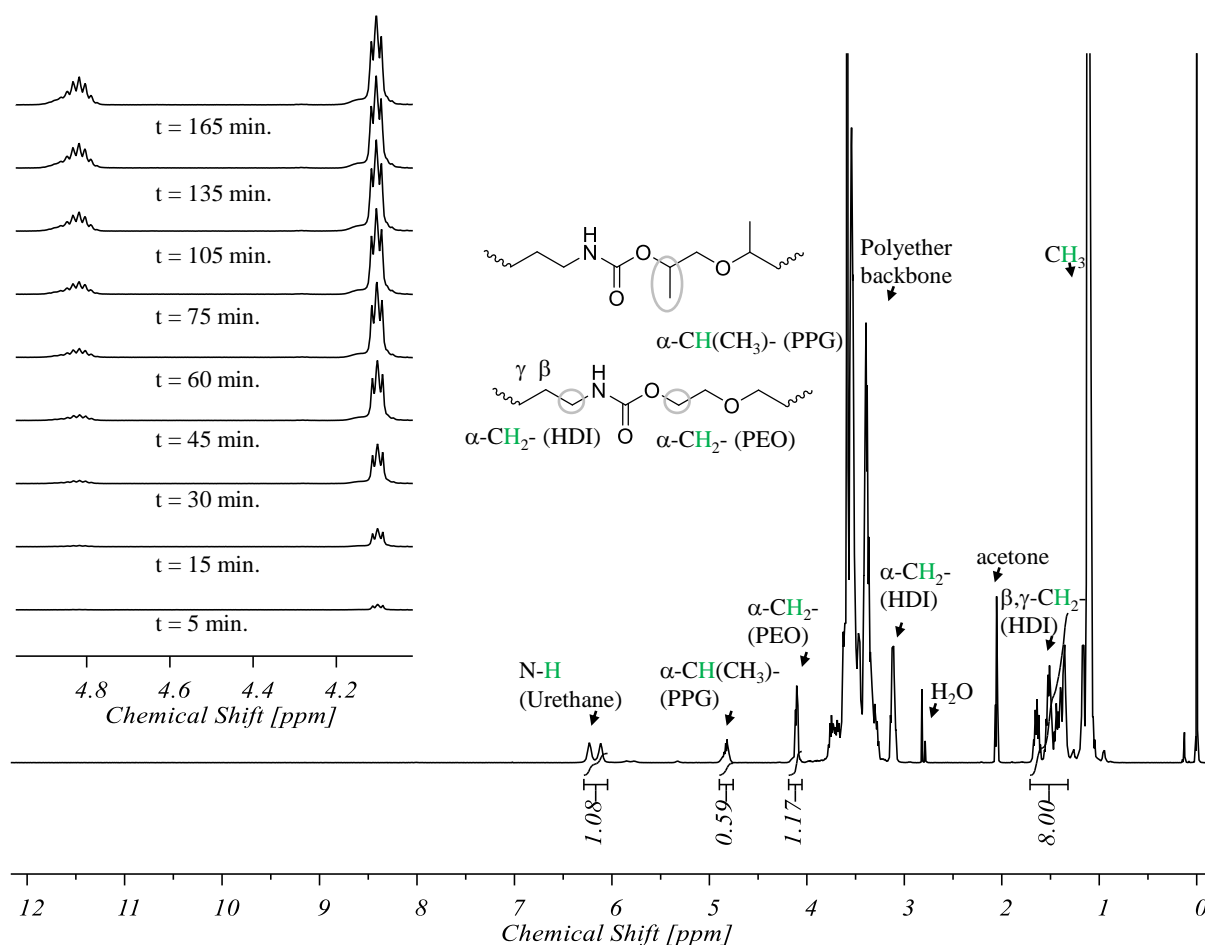


Figure 4-13. ¹H-NMR spectrum of the resulting ITPU comprising 50/50 mol.% PEO600 and PPG2k. The inset shows the evolution of the α -CH and α -CH₂ groups with proceeding reaction. The signal of the β,γ protons of HDI (8H) were used as an integral reference.

The total conversion of the hydroxy groups (rhombus in Figure 4-14) is in excellent agreement to the conversion obtained by the NCO%-content titration method (turned triangle in Figure 4-14). To be more specific, integration of the relevant signals provides evidence that in case of a stoichiometric polyol mixture 80 mol.% of the primary alcohols (triangle in Figure 4-14) was reacted within the first 60 minutes of the reaction. In comparison to this, only 30 mol.% of secondary hydroxyl groups was consumed in the same period of time (square in Figure 4-14). While complete primary alcohol consumption was accomplished after ~100 minutes, the addition of secondary hydroxyl groups was still progressing for further

60 minutes. Interestingly, the overall kinetic of the reaction showed second order behaviour with respect to the isocyanate concentration, as demonstrated by the grey squares in Figure 4-14.

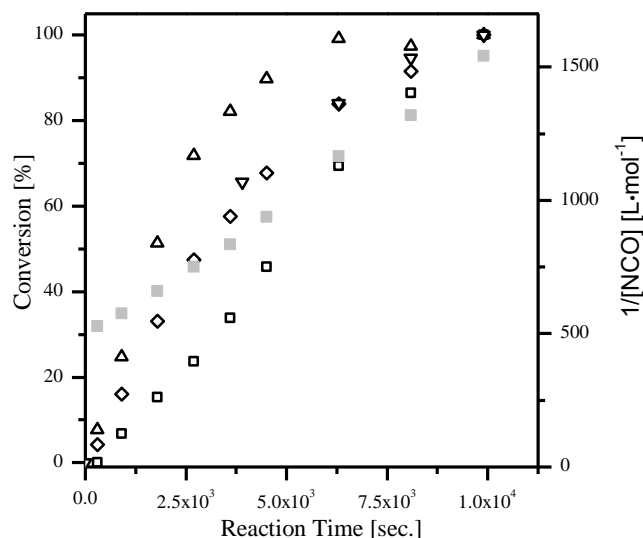


Figure 4-14. Conversion of the primary and secondary OH groups from PEO and PPG determined by $^1\text{H-NMR}$. (Δ : $\alpha\text{-CH}_2$, \square : $\alpha\text{-CH}$, \diamond : $\alpha\text{-CH}_2 + \alpha\text{-CH}$; ∇ : titrated NCO%-content) The isocyanate concentrations used in the second order plot (\blacksquare) are based on the accumulated conversion of secondary and primary hydroxy groups.

The kinetics of the reaction can be interpreted as a competing second order kinetic. Figure 4-15 shows the two occurring reactions between the primary and the secondary hydroxyl groups and the isocyanate. In general, the reaction rate constant of primary OH groups k_1 is greater than the rate constant of secondary OH groups k_2 .^[37,123,125]

Entelis and Nesterov showed earlier in separate model reactions of phenyl isocyanate with 1-butanol and 2-butanol in the presence of DBTDL that the rate constant of primary alcohols is 12-times higher than the secondary one.^[37] In this study a quantitative evaluation the rate constants is spared. As the rate constants depend on the catalyst concentration,^[40] which is varied throughout the different syntheses in this work, there is no comprehensive interpretation achievable in regard of the absolute values of the rate constants.

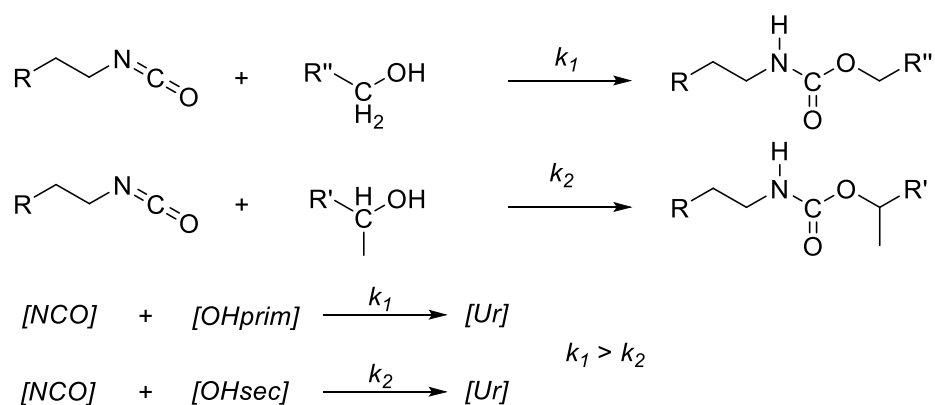


Figure 4-15. Illustration of the competing second order kinetics.

To the best of my knowledge, the kinetics of ternary mixtures containing primary and secondary hydroxyls and isocyanate groups has not been in focus of many investigations. This is surprising as similar conditions may be found in the formation of typical segmented thermoplastic polyurethanes. Here, most commonly a short diol like 1,4-butandiol in combination with a macromolecular diol like PPG is reacted with diisocyanates. In this case, the circumstance of different reactivities is often circumvented by the two-step prepolymer procedure.^[11]

Figure 4-16 shows second order plots of all performed polymerizations based on the titrimetrically determined NCO conversions. The ITPU containing only PPG2k showed the best agreement to the second order kinetics, which is not surprising as it contains only secondary hydroxyl groups.

Comparing the ITPU formations with initial PPG2k/PEO600 fractions $\Phi_{\text{PPG2k}} = 10\text{-}50$ vol.%, it was observed that the reaction times became shorter at higher initial PPG2k contents. Subsequently, the trend is inverted the way that by further increase of the initial PPG2k content the reaction times increased again. This is due to the difference in reactivity between primary and secondary hydroxyl groups and the applied attempt to balance the reaction times by addition of different amounts of catalyst. The catalyst concentration was increased concurrently with the initial PPG2k content, as the secondary hydroxyl groups are less reactive. The addition of the catalyst led to higher reaction rates of both, primary and secondary hydroxyl groups and thus the reaction time decreased rapidly in the cases of high amounts of primary hydroxyl groups (PEO600). As soon as the secondary hydroxyl groups become the critical quantity of the reactive moieties, their reaction rate starts to dominate the overall kinetics. Consequentially, with increasing PPG2k content the reaction begins again to take more time, even though the catalyst amount is increased.

However, it can be seen in the second order plots that the slope in the first stage of the reactions is increasing with respect to the initial PPG2k content and thus with increasing applied amount of catalyst.

Interestingly, a pronounced drop in the second order plots at the end of the polymerizations was found, which points to a decrease in the reaction rate. This was especially the case for the ITPUs containing high volume percentage of PEO600 ($\Phi_{PEO600} > 60$ vol.%). To highlight this phenomenon, the data from the bi-soft segment ITPUs reactions was fitted to two linear stages (Figure 4-16). In the view of the results from the $^1\text{H-NMR}$ study it is assumed that in the first linear stage predominantly primary alcohol react with isocyanates, while in the second stage only secondary alcohols are left for the addition to NCO groups. Interestingly, no second stages were observed in the kinetic data from the reaction mixtures based on polyether polyol mixtures with Φ_{PPG2k} ranging from 70 to 100 vol.%.

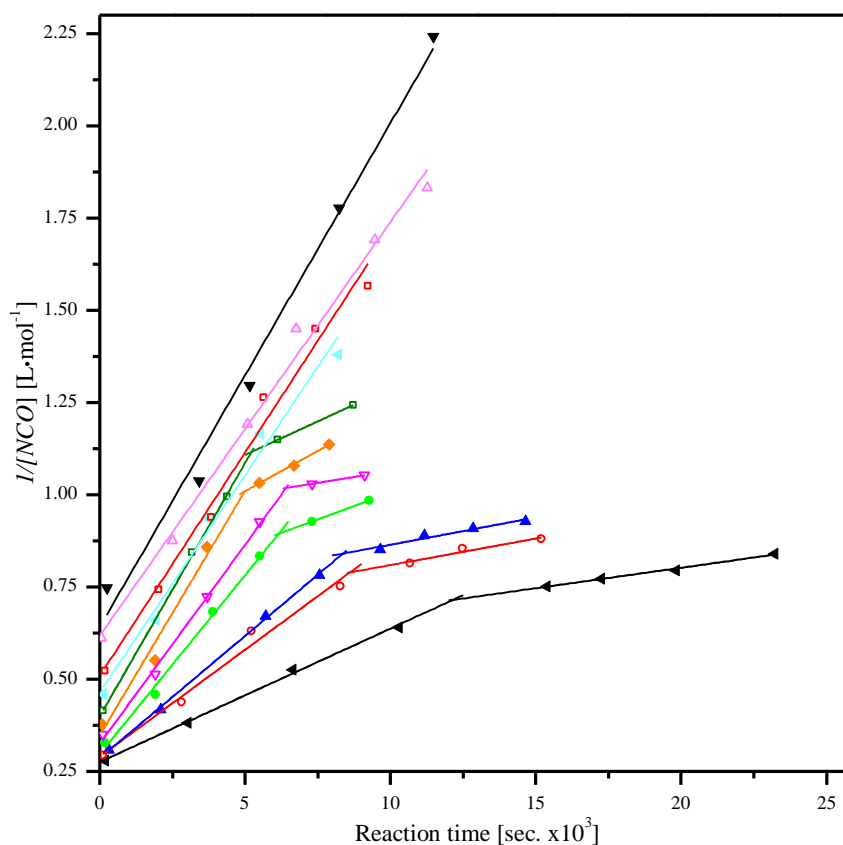


Figure 4-16. Second order plots of the kinetic data from the NCO%-content titration during all polymerisations. The linear fits illustrate the two staged linearity in case of low catalyst concentrations at high PEO600 contents. (◄: ITPU 11; ○: ITPU 1; ▲: ITPU 2; ●: ITPU 3; ▼: ITPU 4; ◆: ITPU 5; □: ITPU 6; ◄: ITPU 7, □: ITPU 8; △: ITPU 9; ▼: ITPU 10)

Very recently, Ismail et al. discussed a similar finding.^[126] They reacted palm oil based sustainable polyols that contained primary and secondary hydroxyls on the same molecule. Interestingly, they argued that the application of DBTDL as a catalyst in the reaction of the palm-based polyol with 4,4'-diphenylenemethane diisocyanate led to a decrease in the difference of the reactivity of primary and secondary OH-groups.

The kinetic data of the conducted polymerizations in this study indeed points to the same conclusion. The second order plots in Figure 4-16 showed that the reaction mixtures with the highest content of catalyst exhibited lowest deviation from a linear second order kinetic implying that the difference in reactivity of the types of hydroxy groups diminished.

The occurrence of two linear stages and thus two reaction rate constants is a fact that has also been found in the kinetics of 2,4-toluene diisocyanate (TDI) in the reaction with alcohols.^[120,121] TDI holds two isocyanate groups with unlike reactivity owing to the deactivation of the 2'-NCO group by a methyl substituent. In accordance to Ismail et al., Kothandaraman and Naser demonstrated in their study that the difference in the reaction rate constants is reduced by increasing catalyst contents.^[120]

Unfortunately, the data obtained by in-line FTIR monitoring in bi-soft segment IPTU formation could not give reliable information about the kinetics of the NCO conversion. The striking discrepancy between both types of measurement is presented and discussed in the following chapter. Here it is just mentioned that on the one hand the single soft segment ITPUs showed excellent agreement in the results derived on basis of FTIR and NCO%-content titration (see Figure 4-12). On the other hand, the results for the bi-soft segment ITPUs, especially the ones that showed phase separation revealed to some extent great deviations between the two resulting methods to determine the NCO conversion. For this reason, the FTIR based NCO conversion is not regarded in view of the kinetics of bi-soft segment polyurethanes.

4.2.2 Onset of phase separation

Reaction monitoring via FTIR analysis and NCO%-content titration was carried out to evaluate the polymerisation progress. In addition to this, in-line UV-Vis based turbidity analysis was employed to receive time resolved information about the onset of phase separation. Combination of these datasets permits to draw conclusions about a possible dependency of the phase separation on the reaction progress. The aim of this investigation was to generate experimental results that can be evaluated in coherence to the results from the miscibility studies in section 4.1.

In the beginning of this chapter it should be stressed that bi-soft segment ITPU 9 shows no phase separation. No onset of turbidity was found in the respective reaction monitoring (see Figure 4-18 c). This is in excellent agreement with the computational and experimental phase diagram of PPG2k/PEO600 mixtures already shown in section 4.1. The phase diagram demonstrated a miscibility window at a polyether polyol composition of 90 vol.% PPG2k and 10 vol.% PEO600 (Figure 4-4). The clear appearance of ITPU 9 revealed that the miscibility is still given regardless of the increase in chain length due to the polymerisation.

In contrast to this, all remaining ITPUs with PEO600 contents Φ_{PEO600} ranging from 20 - 90 vol.% resulted in turbid liquids (see Figure 4-17 and Figure 4-18). Again, this is in accordance with the determined phase diagram of the binary polyol mixture.

As seen in the miscibility study beforehand, HDI acts as a solvent for both polyols in the initial ternary mixture. Against this background, it is presumed that primarily the depletion of the content of monomeric HDI during the reaction led to the phase separation rather than the formation of higher molecular weight products. In this context, the remaining extent of unreacted molecular HDI is defined as residual HDI $\phi_{HDI, res}$. The hypothesis is that there is a critical residual HDI content at which the phase separation is thermodynamically induced. This would imply that the polyol composition is affecting the phase separation as well as the initial and residual HDI content. In this regard, the onset of turbidity of the different reactions was investigated in detail. It is defined as the abrupt increase in turbidity during the reaction.

Figure 4-20 shows the results from the UV-Vis monitoring (open triangles) in combination with the previously illustrated NCO conversion. Starting from clear initial mixtures (turbidity = 0 cm⁻¹), the proceeding reaction led to inhomogeneous emulsions in the cases of ITPU 1 to ITPU 8. A distinct onset of turbidity was apparent in the mentioned instances.

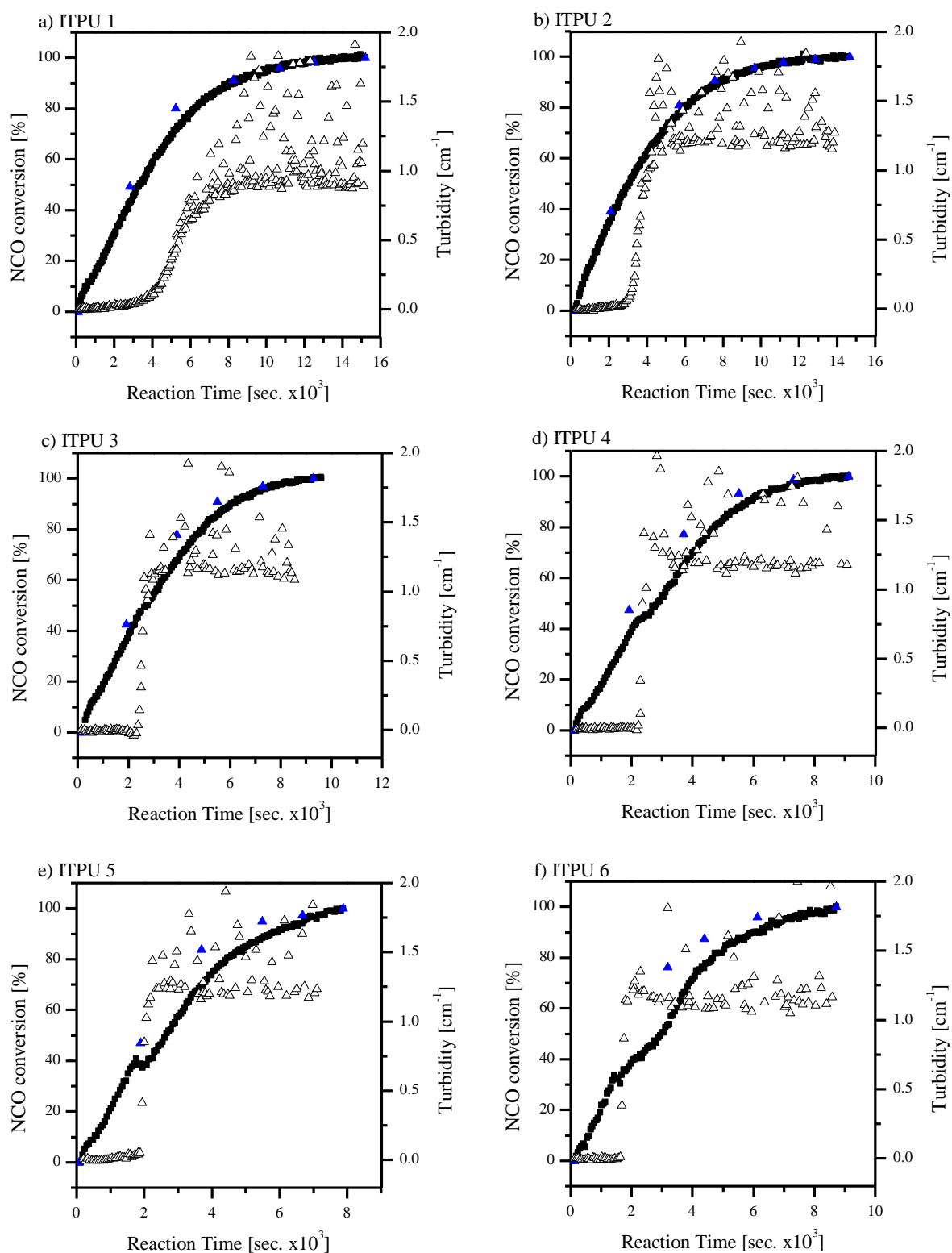


Figure 4-17. Collection of the results from the reaction monitoring of the bi-soft segment polymerisations with Φ_{PEO600} ranging from 10 to 90 vol.%. FTIR NCO conversion (\blacksquare), titrimetric NCO conversion (\blacktriangledown) and turbidity (\triangle). (Continued on the next page)

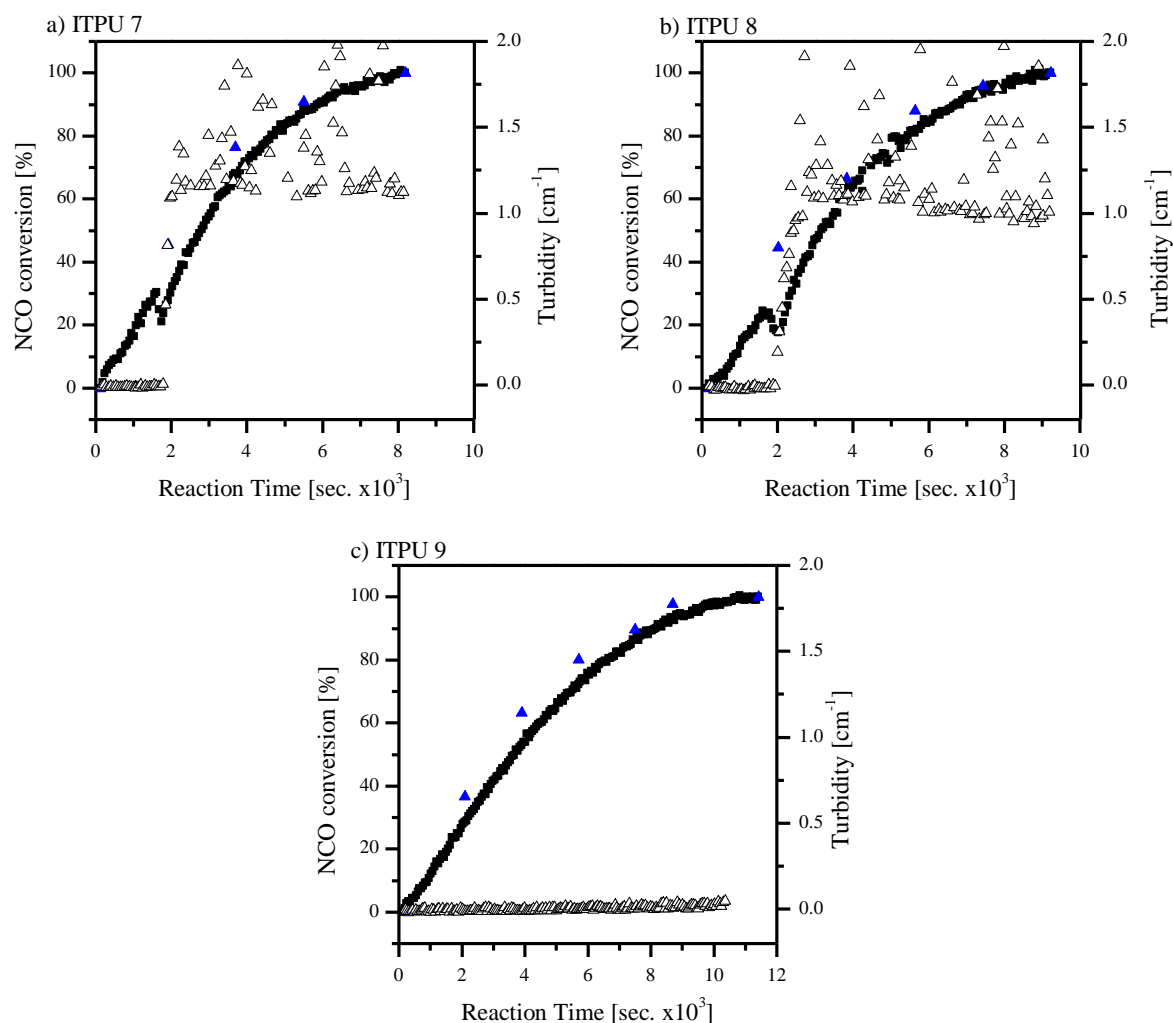


Figure 4-18. Collection of the results from the reaction monitoring of the bi-soft segment polymerisations with Φ_{PEO600} ranging from 10 to 90 vol.%. FTIR NCO conversion (■), titrimetric NCO conversion (▼) and turbidity (△).

Interestingly, the onset of turbidity showed a significant trend depending on the polyol composition. Increasing the content of PEO600 in the polyol mixture led to a shift of the onset of phase separation towards higher NCO conversion.

At this point, afore mentioned inconsistencies between the datasets of the NCO conversions should be addressed. The comprehensive results from UV-vis, FTIR and NCO%-content titration clearly demonstrate that apparently the FTIR analysis has been affected by the occurring phase separation. This becomes obvious as the deviations of the NCO conversions based on FTIR from the NCO%-content titration results become apparent at the onsets of turbidity (see Figure 4-17 and Figure 4-18).

Interestingly, the effect has not been observed in the cases of ITPU 1 and 2 despite the fact that they present a clear onset of phase separation in the turbidity analysis. The deviation

turned out to be more pronounced when nearly equal proportions of PPG2k and PEO600 soft segments were used in the ITPU. Generally spoken, the effect influenced the FTIR results in the way that lower NCO conversions were detected compared to the results based on the titrational method. Strikingly, besides the overall divergence between both results in ITPU 3 or 4 (see Figure 4-17 c & d), distinct sharp drops were found in the derived NCO conversions of the ITPUs with Φ_{PPG2k} varying from 40 to 80 vol.% (see Figure 4-17 d - f and Figure 4-18 a & b).

The observed drop of NCO conversion implicates that the detected NCO stretching signal in the FTIR spectrum experienced a sudden increase. The event that led to the observed increase is not yet clearly identified but at this point it is discussed in the following.

As a start, it is excluded that already formed urethane bonds had been cleaved back to isocyanate groups because of its unlikeliness at temperatures below 200 °C.^[127] Moreover, this explanation would not correlate to the concurrently arising turbidity at all.

The more plausible explanation comes from the fact that the liquid mixture becomes inhomogeneous at the onset of turbidity. In general, liquid systems phase separate by forming emulsions which in the most simple form consist of a continuous phase and dispersed droplets.^[128] This inhomogeneity can affect the ATR-FTIR analysis by twofold aspects:

1. by non-uniform distribution of the absorbing compounds due to inhomogeneity
2. by a scattering effect due to droplets

The latter might be the case since in ATR-FTIR analysis only a very small sample layer that wetting the crystal is analysed.^[129] ATR-FTIR analysis is based on total internal reflection of the infrared light at the interface between the crystal and the sample. An evanescent wave is formed and penetrates the sample at the centre of reflection. The thickness d_{sl} of this sample layer is dependent on the refractive indices of the sample n_{sample} and of the crystal n_{ZnSe} , on the wavelength λ and of the angle of incidence θ of the electromagnetic wave as given in Eq.(4-6).^[129] The wavelength of the NCO band is $\lambda_{NCO} = 4.5 \mu\text{m}$, $\theta = 45^\circ$ and $n_{ZnSe}(4.5\mu\text{m}) = 2.43$ ^[130].

$$d_{sl} = \frac{\lambda}{2\pi \cdot (n_{ZnSe}^2 \cdot \sin^2 \theta - n_{sample}^2)^{1/2}} \quad \text{Eq.(4-6)}$$

The refractive index of the sample mixture n_{sample} is estimated to lie in the range 1.4 - 1.5 based on the refractive indices of the main components PPG^[131] and PEO^[131]. Based on this assumption, the sample layer thickness d_{sl} adds up to 0.47 - 0.50 μm .

Concerning the in-line analysis, this might directly influence the obtained signal in the way that not an average signal from the inhomogeneous emulsion is analysed but just a very distinct sample layer near the crystal. Although the fact that in the applied method 64 scans were averaged in each individual IR spectrum, the resulting spectrum might not reflect the average FTIR transmission of all constituents in the inhomogeneous sample .

Relating this, Kiefer et al. showed in their ATR-FTIR study on water-in-oil emulsions that the distance of the dispersed droplets to the ATR crystal is of significant importance.^[132,133] They postulated that the surface of the ATR crystal is mainly in contact with the continuous phase and only to small extent with the interfacial layer of the droplets. Taking this into account it is presumed that the FTIR absorption is predominantly controlled by the continuous phase.

On the other hand, elastic scattering can disturb FTIR analysis as its applicability is based on Lambert-Beer's assumption.^[134] It states that the incident infrared light intensity I_0 is only lowered by the absorption I_{Abs} via molecular vibrations (see Eq.(4-7)).

$$I(\lambda) = I_0(\lambda) - I_{Abs}(\lambda) \quad \text{Eq.(4-7)}$$

In the case that scattering takes place a new factor I_{Sca} needs to be introduced into Eq.(4-7) resulting in Eq.(4-8). Only little fraction of scattered light reaches the detector on axis. The sum of absorbed and scattered light is known as extinction.^[134]

$$I(\lambda) = I_0(\lambda) - I_{Abs}(\lambda) - I_{Sca}(\lambda) \quad \text{Eq.(4-8)}$$

Elastic scattering (without energy loss) of electromagnetic radiation results from the three-dimensional inhomogeneity of the refractive index in a medium. Three different kinds of elastic scattering are distinguished. Their definition is depending on the particle size d of the scatterer and the wavelength of the light λ , i. e. Rayleigh ($d_p \ll \lambda$), Mie ($d_p \approx \lambda$) and geometric scattering ($d_p \gg \lambda$).^[134] Taking into account that the range of the wavelength in the infrared analysis is 3 - 13 μm and that microscopic images (see section 4.2.5) demonstrated that the droplet size in the presented emulsion is in the same scale, only Mie-type scattering is considered in the following.

The influence of Mie-type scattering in transmission and reflection mode ATR-FTIR analysis has been investigated mainly in biophysical aspects.^[135–138] The effect of scattering due to anomalous dispersion of the refractive index is nowadays used in imaging infrared microscopy of human cells.^[137,138] Miljković et al.^[136] and Boulet-Audet et al.^[135] discussed the influence of dispersion effects on the spectral appearance of the amide region of proteins in detail. They demonstrated that scattering can result in the occurrence of distorted bands^[136] and shifts^[135] in maxima and intensity of the band. In addition to this, Mohlenhoff et al. showed that scattering can lead to a broad wave-like background that superimposes absorption bands.^[137]

Figure 4-19 displays the four FTIR spectra of ITPU 7 representing the NCO conversion instant right before the drop ($t = 1617$ sec.) and the three following measurements. By a look at the full spectrum, one can tell that there is neither obvious distortion of any bands nor an abnormality of the background. Five different vibrational modes, i. e. $\nu_{As}CH_2$, $\nu_{As}CH_3$, $\nu_{Sy}CH_3$, $\nu_{As}COC$ and νNCO , are highlighted to investigate the absorption behaviour of particular functional groups and the corresponding substructures.

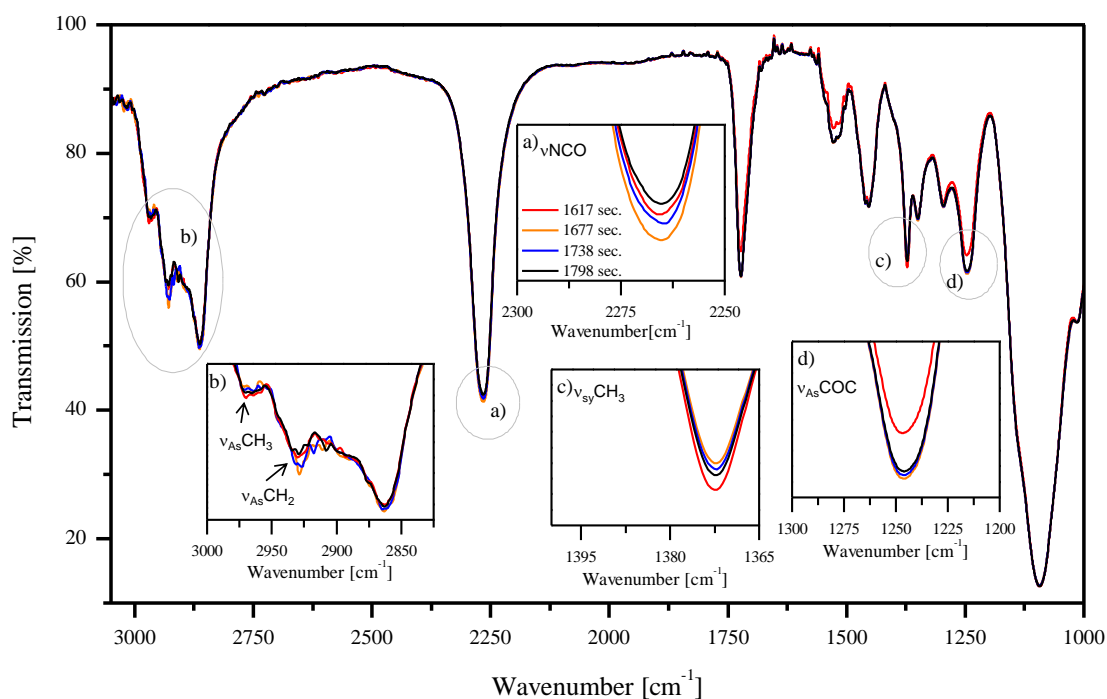


Figure 4-19. FTIR spectra at the time right before and in the drop of the NCO conversion of ITPU 7. The insets demonstrate the evolution of the intensity of the NCO-(stretching), CH_3 -(asymmetric stretching), CH_2 -(asymmetric stretching), COC -(asymmetric stretching) and the CH_3 -(symmetric bending) vibrations.

On the one hand, the maxima of vibrations $\nu_{\text{As}}\text{CH}_2$ and ν_{NCO} are behaving in a parallel manner. Indeed, at first there is a mutual instant decrease in transmission of these groups followed by an increase. Both groups are mainly assigned to HDI molecules or already formed ITPU oligomers. On the other hand, there is an increase in the transmission of both CH_3 modes ($\nu_{\text{As}}\text{CH}_3$, $\nu_{\text{Sy}}\text{CH}_3$). It turned out to behave exactly the opposite way than the before mentioned NCO and CH_2 vibrations. The transmission maxima of the CH_3 vibrations suffer a rather steep increase at first and approximate their initial values in the following. In this respect, it should be noted that the region of $\nu_{\text{As}}\text{CH}_2$ and $\nu_{\text{As}}\text{CH}_3$ is influenced by quite intense background noise. This observation rises from the low transmission of the ZnSe probe above $2\,800\text{ cm}^{-1}$ (see background spectrum in Appendix IV-4). However, the symmetric bending vibration $\nu_{\text{Sy}}\text{CH}_3$ is clearly demonstrating the mentioned behaviour (see Figure 4-19 c). In addition to this, it is found that the asymmetric ether vibration $\nu_{\text{As}}\text{COC}$ exhibited a sharp increase between the particular first two spectra. This vibration is assigned to the polyether polyols and according to the reference spectra (see Appendix IV-3) it is most intense in PEO600.

Regarding these observations, it is presumed that the FTIR analysis is sensitive to the phase separation in the way that it predominantly detects the continuous phase rather than the dispersed droplets. This is in accordance to the observation of Kiefer et al. ^[132,133] Considering the fact that the transmission in the vibrations belonging to HDI and PEO600 is diminished during phase separation, the conclusion can be drawn that they are predominantly present in the continuous phase. In contrast to this, the dispersed phase is enriched with PPG2k as the transmission of the respective vibrations increases. This information can be of significant importance regarding the understanding of the overall phase behaviour during the reaction, which is further discussed in section 4.2.5.

However, notwithstanding the issues shown concerning the observation of the reaction progress by FTIR spectroscopy, the recorded turbidity dataset should be correlated to the NCO conversion values. This procedure makes it possible to conclude the distinct NCO conversion at the onset of turbidity. In this context, the discrepancies between FTIR monitoring and NCO%-content titration are circumvented in the way that both datasets are processed individually. The derived NCO conversion datasets are fitted separately to a polynomial function f_P (Eq.(4-9)). The individual fitted parameters of the functions can be found in the Appendix IV-7.

$$f_P = a + bx + cx^2 + dx^3$$

Eq.(4-9)

The resulting polynomial functions were used to merge the turbidity vs. time data with the NCO conversion vs. time datasets. This procedure allows for the expression of the individual onsets of phase separation in the unit of NCO conversion. Two individual results for the onset of turbidity relating to the FTIR spectroscopy or the NCO%-content titration respectively were derived.

It has already been briefly addressed that the onset of phase separation seemed to exhibit a trend depending on the initial polyol composition of the bi-soft segment ITPU. This effect is highlighted in the stacked plot of the turbidity versus the NCO conversion (see Figure 4-20 a + b). With respect to the NCO%-content titration, the latest onset of phase separation was observed in ITPU 1 with Φ_{PPG2k} of about 10 vol.%. Here the reaction progresses in homogeneous conditions up to a NCO conversion of $\sim 70\%$. In contrast to this, IPTU 8 showed phase separation already at a NCO conversion of $\sim 40\%$. The remaining onsets of turbidity followed a steady nearly linear trend within the presented limits (see Figure 4-20 c). Solely the two reactions towards ITPU 2 and 3 showed a minor deviation from the linearity.

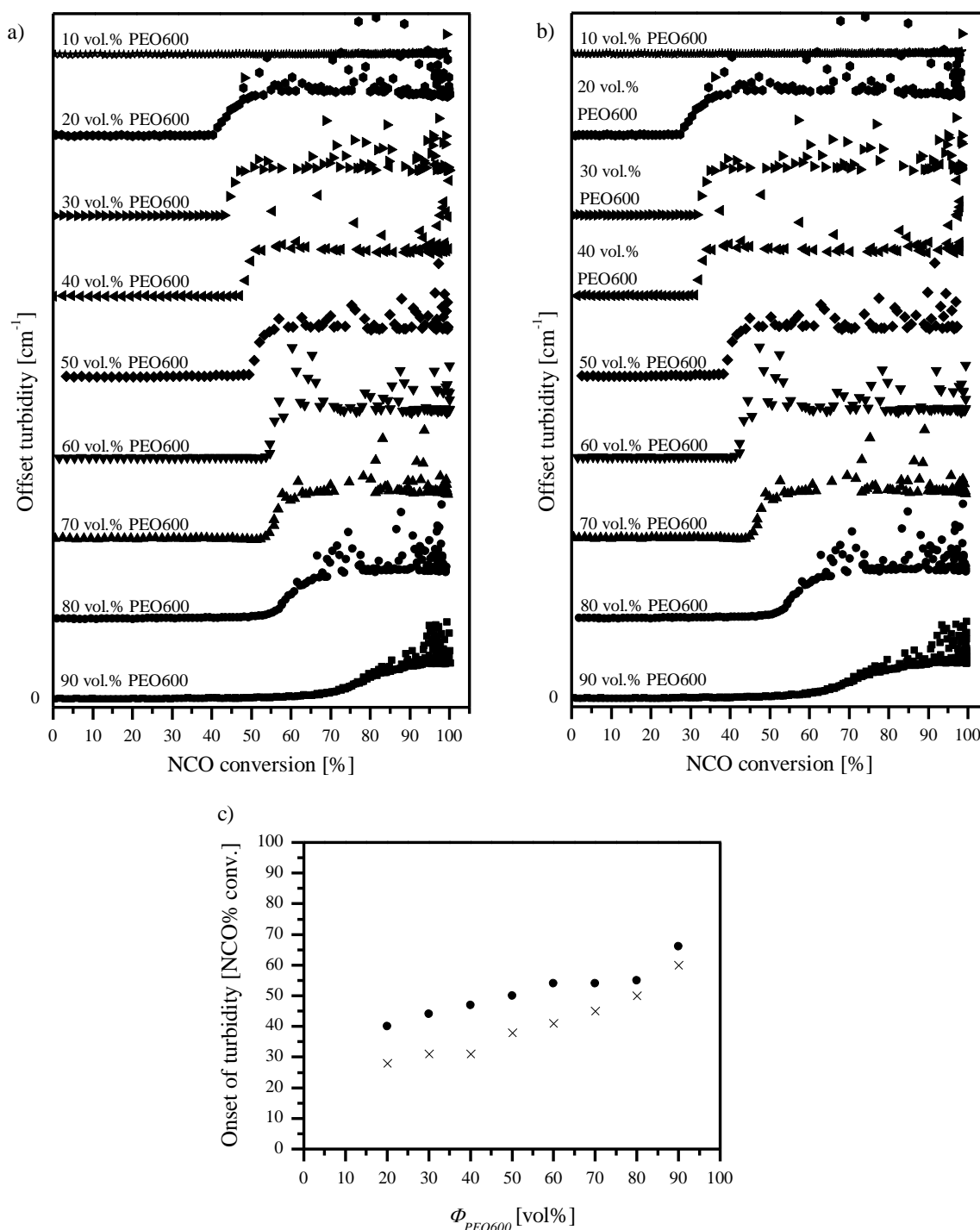


Figure 4-20. Turbidity versus NCO conversion based on the NCO%-content titration (a) and FTIR analysis (b). Inset c) shows the derived onsets of turbidity in dependence on the polyol mixture composition (x: FTIR; •: NCO%-content).

In Figure 4-20 b) it is shown that the consideration of the FTIR based conversion data led to a shift of the onsets of turbidity towards lower values. The deviation becomes larger with increasing PPG2k content in the polyol mixture. Bi-soft segment IPTU 6 comprising a composition of with Φ_{PEO600} of about 40 vol.% presented the greatest deviation with 16 %.

Nevertheless, the described trend towards delayed onsets of turbidity at increased initial contents of PEO600 is as well recognisable in the FTIR based results. But it should be mentioned that in view of absolute values the NCO%-content based correlation is considered more trustworthy.

The significant trend of the onset of phase separation is in accordance to the postulated hypothesis that the residual HDI content is critical for the phase separation. As illustrated by the crosses in Figure 4-21, the initial content of HDI in the different reaction mixtures was lower at increased PPG2k content. This is a consequence of the lower amount of reactive OH moieties per volume in PPG2k compared to PEO600 (see *OH#s* in Table 6-2). The dashed arrows in Figure 4-21 indicate how the residual HDI content continuously decreases as the reaction progresses until it reaches its final value prescribed by the Schulz-Flory^[56] distribution.

Here it should be stressed, that the reaction changes the initial ternary situation to a higher order. As soon as the first oligomers are formed, the mixture is comprising two additional components namely [-PEO600-HDI]_n and [-PPG2k-HDI]_n oligomers. The situation becomes even more complex as soon as a third type of compound, i.e. mixed soft segment oligomers is formed. In this case this would lead to a hexanary reaction mixture due the possible formation of the mentioned three types of adducts.

In the context of FH theory, the evolution of the molar weight distribution of the oligomers would needed to be considered in the calculation of the combinatorial part of the free energy of mixing. It is not subject of this work to modify the FH theory in order to account for these concurrent effects. Indeed, here the situation is simplified by the means that the phase separation is discussed on basis of the phase diagram of the initial reactant mixture. However, to illustrate the ongoing reaction, the ternary phase diagram is modified in the way that the [-PEO600-HDI]_n and [-PPG2k-HDI]_n segments are accounted for at the axis of the respective polyether polyols. This makes it possible to display the path of the reaction in the phase diagram.

The modified ternary phase diagram is displayed in Figure 4-21 comprising the respective axes of HDI, PEO600 ([-PEO600-HDI]_n) and PPG2k ([-PPG2k-HDI]_n). The reaction path is illustrated by three different examples, i.e. ITPU 1, ITPU 5 and ITPU 9. At this point, the difference in the kinetics of the reaction of PEO600 and PPG2k with HDI is not considered. This is addressed in the comprehensive description in section 4.2.5.

The indicated reaction paths reflect the formation of [-PEO600-HDI]_n and [-PPG2k-HDI]_n segments and the simultaneous reduction of the HDI volume fraction. The sole formation of

$[-\text{PEO600-HDI}]_n$ trails parallel to the HDI/ $[-\text{PEO600-HDI}]_n$ axis. Analogously the reaction towards $[-\text{PPG2k-HDI}]_n$ is represented by the path parallel to the HDI/ $[-\text{PPG2k-HDI}]_n$ axis. In the distinct case of ITPU 1 ($\Phi_{\text{PEO600}} = 90$ vol.%) this implicates that the overall reaction path points at the composition of 10:90 vol.% PPG2k:PEO600 of the horizontal axis. The same respective behaviour applies to the other reactions.

The proposed reason for the phase separation is a hypothetical binodal as it was found in the initial ternary phase diagram. The shape of the hypothetical binodal line is derived by the experimental cloud point curve. This explanation would imply that each reaction (excluding ITPU 9 because of the miscibility window) exhibits a critical residual HDI concentration at which phase separation is induced. In this instant, the binodal line is crossed and two phases comprising the equilibrium compositions are emerging.

The striking linear dependence between the onset of turbidity and the initial PEO600 contents is presumed to be caused by the concurrent circumstance of increased levels of HDI content. Higher volume fractions of HDI lead to a longer path for the reaction to progress in the homogeneous region of the phase diagram. In the view of this, the length of the distance between the initial and the critical HDI concentration is responsible for the differences in the onsets of phase separation.

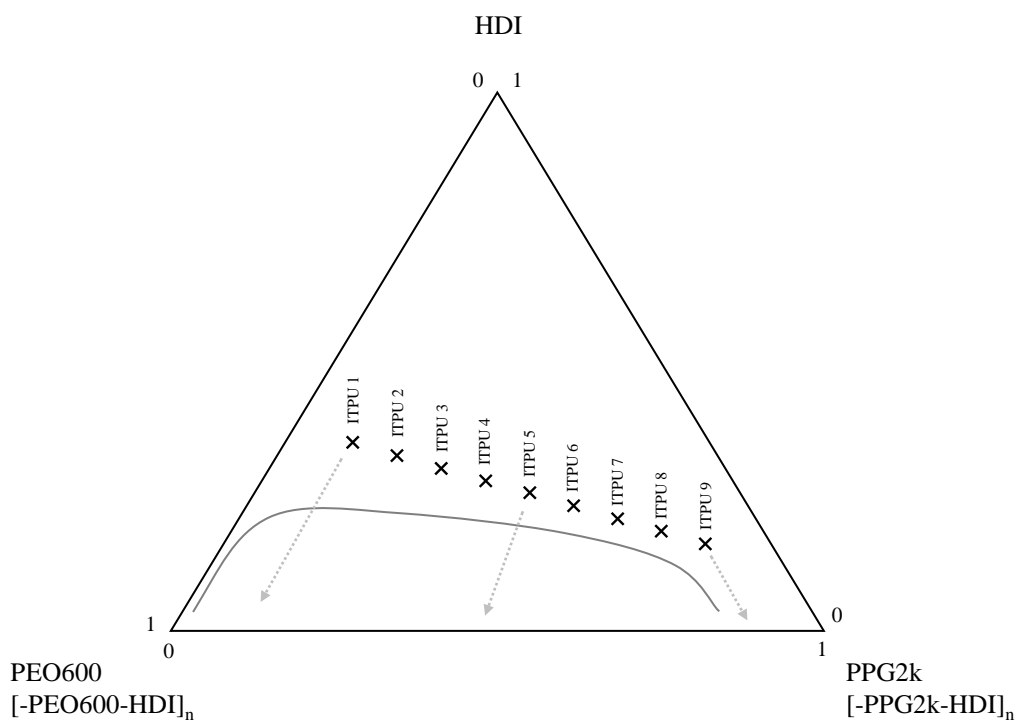


Figure 4-21. Schematically simplified illustration of the hypothetical binodal (grey curve) in the ternary phase diagram. The crosses represent the initial compositions in the reaction mixtures of ITPU 1 to ITPU 9. Grey dashed arrows indicate the reaction progress.

4.2.3 *Thermal properties and glass transitions of the ITPUs*

Typical phase separation in polyurethane technology comes from the fact that the hard segments segregate into hard domains due to their strong interaction via hydrogen-bonding.^[9,17,139–141,141–143] DSC allows for the confirmation of separated phases in the morphology of a polymer by the detection of multiple (glass) transition signals.^[144–146] Nevertheless, it is well known that hard segments can be miscible to a large extent with compatible, polar soft segments like polyether polyols.^[141] In these cases, there is no additional transition signal of the hard domains.^[47] Here, DSC was performed to answer the question if the phase separation and thus the turbidity was by virtue of immiscibility of the soft segments or by hard/soft segment segregation.

The first topic that was addressed by DSC in this thesis was the analysis of bi-soft segment ITPUs containing PEO600 in combination with the M_n series of PPGs. It was shown in section 4.1.1 that low molecular weight PPGs ($M_n < 2\,000\text{ g}\cdot\text{mol}^{-1}$) were miscible with PEO600 in binary mixtures. Respective IPTUs were prepared that contain a 50:50 vol.% mixture of each PPG (400, 1 000, 2 000 and 4 000 $\text{g}\cdot\text{mol}^{-1}$) with PEO600 and HDI. The thermograms are shown in Figure 4-22.

Single glass transitions were observed for both bi-soft segment ITPUs based on PPGs with number average molecular weight below $2\,000\text{ gmol}^{-1}$. The ITPU comprising PPG400 exhibited a glass transition at $T_g = -49\text{ }^\circ\text{C}$, while PPG1k resulted in $T_g = -54\text{ }^\circ\text{C}$. This glass transition temperature region is typical for polyether soft segments.^[47]

Interestingly, the T_g of the polymer with higher molecular weight is lower. Flory and Fox showed the opposite effect of an increase in T_g at higher molar weights on polystyrene polymers in 1950.^[147] However, in this regard it should be stressed that the hard segment content in the PPG400/PEO600 based ITPU is higher compared to PPG1k/PEO600. This is a consequence of the shorter average chain length of the polyether polyols. The concentration of urethane groups c_{Urethane} in PPG400/PEO600 amounts to $2.66\text{ mol}\cdot\text{kg}^{-1}$. This compares with $2.00\text{ mol}\cdot\text{kg}^{-1}$ in the ITPU based on the combination of PPG1k and PEO600. In both cases, the presence of a single glass transition demonstrated that the hard segments are incorporated in the soft segment matrix. Against this background, the higher T_g in the ITPU based on PPG400/PEO600 results from the higher hard segment content present in the vicinity of the soft segments.

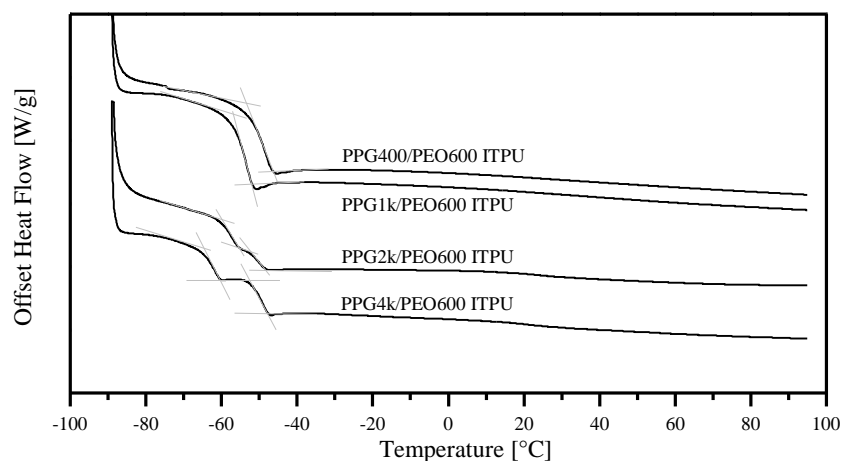


Figure 4-22. Effect of increasing PPG molecular weight on the glass transitions of mixed soft segment PPG/PEO600 ITPUs. The scan was performed at a heating rate of 20 Kmin^{-1} .

In addition to this, the single T_g confirmed that the two soft segments are contained in one phase. In fact, these products were visually clear liquids. The observed miscibility of the two soft segments is in accordance to the previously discussed predicted and observed miscibility of the two binary mixtures of PPG400/PEO600 and PPG1k/PEO600 (see section 4.1.1). This demonstrates the predictive capability of the FH theory for bi-soft segment ITPUs. The result is remarkable since the increase in molar weight due to the formation of covalent urethane bonds did not induce phase separation. According to FH theory, the formation of higher molar weights leads to a reduction of the configurational entropy of mixing which can be responsible for phase separation. On the other hand, it was already shown by Duffy et al. that urethane groups can even enlarge the region of miscibility due to their strong specific interactions.^[54] It is presumed that both effects influence the observed miscibility behaviour in ITPUs.

In contrast to PPG400 and PPG1k, two glass transitions were found for PPG2k and PPG4k in combination with PEO600 (see Figure 4-22). Again, no additional signal was found in higher temperature range. The two glass transitions observed for the combination of PPG2k/PEO600 were $T_{g,1} = -57 \text{ °C}$ and $T_{g,2} = -50 \text{ °C}$. Concluding from this, the two soft segments are organized in separate phases. The same observation holds for the IPTU consisting of PPG4k and PEO600 (see Figure 4-22). The only difference lies in the shift of the first glass transition temperature $T_{g,1}$ which is assigned to the [-PPG4k-HDI] units to -63 °C . The shift again relies on the lower hard segment content of $1.56 \text{ mol}\cdot\text{kg}^{-1}$ in the PPG4k/PEO600 based ITPU compared with $1.72 \text{ mol}\cdot\text{kg}^{-1}$ in the ITPU comprising PPG2k and PEO600 due to the longer PPG chain. Apparently, the step size of the individual glass

transitions in PPG2k/PEO600 and PPG4k/PEO600 ITPU did resemble the volume fraction (50 vol.%) of each soft segment.

To sum it up, it was shown that the average molar weight of PPG soft segment affects the compatibility with PEO600 soft segments in bi-soft segment IPTUs. As previously shown for the binary mixtures of PPGs with PEO600, increasing the chain length of PPG led similarly to incompatibility and phase separation in the respective IPTUs. In fact, there is excellent agreement between the experimental and theoretical outcomes. Immiscibility of PPGs with PEO600 was predicted and confirmed at molar weights above $2\,000\text{ g}\cdot\text{mol}^{-1}$, while apparently incompatibility was induced at the same limit. Indeed, the DSC results confirmed that the turbidity and thus the phase separation in the IPTUs results from the incompatibility of the soft segment units.

In addition to this, DSC was applied to study the influence of the composition of PPG2k/PEO600 mixtures on the thermal properties of the resulting bi-soft segment IPTUs. Of particular interest was to address the question if the only fully transparent product (IPTU 9) demonstrates a single glass transition. Besides the visual clear appearance, this would be a second independent confirmation that the miscibility window seen in the PPG2k/PEO600 phase diagram (see section 4.1.1) is reflecting the compatibility of the soft segments quantitatively.

The DSC thermograms of the IPTU series containing different amounts of PEO600 in combination with PPG2k are shown in Figure 4-23. The thermal behaviour of the bi-soft segment IPTUs is compared to the respective single soft segment products (see Figure 4-23 a).

The single soft segment ITPU based on PPG2k and PEO600 exhibited both single glass transitions at $T_{g,IPTU\,10} = -56.0^\circ\text{C}$ and $T_{g,IPTU\,11} = -45^\circ\text{C}$, respectively. Rather intensive endothermic overshoots were observed immediately after the glass transitions. This is typical for amorphous materials that have been annealed in the first run prior to the analysed run.^[148–150]

Two well defined glass transitions were detected for the bi-soft segment IPTUs with Φ_{PPG2k} ranging between 20 and 80 vol.%. The two glass transitions at $T_{g,1} = -54.0^\circ\text{C}$ and $T_{g,2} = -45^\circ\text{C}$ were nearly identical to the individual transitions of the single soft segment IPTUs and did not alter with soft segment composition. On closer inspection a point of inflection near -54°C in the ITPU comprising Φ_{PEO600} of about 90 vol.% indicates the second T_g assigned to the PPG2k segments. In the entirety of the results, it is obvious that the initial soft segment fraction affected the individual step sizes of the glass transitions.

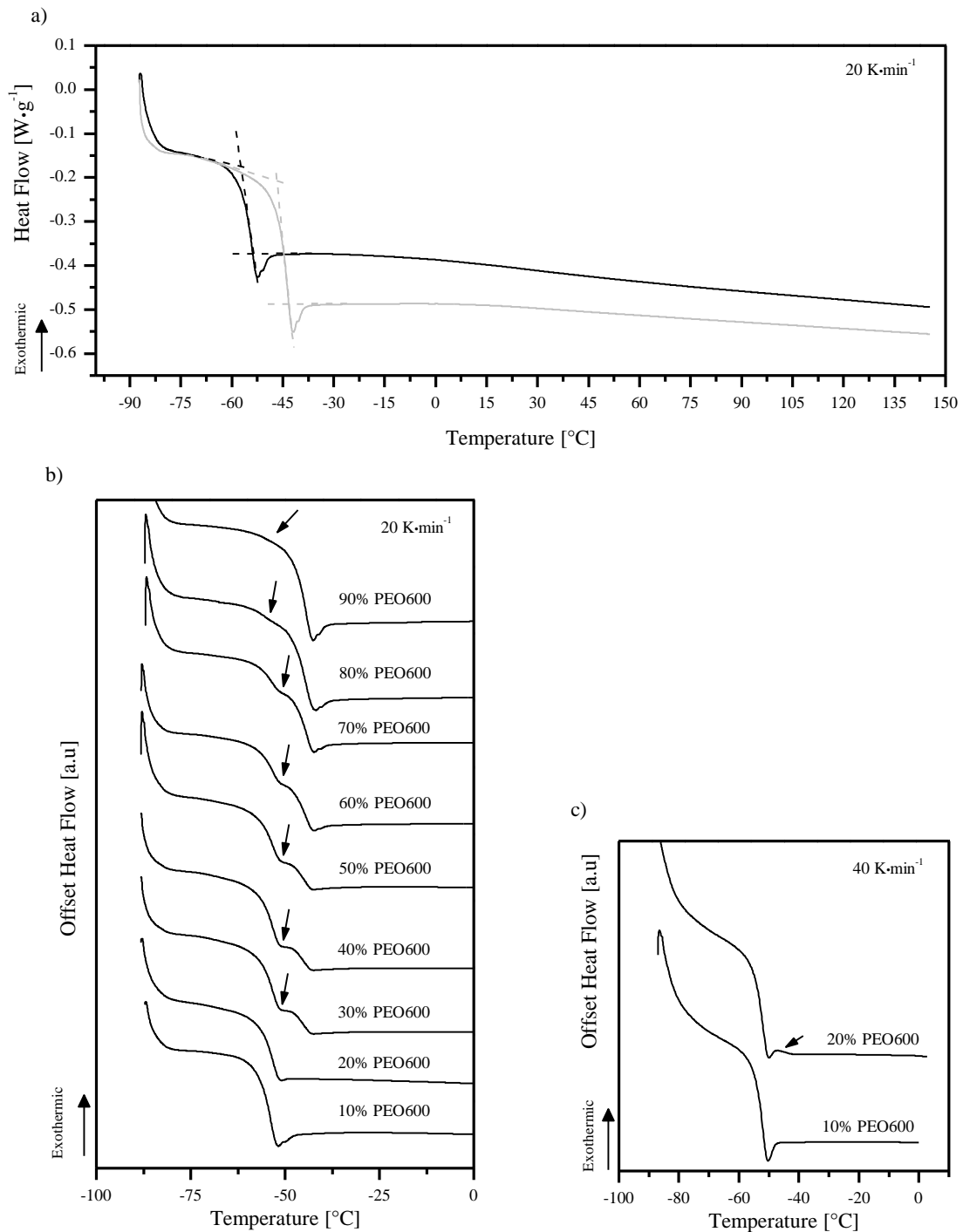


Figure 4-23. DSC thermograms of different PPG2k/PEO600 ITPUs. a) The single soft segment ITPUs containing PEO600(-) or PPG2k(-). b) Bi-soft segment ITPUs with increasing Φ_{PEO600} in the polyol mixture. Two glass transitions were detected for Φ_{PEO600} ranging from 30 to 90 vol.% (indicated by the arrows). c) Glass transition of ITPU 8 and 9 at an increased heating rate of 40 Kmin⁻¹.

The two remaining products with Φ_{PEO600} of about 20 and 10 vol.% did show single T_g s at approximately $-55\text{ }^\circ\text{C}$ (see Figure 4-23 b). Against the background of the turbid optical appearance of the IPTU 8 with Φ_{PEO600} of about 20 vol.% it was surprising that only a single glass transition has been detected. In a further experiment, samples of both ITPUs were analysed at increased heating rate of $40\text{ K}\cdot\text{min}^{-1}$. Higher heating rates improve the sensitivity for the detection of glass transitions.^[151] Indeed, an additional glass transition was found at $T_{g,2} = -45\text{ }^\circ\text{C}$ (see Figure 4-23 c)). This confirmed the phase separation of the soft segments.

Still a single T_g with an endothermic overshoot was found in the thermogram of the ITPU based on the PPG2k:PEO600 mixture with Φ_{PEO600} of about 10 vol.%. This result and the fact of its transparent appearance support the conclusion that [-PPG2k-HDI] segments were miscible with up to amounts of at least 10 vol.% [-PEO600-HDI] segments. This is in very good agreement with the predicted and experimentally found miscibility in the initial binary polyol mixture.

4.2.4 Molecular weight distribution of the ITPUs

SEC was performed to investigate the MWD of the prepolymers and to determine their residual content of monomeric HDI $\omega_{HDI,res}$. The products were quenched with an excess of methanol prior to analysis to ensure the absence of uncontrolled secondary reactions of the residual terminal isocyanate groups.

Table 4-6 gives an overview of the results obtained by the SEC analysis of samples from the different PPG2k/PEO600 ITPUs. The experimental molecular weights and $\omega_{HDI,res}$ values are compared with theoretical values which were calculated on basis of Schulz-Flory distribution.^[56]

The SEC analysis of the single soft segment ITPUs 10 and 11 resulted in the number average molar weights of $M_{n,ITPU\ 10} = 5\ 312\text{ g}\cdot\text{mol}^{-1}$ and $M_{n,ITPU\ 11} = 2\ 068\text{ g}\cdot\text{mol}^{-1}$, respectively. With respect to their theoretical values, a deviation of approx. 15 – 20 % was observed. However, considering the fact that the residual NCO groups were capped with methanol and that the SEC was calibrated with polystyrene standards a systematic deviation is not surprising. Nevertheless, the trend of increasing M_n with respect to the varied Φ_{PEO600} values is in excellent agreement to the theoretical values. The theoretical difference $\Delta M_{n,theo}$ between the average molar weight of ITPU 1 and ITPU 9 amounts to $1\ 912\text{ g}\cdot\text{mol}^{-1}$. This compares to the experimentally determined $\Delta M_{n,exp}$ of about $1\ 855\text{ g}\cdot\text{mol}^{-1}$.

Table 4-6. SEC results for the PPG2k/PEO600 ITPUs.

Product	Φ		M_n [g·mol ⁻¹]	M_w [g·mol ⁻¹]	$\omega_{HDI,res}$ [wt.%]	$M_{n,theoretical}^a$ [g·mol ⁻¹]	$\omega_{HDI,theo}^a$ [wt.%]
	PEO600	PPG2k					
ITPU 1	90	10	2 118	5 903	3.53	1 767	3.17
ITPU 2	80	20	2 218	6 427	3.39	1 863	3.01
ITPU 3	70	30	2 352	7 062	3.20	1 977	2.84
ITPU 4	60	40	2 503	7 726	3.05	2 114	2.65
ITPU 5	50	50	2 623	8 788	3.11	2 283	2.46
ITPU 6	40	60	2 667	8 616	2.87	2 496	2.25
ITPU 7	30	70	2 867	9 245	2.65	2 771	2.02
ITPU 8	20	80	3 301	10 811	2.37	3 145	1.78
ITPU 9	10	90	3 973	12 886	2.00	3 679	1.52
ITPU 10	-	100	5 312	15 710	1.46	4 505	1.24
ITPU 11	100	-	2 068	5 545	3.62	1 686	3.33

^a based on Schulz-Flory distribution

Due to the excess of HDI in the reaction mixture, there is still monomeric residual HDI left at the end of the polymerisation. After quenching with methanol, the resulting MeO-HDI-OMe units could be detected in the SEC chromatograms in the molar weight range from 100 to 300 g·mol⁻¹ (see Figure 4-24). The area of the signal is calculated via the software *WinGPC* and the resulting weight percentage is defined as the residual HDI content $\omega_{HDI,res}$.

For the reasons discussed above, the values obtained by this procedure presented deviations of about 10 - 20 % with respect to the estimated residual HDI contents based on Schulz-Flory distribution (see Table 4-6). But still, the trend of increasing residual HDI content with increasing Φ_{PEO600} was well reflected. The experimentally determined overall difference between the ω_{HDI} values of ITPU 1 and ITPU 9 matched very well the theoretical predicted difference ($\Delta\omega_{HDI,res} = 1.53$ wt.% $\approx \Delta\omega_{HDI,theo} = 1.65$ wt.%).

Figure 4-24 displays the individual MWDs of the bi-soft segment ITPUs and allows a comparison with the respective single soft segment prepolymers. The MWDs make further assignment of peaks to distinct oligomers possible. In this regard, the adduct MeO-HDI-PEO600-HDI-OMe (see Figure 4-24 B) was identified at the front of the broad polymeric peak ($\sim 1\,200$ g·mol⁻¹) in all samples excluding the PPG2k single soft segment

ITPU. Similarly, the MeO-HDI[-PEO600-HDI]₂-OMe unit (see Figure 4-24 D) was detected in the vicinity of $\sim 2\,400\text{ g}\cdot\text{mol}^{-1}$. Correspondingly the equivalent first adduct of PPG2k, HDI and MeOH (see Figure 4-24 C) was assigned to the first signal at $\sim 3\,000\text{ g}\cdot\text{mol}^{-1}$ at the start of the oligomeric compounds in the single soft segment ITPU 10. The dimer of PPG2k and HDI was ascribed to the peak signal at $6\,000\text{ g}\cdot\text{mol}^{-1}$ (see Figure 4-24 E).

Unfortunately, the separation efficiency of the applied column was not sufficient to distinguish between the oligomers in the bi-soft segment ITPUs 1 - 9. Only adducts A and B could be identified without doubt. At higher molecular weights ($M_n > 2\,000\text{ g}\cdot\text{mol}^{-1}$) the signals of the oligomers start to overlap and could not be clearly assigned.

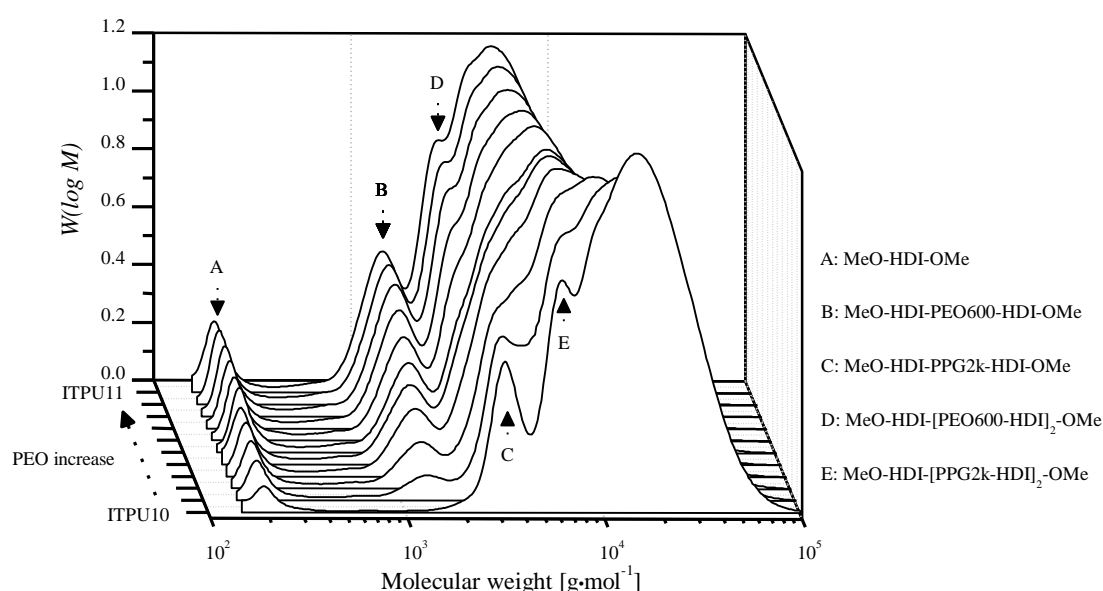


Figure 4-24. Molecular weight distributions of the synthesised ITPU products listed in Table 3-9.

4.2.5 Phase behaviour of the ITPU

The reaction-induced phase separation led to an inhomogeneous reaction mixture. The DSC analysis demonstrated that the phase separation was due to the incompatibility of the different soft segment units and confirmed the absence of hard segment domains. Based on these findings it is presumed that the occurring demixing process resembles a liquid/liquid phase separation resulting in two phases with equilibrium compositions. This implicates that the onset of phase segregation in the course of the reaction led to an emulsion, presumably consisting of a continuous and a dispersed phase. This is typical for phase separated liquid systems.^[128]

Here it should be mentioned that the prepared ITPUs were stable emulsions and that they did not separate into two layers spontaneously. In order to accelerate the demixing process, centrifugation was applied as displayed in Figure 4-25. It is a typical method to destabilize emulsions and dispersions.^[152] By this procedure emulsions separate into their individual phases and form clearly separate layers that can be analysed. In this case it is based on the different specific gravities of PEO600 and PPG2k (see Table 6-2). The upper and the lower phase are denoted by prime and double prime respectively in the following. Samples were drawn from the resulting layers and characterized by NMR and SEC in order to investigate the composition and the MWD in the individual phases. Of particular interest was the quantification of the volume fractions of PPG2k and PEO600 soft segments in the layers as this expresses the quantitative partial miscibility. The observed volume fraction of PEO600 and PPG2k with respect to the total soft segments is denoted by $\Phi_{PEO600,obs}$ in the following.

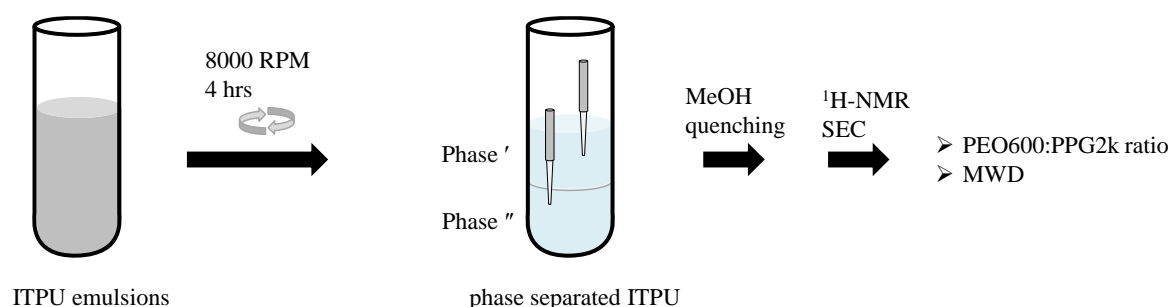


Figure 4-25. Schematically illustration of the experimental approach to analyse the separate phases. Centrifugation of the ITPUs 3,4,5,6 and 7 led to two separate phases which were further analysed by $^1\text{H-NMR}$ and SEC. ITPU 1,2 and 8 remained turbid and were stable.

It has been shown previously that $^1\text{H-NMR}$ allows for the discrimination between secondary and primary alkoxy groups located in the urethane linkages. In order to derive the soft segment composition in the individual phases, the ratio of the intensities I of the signals from primary $\alpha\text{-CH}_2\text{-O-CO-NH-}$ and secondary $\alpha\text{-CH(CH}_3\text{)-O-CO-NH-}$ moieties in the $^1\text{H-NMR}$ spectra was investigated. Based on this, the molar fraction of PEO600 with respect to the total soft segments in the isolated samples could be calculated.

It should be mentioned that in order calculate the individual molar fractions of PEO600 : PPG2k in the isolated phases, it was needed to take into account that PEO600 contains small amounts of secondary hydroxyl groups. The secondary hydroxyl content in PEO600 was quantified by $^1\text{H-NMR}$ analysis of the single soft segment ITPU 11 to amount 8 mol.% with respect to the primary hydroxyl content (see Figure 4-26 a). Without considering this fact, the obtained ratio of $I_{\alpha\text{-CH}_2}$ divided by the secondary $I_{\alpha\text{-CH(CH}_3\text{)}}$ would not

represent the actual molar fraction of PEO600:PPG2k soft segments. Therefore, a two point calibration was derived to assign the determined molar ratio of the intensities $\alpha\text{-CH}_2/\alpha\text{-CH}$ to molar fraction of PEO600/PPG2k units, denoted as $x_{\text{PEO600,obs}}$.

For the set-up of the calibration, it was made use of the fact that polyurethane prepolymer ITPU 9 was a clear homogeneous product. The polyether mixture used for ITPU 9 comprised 30 mol.% of PEO600 and 70 mol.% of PPG2k. Therefore, the determined molar ratio $I_{\alpha\text{-CH}_2} : I_{\alpha\text{-CH}(\text{CH}_3)}$ in this sample could be assigned to a molar fraction of PEO600 : PPG2k units of 30 mol.% : 70 mol.%. The second sample used in this linear calibration was the PEO600 single soft segment ITPU itself. The $^1\text{H-NMR}$ spectra of the two samples and the assumed linear dependency between the molar ratio $I_{\alpha\text{-CH}_2} : I_{\alpha\text{-CH}(\text{CH}_3)}$ and the molar fraction of PEO600 soft segments are shown in Figure 4-26 and Eq.(4-10).

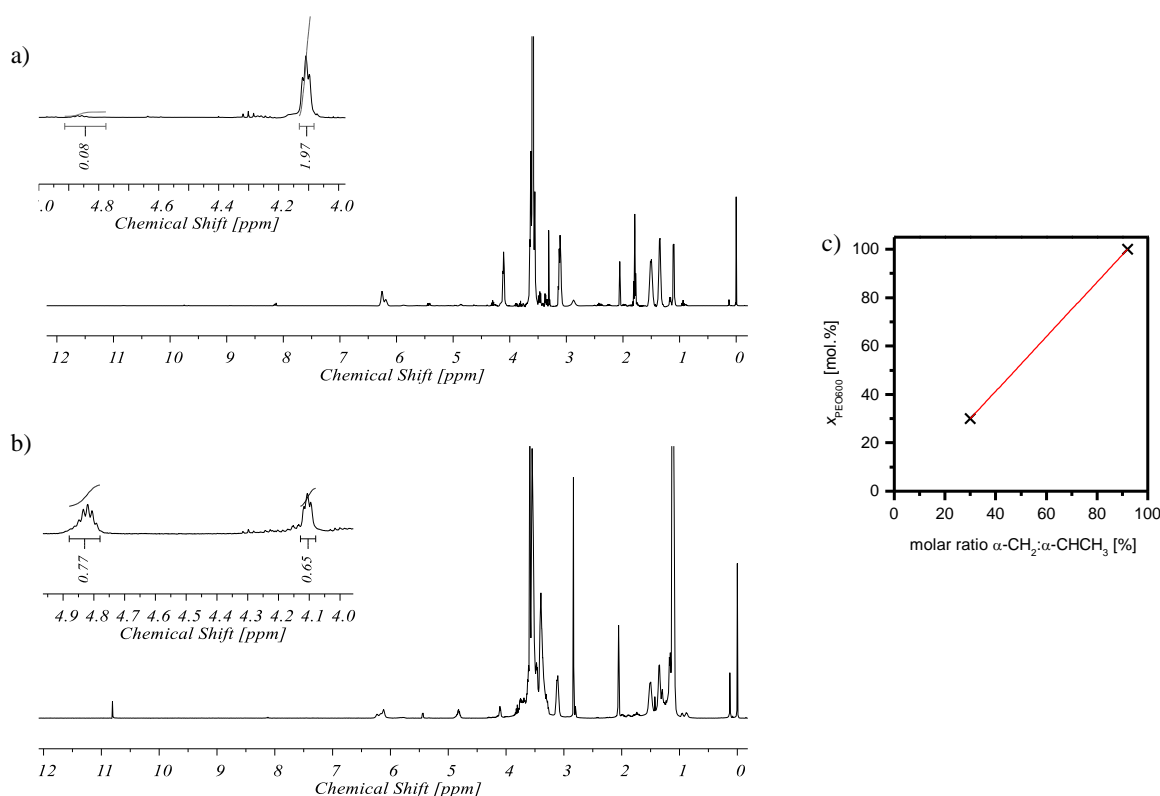


Figure 4-26. Illustration of the estimation procedure of the molar ratios of PEO600 with respect to PPG2k in the separate phases. a) $^1\text{H-NMR}$ spectrum of ITPU 11 b) $^1\text{H-NMR}$ spectrum of ITPU 9 and c) Linear calibration.

$$x_{\text{PEO600,obs}} = \frac{0.5 \cdot I_{\alpha\text{-CH}_2}}{I_{\alpha\text{-CH}(\text{CH}_3)}} \cdot 0.0112 - 0.0387 \quad \text{Eq.(4-10)}$$

It should be noted that the $^1\text{H-NMR}$ spectra of the ITPUs revealed in some cases an additional signal at a chemical shift of about 10.8 ppm that can be assigned to allophanate groups. These groups are forming by a successive reaction of residual isocyanates with urethane groups. The storing time and the centrifugation process did not make it possible to avoid their formation completely. In the following, it is assumed that the low extent of allophanate groups did not have significant impact on the composition of the isolated phases and on the quantification of the PEO600 : PPG2k ratio. The assumption is based on the premise that the signal intensities of the $\alpha\text{-CH}_2$ and the $\alpha\text{-CH}(\text{CH}_3)$ units are not altered by the additional signal of allophanates.

On basis of the calibration, the molar ratio of the $\alpha\text{-CH}_2 : \alpha\text{-CH}(\text{CH}_3)$ signals in the different samples could be converted to the molar fraction $x_{\text{PEO600,obs}}$ of PEO600 soft segments with respect to PPG2k. The molar ratio was then further converted to the observed volume fraction $\Phi_{\text{PEO600,obs}}$ by consideration of the molar volume V_m of the polyether polyols (see Table 6-2 for V_m values).

The resulting values obtained for $x_{\text{PEO600,obs}}$ and $\Phi_{\text{PEO600,obs}}$ in the individual isolated phases are illustrated in Figure 4-27. Remarkably, the experimentally determined molar ratios of the $\alpha\text{-CH}_2 : \alpha\text{-CH}(\text{CH}_3)$ signals in the respective upper phases (phase') of the different ITPUs was found to be nearly identical throughout the samples. The same applies for the samples from the lower phase (phase'').^b

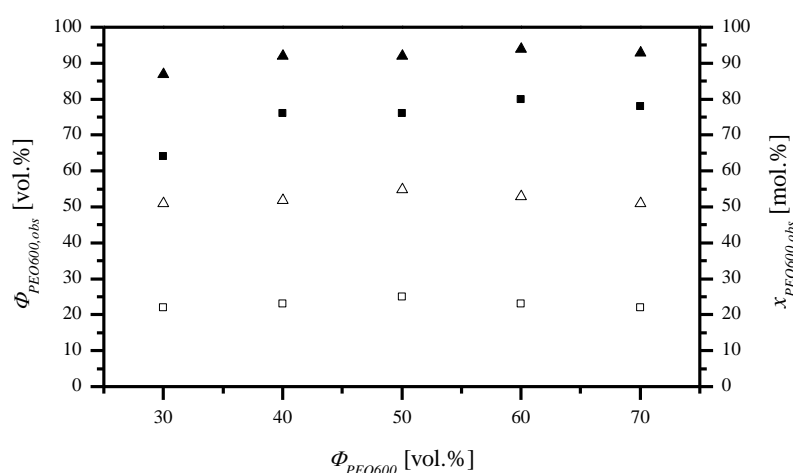


Figure 4-27. Determined volume and molar ratios of PEO600 soft segments in the isolated phases from the ITPUs after centrifugation. Triangles represent $x_{\text{PEO600,obs}}$ and squares $\Phi_{\text{PEO600,obs}}$ respectively. Phase' is represented by the open symbols and phase'' by the solid ones.

^b See all relevant $^1\text{H-NMR}$ spectra in Appendix IV-12 ff.

Overall, phase' entirely contained nearly equimolar amounts of primary and secondary α -CH_x groups whereas phase'' comprised throughout a high excess of primary moieties. Based on the presented two-point calibration, an average soft segment composition with $x_{PEO600,obs}$ of about 92 mol.% was found in phase''. In contrast to this, a balanced PEO600 : PPG2k soft segment fraction of about 52 mol.% was detected throughout phase'.

Considering the molar volumes of the soft segments, the results revealed the existence of a PEO600- and a PPG2k-rich phase. The volume fraction of PEO600 soft segments amounted to an average of about 75 vol.% in the individual PEO-rich phases. Compared to this, the PPG2k-rich phases revealed average values of about ~23 vol.% for $\Phi_{PEO600,obs}$, respectively. Especially in the PPG2k-rich phases, the PEO600 content was particularly constant with a standard deviation of about 1 vol.%. On the other side, a slightly decreasing trend in $\Phi_{PEO600,obs}$ was observed throughout the samples of phase'' at increasing Φ_{PPG2k} amounts.

Overall, these results are of particular importance regarding the understanding of the phase behaviour during the reaction progress. They demonstrate that the composition of the resulting phases was practically independent of the initial composition of the components and thus independent of the reaction path in the ternary phase diagram. This strongly suggests a thermodynamically controlled phase separation process as it was already proposed in the shape of the presented hypothetical binodal in the ternary diagram in section 4.2.2.

In addition to the ¹H-NMR study, the samples were analysed by SEC in order to investigate their MWD. The obtained MWDs of the isolated phases are shown in Figure 4-28. The PPG2k-rich phases revealed a broad polydispersity and significantly lower average molar weight compared to the respective PPG2k single soft segment ITPU (dotted line). The MWDs of the samples from phase' did not extensively differ from one another throughout the different products. However, it was found throughout the samples that increasing Φ_{PPG2k} systematically resulted in lower contents of residual monomeric HDI and of MeO-HDI-PEO600-HDI-OMe units (PEO600 unimer). In addition to this, concurrently a minor shift towards higher chain length was observed (see Figure 4-28).

In fact, the mentioned trends of reduced HDI and PEO600 unimer fractions and slightly higher chain length at increasing Φ_{PPG2k} are analogously observed in the samples from phase'' (see Figure 4-28). The reduced residual HDI fraction is coherent against the background of the reduced initial content of HDI at increased Φ_{PPG2k} (see Table 6-4). On the other hand, the systematic decrease of the PEO600 unimer was surprising as the PEO600/PPG2k soft segment fraction throughout the samples was proofed to be almost constant (Figure 4-27). In this regard, it is assumed that increased Φ_{PPG2k} values result in the presence of PEO600 soft

segments in higher chain length mixed soft segment oligomers. Keeping in mind that PPG2k is predominantly reacting at a later stage compared to PEO600, these observations suggest that the low molecular PEO600 adducts were subsequently further extended with PPG2k. Unfortunately, the resolution of the MWDs did not suffice to identify such oligomers.

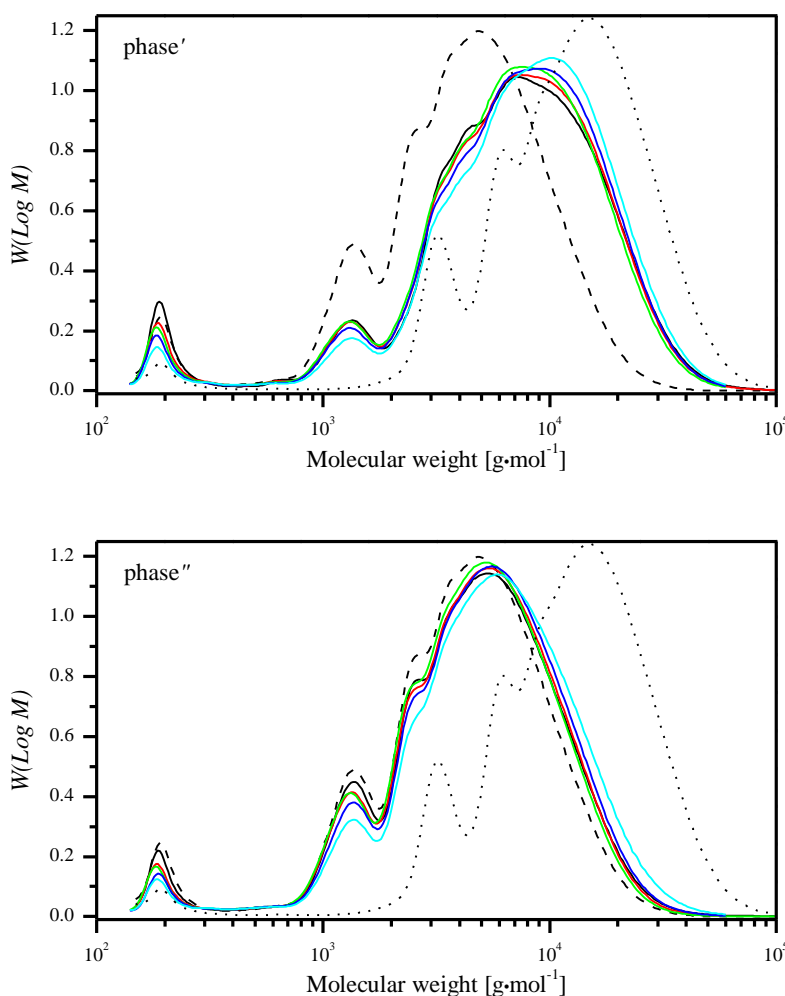


Figure 4-28. MWDs of the samples from upper (phase') and lower (phase'') phase after centrifugation of ITPU 3(—), 4(—), 5(—), 6(—), and 7(—). The dashed and dotted line represent the respective single soft segment ITPUs 11 and 10 respectively.

Nevertheless, the presence of the PEO600 unimer in the PPG2k-rich phase is remarkable as this confirmed its solubility. For the exemplary case of phase' of ITPU 5, the weight fraction of the PEO600 unimer with respect to the total signal of oligomers was estimated at ~6 wt.% by integration. Considering the specific gravities of the polyether polyols the PEO600 unimer makes up 5.5 vol.% of the oligomers. Against the background of the average value of about 23 vol.% for $\Phi_{PEO600,obs}$ (phase' of ITPU 5 in Figure 4-27) it is concluded that PEO600 soft segments should also be present in the higher molecular weight oligomers. In

this concern it should be stressed, that the dimeric single soft segment MeO-HDI-[PEO600-HDI]₂-OMe unit seemed to be absent in the MWDs of the PPG-rich phases (phase' see Figure 4-28). Consequentially the remaining content of PEO600 might be contained in mixed soft segment oligomers.

The MWD in all samples from phase'' was nearly identical to the MWD of the single soft segment PEO600 ITPU 11. This is in accordance to the estimated value for x_{PEO600} of about ~92 mol.% in these samples (see Figure 4-27). Similar to the results previously described for phase', there was a slight but steady decrease in the contents of monomeric HDI and in the unimeric and dimeric oligomers of PEO600 from ITPU 3 to ITPU 7. Once more, this occurred concurrently with a minimal tendency towards higher molar masses (see Figure 4-28). This matched the observations concerning the MWDs in phase' and supported the hypothesis that low-molecular PEO600 adducts were extended by PPG2k. However, the similarity of the individual MWDs of phase'' with the single soft segment is remarkable as it demonstrates the marginal influence of Φ_{PPG2k} .

Moreover it should be stressed that the detected MWDs demonstrated that the HDI content was shared between the two phases as in both a typical Schulz-Flory distribution and fairly balanced contents of residual monomeric HDI were found (see Figure 4-28).

Interestingly, in the case of the opaque ITPUs with Φ_{PPG2k} below 30 vol.% and greater than 70 vol.% the centrifuged samples appeared persistently turbid and did not show divided phase layers even at prolonged periods of centrifugation. In the following, the possible reason(s) for the stability of these remaining emulsions is briefly addressed. It will be focused on ITPU 1 ($\Phi_{PPG2k} = 10$ vol.%) and ITPU 12 ($\Phi_{PPG2k} = 79$ vol.%). Although there were no clearly distinguishable phases after centrifugation, samples were drawn at the top surface and the bottom of the liquid in order to investigate if there was an enrichment of either PEO600 or PPG2k.

For ITPU 1, ¹H-NMR analysis quantified the values for $\Phi_{PEO600,obs}$ to be 87 vol.% at the top surface and 88 vol.% at the bottom. The samples at the top surface and the bottom of ITPU 12 revealed identical $\Phi_{PEO600,obs}$ values of about 20 vol.% (¹H-NMR spectra shown in the appendix). These values are nearly identical to the initial PEO600 contents in these ITPUs ($\Phi_{PEO600} = 90$ vol.% and $\Phi_{PEO600} = 21$ vol.%, see Table 6-4). Thus no significant enrichment of either PEO600 or PPG2k at the top surface or the bottom of the liquids was observed after centrifugation. In other words, the distribution of the soft segments throughout the sample was uniform on macroscopic scale. This is further supported by the almost identical MWDs

of the two samples from ITPU 1 and 12 determined by SEC analysis (MWDs shown in Appendix IV-24).

To investigate the morphology of the two phases in more detail, micrographs were taken of liquid emulsion films. A drop of the respective turbid ITPUs was dispensed on a microscope slide and covered with a cover glass. Figure 4-29 demonstrates that in cases of ITPU 1 and ITPU 12 fairly monodisperse symmetrical droplets with radii in the range of 1 – 10 μm could be observed. These pictures point to the typical structure of an emulsion comprising a dispersed phase in a continuous matrix. Inspecting the morphology of ITPU 5 no clear differentiation between continuous and dispersed phase is possible. Indeed, the appearance of the interfaces of the phases in this emulsion did indicate bi-continuous morphology. This is a characteristic appearance of polymer blends exhibiting spinodal decomposition (SD).^[102]

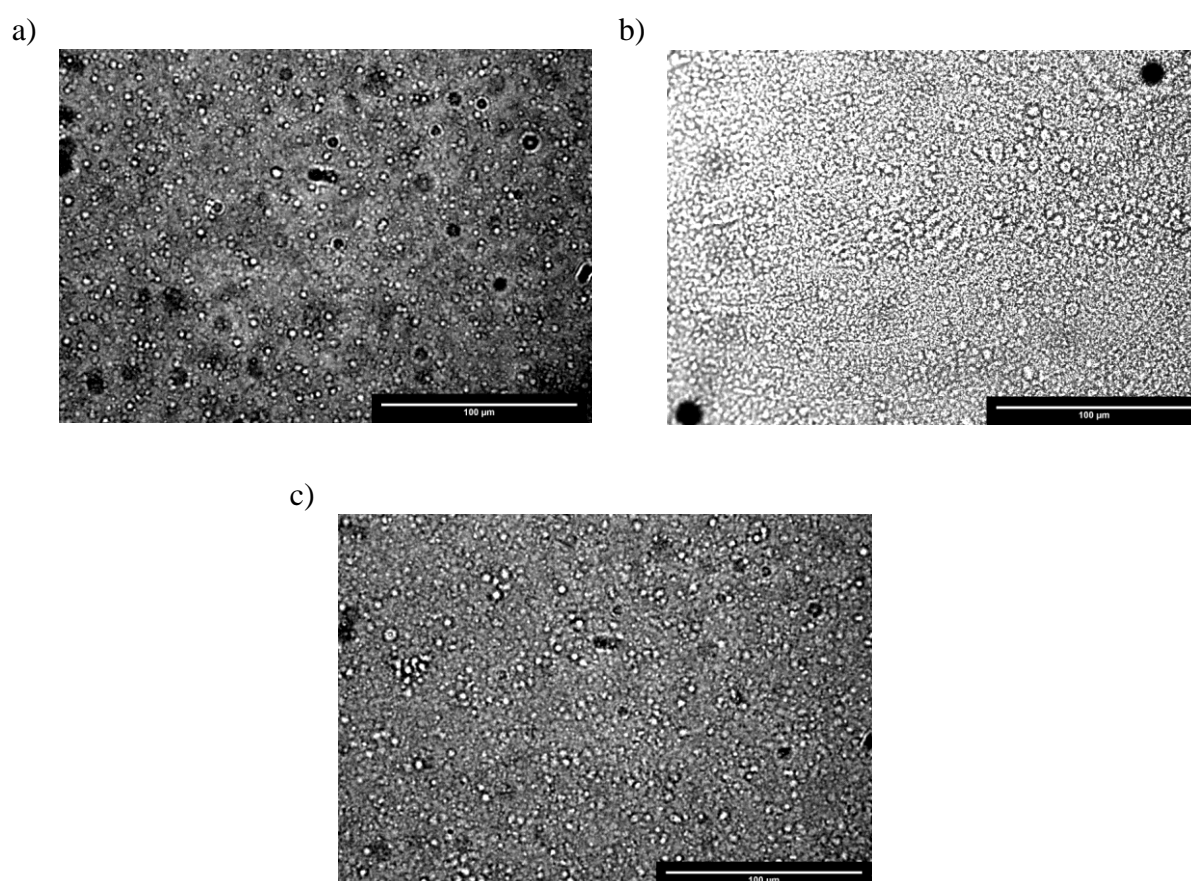


Figure 4-29. Micrographs of emulsions (a) ITPU 1 ($\Phi_{\text{PPG}2k} = 10 \text{ vol.}\%$), (b) ITPU 5 ($\Phi_{\text{PPG}2k} = 50 \text{ vol.}\%$) and (c) ITPU 12 ($\Phi_{\text{PPG}2k} = 79 \text{ vol.}\%$).

SD is taking place when the second derivative of the Gibbs free energy of mixing is zero.^[102] This condition controls the mechanism of phase separation to occur via SD or via “nucleation and growth” (NG).^[107] Latter is observed in the metastable region between binodal and spinodal curve in the phase diagram. The mechanism of SD follows a periodic

fluctuation of the concentrations that finally results in the characteristic co-continuous morphology. In NG nuclei comprising the equilibrium concentrations are formed randomly and grow as time proceeds.^[102] In this regard, the droplets comprised in ITPU 1 and 12 were most likely formed by NG.

In order to provide a comprehensive discussion of the RIPS and the consequential occurrence of either SD or NG, the phase behaviour during the formation towards the prepolymer needs to be addressed in detail. The proposed phase evolution process during the reaction progress is schematically illustrated in Figure 4-30.

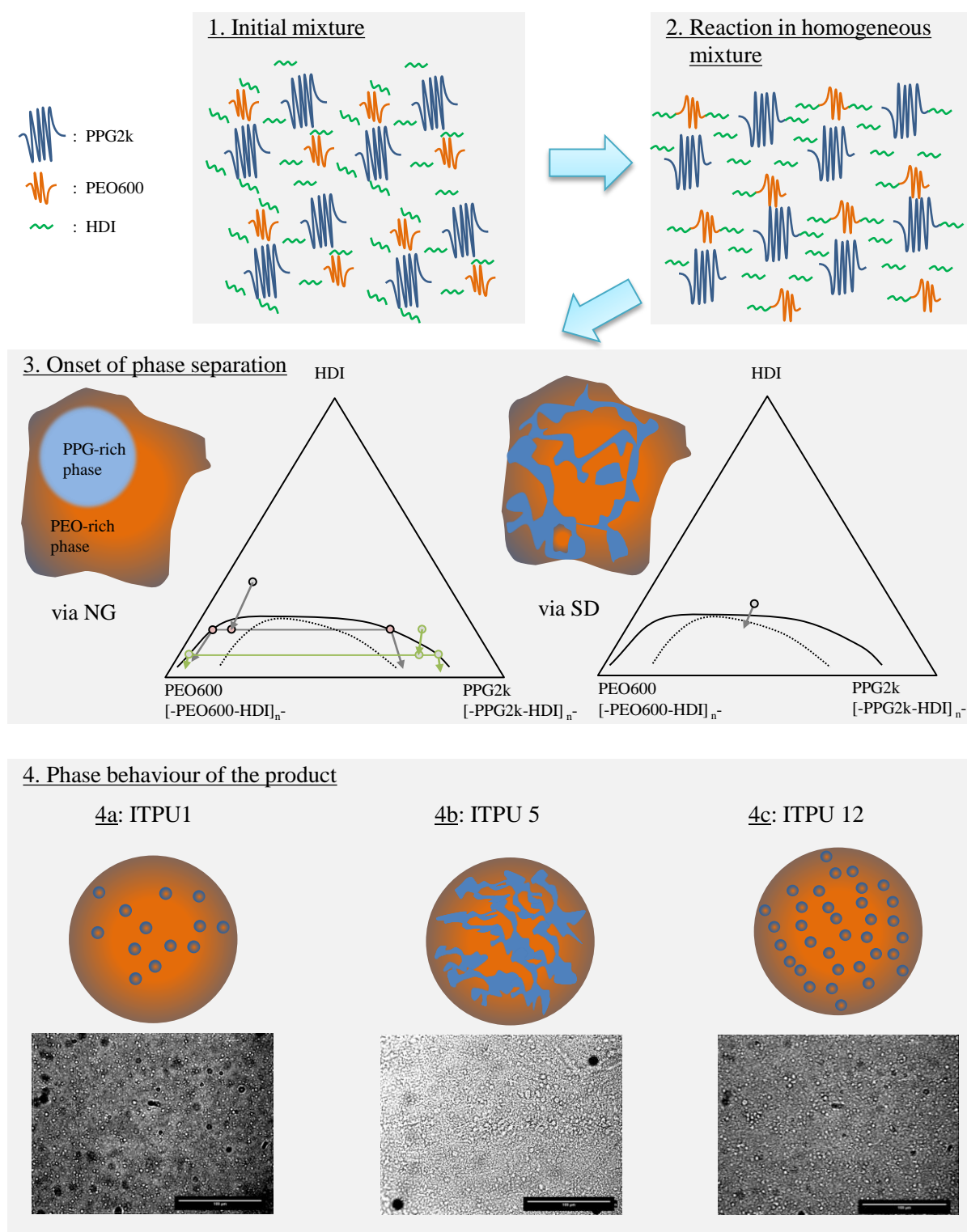


Figure 4-30. Schematic illustration of the phase evolution during the reaction progress including optical micrographs of the products. (4a) ITPU 1 (4b) ITPU 5 (4c) ITPU 12.

The scheme illustrates the phase evolution on the example of the two stable ITPUs 1 and 12 and the spinodal emulsion ITPU 5. On the whole, the results from the phase analysis via $^1\text{H-NMR}$ and SEC supported the hypothesis that the phase separation of these bi-soft segment IPTUs followed the principle of the previously proposed ternary phase diagram due to the fact that the demixing results in two phases with compositions that are evidently predefined by a binodal line (section 4.1.2).

Regarding the presented reactions, the polymerisation started in an initially homogeneous mixture in all cases (1. period). Considering the observations from the kinetic study in section 4.2.1, predominantly PEO600 molecules react with HDI to form first adducts. This reaction causes the overall composition to change towards higher [-PEO600-HDI]- concentration as depicted by the arrows in the phase diagrams in Figure 4-30. While the reaction continues still in homogeneous conditions HDI is consumed until a critical volume fraction of HDI $\phi_{crit,HDI}$ is reached. At this point, the binodal is crossed meaning that NG might spontaneously occur.

Indeed, in the cases of ITPU 1 and ITPU 12 an emulsion containing a continuous and a dispersed phase was formed. Interestingly, this onset of phase separation can be considered as the origin of two individually, locally distinct reaction ‘containers’. The compositions in these ‘containers’ is thermodynamically controlled by the proposed binodal in the ternary phase diagram. The PEO600-rich phase had very poor solubility for PPG2k segments ($x_{PEO600,obs} = \sim 92\%$, $\Phi_{PEO600,obs} = \sim 75\%$), while on the other hand PEO600 segments were soluble to a much greater extent in the PPG2k-rich phase ($x_{PEO600,obs} = \sim 52\%$, $\Phi_{PEO600,obs} = \sim 23\%$).

Starting from the binodal compositions, the reaction continues inevitably in the metastable region of the phase diagram. ϕ_{HDI} reduces continuously and the reaction mixture might eventually phase separate further by NG. Due to the differences in the concentration of the reactants between the phases, the subsequent pathways vary as illustrated in the phase diagram. In the PEO600-rich phase predominantly [-PEO600-HDI]_n- is formed and vice versa.

Concerning ITPU 5 it is presumed, that the pathway between the binodal and the spinodal line is very narrow. This implicates that the period given for NG is very short. The advancing reaction and consequential consumption of HDI might have caused that the spinodal line is crossed before NG has been accomplished. SD is induced and the observed morphology is build up.

Regarding the morphology of the emulsions it is furthermore of interest to address if either the PEO600-rich or the PPG2k-rich phase makes up the continuous phase. Here, the findings

from the FTIR analysis concerning the irregular changes in transmission in the NCO, CH₂ and CH₃ vibrations are worthy of note (cf. section 4.2.1). Like mentioned before, it is reasonable to assume that the detected signal of FTIR analysis in emulsions is mainly dominated by the continuous phase.^[132] Considering this, the present findings clearly point to the conclusion that the continuous phase is enriched with PEO600 and HDI, while the discontinuous phase is enriched with PPG2k containing slightly lower content of HDI. This is in excellent agreement to the predicted equilibrium compositions based on $\delta_{HDI,Stefanis}$ (cf. section 4.1.2). In fact, the prediction suggested a slightly favoured miscibility of PEO600/HDI compared to PPG2k/HDI.

In addition to this, it is interesting to discuss why the centrifugation of ITPUs 1, 2, 8 and 12 did not result in isolated phases. There seems to be a stabilization mechanism preventing demixing processes. Responsible for stabilization might be the existence of amphiphilic molecules that stabilize the surface of the dispersed droplets. Amphiphilic mixed soft segment block co-polymer polyurethanes that possess a similar structure to those investigated have been reported as surface active agents.^[153–155] Mixed soft segment oligomers containing hydrophilic PEO600 and hydrophobic PPG2k units could therefore be considered as that type of molecule.

A requirement for the formation of mixed soft segment oligomers is that the different reactants are in contact with each other. In fact, this requirement is fulfilled at the start of the reaction but the phase separation might be a critical parameter. After phase separation, the chance of formation is very low in the PEO600-rich phase as the content of PPG2k in it is around 5 mol.%. On the other hand, balanced molar fractions of both polyether polyols are contained in the PPG2k-rich phase. Following this argumentation, mixed soft segment oligomers can either be formed at the interphase between the two phases or inside the PPG2k-rich phase.

The onset of phase separation directly affects the duration in which polymerisation takes place in a homogeneous mixture. An onset of phase separation at low conversions could imply that the formation of dimers or higher oligomers did not occur until that moment. Here, Carothers^[58] equation for step growth polymerizations is used for a correlation of the conversion p and the polymerisation degree \bar{X}_n . Based on the NCO%-content titrations the onset of phase separation occurred at a NCO conversion of about 65 % in the case of ITPU 1 and hence later in comparison to ITPU 5 (50 %) and 12 (40 %).

Following this, the degree of polymerization \bar{X}_n was 2.08 in ITPU 1 at the onset of phase separation considering the initial molar ratio OH/NCO r of about 0.6667. This implicates that

at this time first adducts in the form of PEO600-HDI-PPG2k-HDI could be expected. For ITPU 5 with $p = 0.50$ and ITPU 12 with $p = 0.40$ this resulted in the degrees of polymerisation \bar{X}_n of about 1.67 and 1.47, respectively. In these cases, the only possibility of formation of mixed soft segment oligomers was in the PPG2k-rich phase due to the early onset of phase separation. Considering the assumption that the PPG2k-rich phase is contained in the droplets, the stabilizing surfactants might be formed in the inside of the droplets and assemble at the interface reducing the surface tension and stabilizing the droplet.

Theoretically, the signal of HDI-PEO600-HDI-PPG2k-HDI chains in SEC chromatograms should be expected at $\sim 3\,500\text{ g}\cdot\text{mol}^{-1}$. Unfortunately, the resolution of the SEC analysis did not suffice to identify of the amphiphilic adduct. Nevertheless, all received results point to the reliable conclusion that the emulsions ITPU 1 and 12 are stabilized by amphiphilic HDI-PEO600-HDI-PPG2k-HDI oligomers.

4.2.6 Summary on the reaction-induced phase separation in PPG2k/PEO600/HDI reaction mixtures

It was found that mixtures comprising PPG2k, PEO600 and HDI exhibit reaction-induced phase separation. Variation of the composition of the initial polyol mixture resulted in a shift of the onset of phase separation with respect to the overall NCO conversion. It was found that an increase of the initial volume fraction of HDI leads to delayed phase separation.

$^1\text{H-NMR}$ analysis revealed that the kinetics in the applied system can be interpreted as competing second order due to the existence of primary and secondary hydroxy groups. DSC measurements demonstrated that the phase separation in the ITPU is a result of the incompatibility of the soft segments and not induced by hard/soft segment segregation. The separate phases could be individually analysed after isolation by centrifugation. $^1\text{H-NMR}$ has proven the existence of two phases, a PEO600-rich and a PPG2k-rich layer. It was found that the MWDs and the soft segment fractions in the two discrete phases were nearly identical throughout the different ITPUs.

Micrographs of the ITPUs suggest that the phase separation followed NG mechanism in cases of ITPU 1 and 12 while bi-continuous morphology in case of ITPU 5 indicates SD. A hypothetical ternary phase diagram serves as a basis to illustrate the proposed phase behaviour during the reaction process.

5 Conclusion and outlook

In this work, the reaction-induced phase separation (RIPS) in bi-soft segment polyurethane reaction mixtures of PPG/PEO/HDI was investigated. In the beginning of this work, the partially miscible mixture of PPG2k/PEO600 and HDI was identified as a potential candidate to exhibit RIPS. The initial miscibility of the ternary reaction mixture has been theoretically and experimentally determined and correlated to experimental observations regarding the RIPS subsequently.

FH theory served as basis for the estimation of the initial miscibility of the reactants. In this approach, the interactions between the substances are accounted for in binary interaction parameters (BIPs). In order to estimate the ternary phase diagram, the three BIPs between PPG/PEO, PPG/HDI and PEO/HDI were assessed. In the light of this, it was practical to investigate the three binary systems stepwise.

In this study, the BIPs were estimated on basis of SPs. Relating to the polyether polyols, group contribution theories of Fedors^[90] and Hoy^[91] were applied in order to determine the SPs. Here, the detailed molecular structure of the macrodiol was considered including the starter molecule structure, the number of EO/PO repeating units and the end-functional hydroxy groups. Implementation of the derived SPs in FH theory-based calculations demonstrated that the SPs based on Fedors' method led to the best reflection of experimentally observed miscibility behaviour. It was found that PPG2k/PEO600 and PPG4k/PEO600 mixtures show UCST behaviour. In fact, numerically determined quantitative phase diagrams of these two mixtures were in excellent accordance to experimentally determined binodal compositions at temperatures below 120 °C.

In the following, the initial miscibility in the ternary system of PPG2k/PEO600/HDI was investigated. In this regard, it was found that the SPs of HDI based on Fedors' and Hoy's group contribution theories led to misleading prediction of the binary miscibility of PPG2k with HDI. For HDI it was shown that the value of the SP depends strongly on the method applied for the determination. In addition to the methods of Fedors and Hoy, the SP of HDI was obtained by Hansen solubility tests and by an alternative group contribution theory introduced by Stefanis^[93]. Their application in the numerical estimation of the ternary phase diagram of PPG2k/PEO600/HDI resulted in a binodal curve, which was in qualitative agreement with experimental cloud points. Both, predicted binodal and cloud points, presented a miscibility gap at low volume fractions of HDI. Nevertheless, significant deviations were found near the critical point.

Here it is assumed that in general more sophisticated prediction tools are needed for a reliable quantitative assessment of the phase diagram of polyols with polyisocyanates. Specific interactions like hydrogen bonds or composition dependent interaction parameters might play a crucial role in these systems.^[85] In addition to this, polydispersity is known to affect the configurational entropy in solutions and thus the thermodynamic equilibria.^[35] This might be of importance as the polyether polyols possess molar weight distributions. In this regard, it is proposed that modified, extended FH models^[33,106] could be applied in a future study. The MATLAB program that was coded for this thesis could be used as a basis for that.

The formation of the ITPU from the PPG2k/PEO600/HDI mixture has been monitored by several independent methods, i. e. in-line FTIR spectroscopy, in-line UV-Vis spectroscopy, NCO%-content titration and ¹H-NMR spectroscopy. ¹H-NMR analysis performed in the course of a model reaction demonstrated the competing second order kinetics in the ternary situation. It was shown that the reaction of the primary alcohol of the PEO with the isocyanate group was kinetically favoured with respect to the secondary hydroxyl group of the PPG. In accordance to this, the kinetic data obtained by NCO%-content titration did present a second linear stage at the end of the reactions, which is apparently a result from secondary alcohol reaction with isocyanate. It would be of great interest to look at these particular findings from the kinetic investigation in future studies. It would be needed to design experiments properly to elucidate the reaction kinetics. In contrast to the experiments done in this thesis, it is suggested to use equimolar $[NCO]/[OH]$ fractions and to operate in solution to ensure homogeneous reaction conditions. In this context, it would also be of interest to address the irregularities that were observed in the FTIR reaction monitoring. Systematic investigation on this topic is needed for a comprehensive understanding of the phenomenon observed.

In-line UV-vis spectroscopy was applied to record the onset of turbidity during the reaction. As presumed based on the limited miscibility of the reactants, the polymerisations of PPG2k/PEO600/HDI mixtures demonstrated RIPS. Several ITPUs were prepared at different soft segment ratios. An apparently linear dependency between the onset of phase separation and the initial soft segment ratio was found. Increased PEO600 contents resulted in a shift of the onset of phase separation towards higher NCO conversions. Due to the fact that throughout the different reactions the initial NCO/OH index is kept constant, an increased PEO600 fraction leads concurrently to increased HDI contents. It is proposed that not the PEO600 content affects the onset of phase separation but the increased HDI content. It is hypothesized that the RIPS is thermodynamically controlled and that it occurs by virtue of the

consumption of the reactive solvent HDI. In correlation to the partial miscibility of the initial reactant mixture, the hypothesis is schematically illustrated in a ternary phase diagram.

For future studies, it would be interesting to quantify the residual HDI volume fractions at the onsets of phase separation. This thesis showed that the HDI content was quantifiable via SEC analysis. Samples could be taken at the onset of phase separation, quenched with an amine to stop the polymerisation and subjected to SEC analysis. This would lead to more detailed knowledge about the relationship between the residual HDI content and the onset of phase separation.

DSC analysis has proven that the phase separation in the prepared ITPUs is a result of incompatible soft segment units. Furthermore, the glass transitions indicated that the hard segments were dispersed in the soft segment matrix and not segregated into hard domains. This confirmed that the phase separation process is resulting from liquid/liquid demixing and that it can be illustrated by the proposed ternary phase diagram.

In addition to this, the phase behaviour during the reaction was discussed in detail in view of the presented morphologies of the prepared ITPUs. They were centrifuged in order to divide the incompatible phases and to investigate their composition and their MWD. ¹H-NMR analysis revealed the occurrence of two phases, a PEO600-rich and a PPG2k-rich one. Interestingly, the initial PEO600/PPG2k contents had no significant influence on the resulting PEO600/PPG2k ratios in the two phases. This finding points to the conclusion that the phase separation and thus the composition in the separate phases are thermodynamically controlled. In accordance to this, SEC analysis demonstrated that not only the compositions were nearly constant but that also the MWDs in the phases were more or less independent from initial polyol composition.

Micrographs indicated that the phase separation in some cases followed the mechanism of NG and in other cases SD. In this regard, a comprehensive illustration of the complete reaction process was presented starting at the initial period of homogeneous reaction and ending in the phase separate product. It is suggested that the initial composition and the inherent reaction path play a major role concerning the final morphology of the emulsion. Microscopy was proofed as a useful tool investigating the morphology. In this context, it is recommended to study the appearance of samples of the presented reaction mixtures in regular intervals during the prepolymerization in order to obtain an in-depth understanding of the phase behaviour.

Furthermore, it would be of great interest to focus on chain extended products of the presented bi-soft segment ITPUs. The preservation of the presented morphologies could

possibly open a door for applications where such structures play a key role regarding functionality, for example in membrane science^[156]. For tailored design of the morphology, the knowledge of the detailed phase diagram and the kinetics of the phase separation are required. In this regard, this study represents a fundamental basis for the understanding of the complex mechanisms involved and provides a starting point for sophisticated investigations.

6 Experimental part

6.1 Materials

Table 6-1. Used chemicals.

Chemical	Supplier	Purity
1,2-Butandiol	Fluka	≥ 98 %
1,3-Propylene glycol	Acros Organics	98 %
1,4-Dioxane	Merck	99.8 %
1,6-hexamethylene diisocyanate	Merck Millipore	≥ 99 %
1-Propanol	Merck Millipore	99 %
Acclaim 2200 (PPG2k)	Covestro Deutschland AG	technical grade
Acclaim 4200 (PPG4k)	Covestro Deutschland AG	technical grade
acetone	various	99.5%
acetone-d ₆	Carl Roth	99.8 Atom%D
Acetonitrile	VWR	≥ 99.95 %
Chlorobenzene	VWR	99.9 %
Chloroform	Carl Roth	≥ 99 %
Chloroform-d ₃	Carl Roth	99.8 Atom%D
Cyclohexane	Merck Millipore	≥ 99 %
Desmophen 1111BD (PPG1k)	Covestro Deutschland AG	technical grade
Desmophen 1262BD (PPG400)	Covestro Deutschland AG	technical grade
Desmophen L300 (PEO600)	Covestro Deutschland AG	technical grade
Dibutyltin dilaurate (DBTDL)	Covestro Deutschland AG	technical grade
Dibutylamine	Merck Millipore	99.0 %
Diethyl ether	Carl Roth	≥ 99.5 %
Dimethyl sulfoxide	Carl Roth	≥ 99.5 %
Dimethyl sulfoxide-d ₆	Carl Roth	99.9 Atom%D
Ethanol	Carl Roth	≥ 99.8 %
Ethyl acetate	Carl Roth	≥ 99.5 %
Ethylene glycol	VWR	99.8 %
Glycerol	Fluka	≥ 99.5 %
n-Hexane	Carl Roth	≥ 95 %
Hydrochloric acid, c = 1 mol·L ⁻¹	Bernd Kraft	titration grade
Methanol	Merck Millipore	99.9 %
N,N-Dimethyl formamide	Merck Millipore	≥ 99.5 %
N-Methyl-2-Pyrrolidone	Merck Millipore	≥ 99.7 %
Tetrahydrofuran	Carl Roth	≥ 99.9 %
Toluene	VWR	100 %

Experimental part

The listed compounds were used without further purification, unless mentioned in the following. The molecular weight series of poly(propylene oxide) (PPG) with number average molar weights of 430 g·mol⁻¹ (Desmophen 1262 BD, PPG400), 1 000 g·mol⁻¹ (Desmophen 1111 BD, PPG1k), 2 000 g·mol⁻¹ (Acclaim 2200, PPG2k), 4 000 g·mol⁻¹ (Acclaim 4200, PPG4k) and poly(ethylene oxide) with a number average molar weight of 590 g·mol⁻¹ (Desmophen L300, PEO600) were dried for 2 hours at 80 °C under reduced pressure of 50 mbar prior to the experiments. Concerning SP calculation it is important to note, that the EO content in PEO600 amounts to 86.6 wt.% and that there is process-related PO and starter molecule content (i. e. 1,2-propylene glycol) of 0.6 wt.% and 12.8 wt.% respectively.^[31] The relevant characteristics of the macrodiols are listed in Table 6-2.

Table 6-2. Characteristics of the linear difunctional polyether polyols.

Polyol	M_n^a [g·mol ⁻¹]	M_w^a [g·mol ⁻¹]	PDI^a	$OH\#^b$ [mg KOH g ⁻¹]	M_n^c [g·mol ⁻¹]	ρ^b [g·cm ⁻³]	V_m^d [cm ³ ·mol ⁻¹]
PPG400	426	501	1.18	260	431	1.00	431
PPG1k	1 331	1 494	1.12	111.4	1 007	1.00	1 007
PPG2k	2 779	2 944	1.06	56.1	2 000	1.01	1 980.2
PPG4k	5 452	7 482	1.37	28	4 007	1.01	3 967.3
PEO600	630	723	1.15	190	590	1.11	531.5

^a Analysed by SEC.

^b based on manufacturer's datasheet.^[157-161]

^c Calculated from OH#.

^d Calculated from M_n and ρ

6.2 Analytical methods

NCO%-content titration

The content of NCO groups in the reaction mixture was determined according to DIN-EN-ISO-11909-2007.^[162] In a typical procedure 400 mg of the reaction mixture were added 10 mL of a 0.2 molar dibutylamine solution in acetone. The mixture is further diluted with 200 mL of acetone and titrated against 0.1 molar hydrochloric acid. The automatic titration was employed on a Titroline 6000 titration unit (SI Analytics). The result is given in weight percentage of the NCO groups with respect to the sample weight.

Differential scanning calorimetry

A TA Instruments Q2000 DSC was used for thermal analysis. It was equipped with an autosampler, a RCS90 refrigerated cooling unit and was calibrated with an indium standard. Samples were prepared in Tzero hermetic aluminium pans which were perforated to secure N₂ atmosphere over the sample during the analysis. Analogue to the SEC experiments, ITPU samples were quenched with methanol prior to the analysis. If not noted otherwise three cycles from -90 °C to 150 °C were run at a heating rate of 20 °C·min⁻¹. If deviating heating rates were applied, they are mentioned in the respective result. The results of the second cycle were used for evaluation. Before the relevant second cycle the samples were held at 150 °C for 5 minutes to ensure proper diffusion/mixing.

In-line FTIR spectroscopy

The FTIR spectra were collected on a Thermo Fisher Nicolet iS50 spectrometer equipped with a probe coupler and a ZnSe ATR probe FlexiSpec[®] from art photonics GmbH, Berlin. The HgCdTe detector was cooled by liquid nitrogen. On basis of the Thermo Fisher software package “*Macros Basic*” a script was developed to automatically collect 1 spectrum per minute with 64 scans at a resolution of 2 cm⁻¹. After collection of the background spectrum in dried N₂ the ATR probe was directly inserted in the sample medium.

The spectrometer and the probe coupler were purged with dried nitrogen to prevent atmospheric absorption especially of carbon dioxide (2 300 cm⁻¹) which overlays the NCO absorption at a wavelength of 2 200 cm⁻¹. A macro was programmed using the “*OMNIC*” software package to calculate the area of the NCO peak in the range from 2 000 – 2 500 cm⁻¹. The difference between the peak area at the beginning $A_{\text{NCO},0}$ and at the end point of the

reaction $A_{\text{NCO, end}}$ was defined as the total converted area $A_{\text{NCO, tc}}$. The degree of conversion DoC at the time t was calculated following Eq.(6-1).

$$DoC(t) = \frac{(A_{\text{NCO},0} - A_{\text{NCO},t})}{A_{\text{NCO},tc}} \quad \text{Eq.(6-1)}$$

Nuclear magnetic resonance spectroscopy

NMR spectra were recorded using a Bruker Ascend 400 spectrometer. If not explicitly stated otherwise deuterated acetone (acetone- d_6) was used as the solvent. Tetramethylsilan was used in all experiments as an internal standard reference. For detailed peak assignments Heteronuclear-Multiple-Bond-Correlation (HMBC) and Heteronuclear-Single-Quantum-Coherence (HSQC) 2D-Experiments were performed.

To study the kinetics of the reaction mixture of secondary (PPG) and primary (PEO) hydroxy groups with HDI, a model experiment was performed as follows:

A polyol mixture comprising 50/50 mol.% PEO600 und PPG2k is reacted at 80 °C with HDI at an index of 1.5 with the catalyst amount equivalent to the amounts in chapter 6.3 14.34 g (0.0242 mol) PEO600 and 48.45 g (0.0242 mol) PPG2k were introduced into a round-bottom flask equipped with a magnetic stirrer and added by 18.5 μL catalyst solution. The mixture is held at 80 °C and 50 mbar for 2 hours to remove water traces. With addition of 12.32 g (0.0727 mol) of HDI the reaction was started. For NMR analysis, 50 μL of the reaction mixture were dissolved in acetone- d_6 and immediately analysed at 298 K. In parallel, NCO%-content is analysed by titration in regular intervals. The peak intensities were referenced on the 8 hydrogens of the β, γ - CH_2 groups of the HDI segment.

In addition to the kinetic study, NMR was used to analyse the composition of the isolated phases of the ITPUs (see chapter 6.4). For sample preparation 70 μL of dissolved samples were dried in a vacuum oven for 1 hour to retain 30 mg of dried ITPU. The remaining sample was dissolved in deuterated acetone (acetone- d_6) and analysed at 298 K. The peak intensities were referenced on the 4 hydrogens of the α - CH_2 groups of the HDI segment.

Optical microscopy

The micrographs were taken on a Motic BA310E microscope equipped with a 5 megapixel Moticam 5. A drop of the emulsion was placed on a microscope slide and covered with a cover glass. The recorded pictures were processed with the software “*ImageJ*” to optimize contrast and brightness.

Size exclusion chromatography

Gel permeation chromatography (GPC) was carried out on a PSS Polymer SECcurity system based on Agilent 1260 hardware modules equipped with SECcurity isocratic pump, vacuum degasser, refractive index and UV-Vis detector (254 nm), column oven and standard autosampler. A styrene-divinylbenzene copolymer column with 5 μm particle size and 1 000 Å porosity was calibrated with polystyrene ReadyCal Kit (PSS Polymer) standards. Measurements were carried out in tetrahydrofuran at 30 °C with a flow rate of 1.0 mL·min⁻¹. Samples contained ~1 wt.% substance in THF. Polyol samples were analysed without further preparation, while the ITPU samples were quenched with methanol prior to the measurement to prevent uncontrolled chain extension. Excess methanol was removed by rotary evaporation prior to the analysis.

In-line UV-vis spectrometry

UV-Vis transmission analysis was carried out on a Thermo Fisher Evolution 220 spectrometer equipped with an Evolution Fibre Optic Coupler. A Hellma Falcata 6 probe with 10 mm optical path length was used. The transmission was determined at a fixed wavelength of 633 nm. The optically clear state of the analysed mixture was used as reference for 100 % transmission (I_0). The turbidity τ was calculated according to Eq.(6-2), where I_0 and I are the light intensity before and after passing the optical path length d in cm. ^[163]

$$\tau = \frac{-1}{d} \cdot \ln \frac{I(633 \text{ nm})}{I_0(633 \text{ nm})} \quad \text{Eq.(6-2)}$$

6.3 Synthesis of isocyanate-terminated polyurethanes

ITPUs with mixed soft-segments were prepared by a one-pot synthesis. A molar ratio of isocyanate to hydroxyl groups of 3:2 (index = 1.5) was employed for all reactions. Polyadditions to yield the NCO-terminated PU were catalysed by a $0.266 \text{ mol}\cdot\text{L}^{-1}$ solution of dibutyltin dilaurate in tetrahydrofuran.

To study the PPG/PEO600 soft segment miscibility in the ITPU, each macrodiol combination (1:1 wt./wt.) was reacted with HDI to yield the bi-soft segment ITPU (see Table 6-3). The reactions were performed at room temperature under nitrogen atmosphere in snap-cap bottles. 100 ppm of catalyst solution was added to the reaction mixture of total 5 grams. The bottles were placed on a roller mixer to ensure proper mixing throughout the reaction. The polyaddition was allowed to proceed until a constant NCO%-content or $\text{NCO}\%_{\text{theo}}$ was reached.

Table 6-3. Experimental details in the synthesis of PPG/PEO600 bi-soft segment ITPUs.

Soft segment	Polyol composition [wt.%]		Polyol content in ITPU [wt.%]	HDI content in ITPU [wt.%]	DBTDL solution [μL]	$\text{NCO}\%_{\text{theo}}$	NCO%
	PEO600	PPG2k	[wt.%]	[wt.%]	[μL]		
PPG400/PEO600	50	50	66.3	33.7	6.3	5.59	5.38
PPG1k/PEO600	50	50	74.6	25.4	4.7	4.21	4.33
PPG2k/PEO600	50	50	78.24	21.76	4.0	3.61	3.69
PPG4k/PEO600	50	50	80.24	19.76	3.7	3.28	3.24

Reaction monitoring was performed on reaction mixtures comprising PPG2k/PEO600 and HDI. Table 6-4 lists all information regarding the composition and notation of the reaction mixtures. The experiments were designed to obtain 250 grams of product. To minimize the difference in reaction time throughout the experiments and to inhibit undesirable rises of the reaction temperature due to the exothermic reaction, the volume of catalyst solution V_{cat} was varied. Based on preliminary experiments, the catalyst solution was dosed in dependency on the initial volume fraction of HDI Φ_{HDI} according to Eq.(6-3). This ensured comparable reaction times and constant reaction temperatures at different polyol mixtures.

$$V_{\text{cat}} = -243.5 \mu\text{L} * \Phi_{\text{HDI}} + 96.325 \mu\text{L} \quad \text{Eq.(6-3)}$$

In a typical procedure to obtain an ITPU containing 50:50 vol.% polyol composition, the dried polyols, PEO600 (101.85 g, 0.172 mol) and PPG2k (92.68 g, 0.046 mol), were introduced into a 250 mL flat flange reaction vessel that was heated to the reaction temperature of $T = 80\text{ }^{\circ}\text{C}$ via a thermal jacket. A mechanical stirrer assured proper mixing. Temperature was controlled by a Julabo FN-25 refrigerated circulator and recorded by an Omega TC-08 thermocouple data logger.

The calculated amount of catalyst solution was then added to the polyol mixture. Immediately with addition of HDI (55.47 g, 0.328 mol), the UV-Vis and FTIR data collection is started. The NCO%-content is determined titrimetrically in regular intervals to analyse the reaction progress. The reaction was allowed to proceed until a constant NCO%-content or $\text{NCO}\%_{\text{theo}}$ was reached.

Table 6-4. Notation and composition of the PPG2k/PEO600 bi-soft segment ITPUs.

Code	Polyol composition [mol.%]		Polyol composition [vol.%]		Polyol content in ITPU [vol.%]	Φ_{HDI}	NCO% _{theo}	NCO%
	PEO600	PPG2k	PEO600	PPG2k				
ITPU 1	97	3	90	10	73.4	0.266	4.75	4.67
ITPU 2	94	6	80	20	75.0	0.25	4.50	4.50
ITPU 3	90	10	70	30	76.6	0.234	4.25	4.25
ITPU 4	85	15	60	40	78.3	0.217	3.97	4.01
ITPU 5	79	21	50	50	80.1	0.199	3.68	3.69
ITPU 6	71	29	40	60	82.0	0.180	3.36	3.21
ITPU 7	61	39	30	70	84.0	0.160	3.03	3.09
ITPU 8	48	52	20	80	86.1	0.139	2.67	2.67
ITPU 9	29	71	10	90	88.2	0.118	2.28	2.30
ITPU 10	-	100	-	100	90.5	0.095	1.86	1.98
ITPU 11	100	-	100	-	71.9	0.281	4.98	5.02
ITPU 12	50	50	21	79	85.8	0.142	2.71	2.73

6.4 Phase isolation and composition analysis

To get detailed information about the composition of the dispersed phases, the turbid ITPUs were centrifuged to separate them quantitatively prior to analysis. For this purpose, samples of each ITPU were placed in falcon tubes under nitrogen atmosphere and centrifuged

at 8 000 RPM for 4 hours at 30 °C in a Sorvall RC5b centrifuge equipped with a SLA3000 rotor. The upper phase is symbolized prime and the lower phase double prime. Subsequently, approximately 0.3 g of sample was drawn from each phase with a Pasteur pipette. In case of persisting turbid dispersed appearance, samples were drawn at the top and bottom of the falcon tubes. The drawn samples were reacted with methanol for 24 hours to quench the reactive NCO groups prior to analysis. Excess methanol was removed by rotary evaporation and the resulting sample was dissolved in two mass equivalents THF to reduce the viscosity and facilitate handling.

¹H-NMR spectra were recorded using a Bruker Ascend 400 spectrometer. For sample preparation 70 μL of dissolved samples were dried in a vacuum oven for 1 hour to retain 30 mg of prepolymer for analysis. The remaining sample is dissolved in deuterated acetone and analysed at 298 K.

For detailed peak assignments Heteronuclear-Multiple-Bond-Correlation (HMBC) and Heteronuclear-Single-Quantum-Coherence (HSQC) 2D-Experiments were performed. This allows for discrimination between the α-CH₂- and α-CH(CH₃)- groups coming from the PEO and PPG bonding to the urethane moieties. Using this information the PPG and PEO content in the respective phases was determined from the ¹H-NMR spectra.

The molecular weight distribution of the isolated phases was analysed by SEC. For sample preparation 40 μL of the dissolved samples was introduced in a vial and diluted with 1 460 μL THF. SEC analysis was performed as described in 6.2.

6.5 Determination of the solubility parameters

The methods of Fedors and Hoy for calculation of the SP allow for dividing molecules in small (functional) parts each of them contributing to the energy of vaporization and the molar volume. As depicted in Figure 6-1, the polyols were divided in propylene oxide (PO), ethylene oxide (EO) and OH-functional units, latter representing the end of the chain. In addition to these parts, the process-related starter molecule (1,2-propylene glycole) was considered as well. The average numbers of PO and EO repeating units in the polyols m_{PO} and m_{EO} were calculated on basis of the manufacturer's information about the number averaged molar weight and the EO-content.

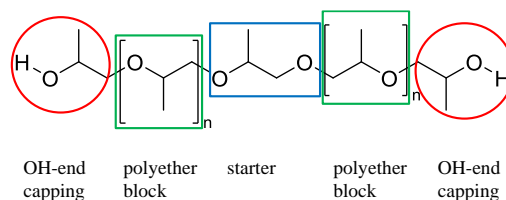


Figure 6-1. Schematic partitioning of the polyether polyol structure for the calculation of the SP.

The molar contributions of typical polyether functional groups were derived to facilitate the mathematical procedure (Table 6-5). The energy of vaporisation and molar volumes were calculated by summing up all chemical units following Eq.(6-4) and Eq.(6-5).

$$E_i = e_{i,\text{starter}} + m_{\text{EO}} \cdot e_{i,\text{EO}} + m_{\text{PO}} \cdot e_{i,\text{PO}} + 2 \cdot e_{i,\text{HO-unit}} \quad \text{Eq.(6-4)}$$

$$V_i = v_{i,\text{starter}} + m_{\text{EO}} \cdot v_{i,\text{EO}} + m_{\text{PO}} \cdot v_{i,\text{PO}} + 2 \cdot v_{i,\text{HO-unit}} \quad \text{Eq.(6-5)}$$

Table 6-5. Derived group contributions for typical chemical units of polyether polyols on basis of Fedors^[90] dataset.

Functional group	Unit	e_i [cal·mol ⁻¹]	v_i [cm ³ ·mol ⁻¹]
PO	O-CH(CH ₃)-CH ₂ -	3 925	52.4
PO-OH	HO-CH(CH ₃)-CH ₂ -	10 245	58.6
EO	O-CH ₂ -CH ₂ -	3 160	36
EO-OH	HO-CH ₂ -CH ₂ -	9 480	42.2
PO starter	O-CH(CH ₃)-CH ₂ -O	4 725	56.2

In the case of Fedors' GCT the Hildebrand SP are given by Eq.(6-6).

$$\delta = \left(\frac{E_i}{V_i} \right)^{1/2} \quad \text{Eq.(6-6)}$$

As Hoy discriminates between small molecules and macromolecules, the SPs of the polyols were calculated on basis of the approach for macromolecules whereas HDI was regarded as a small molecule. The set of equations is listed in Table 3-5. For the

determination of the SP of HDI, Stefanis' GCT was applied in addition to Fedors' and Hoy's approach.

Besides these mathematical methods, the HSP of HDI was determined by miscibility experiments. HDI (1 mL) was mixed with 5 mL of each of the 21 different solvents listed in Table 6-6 in a glass tube and vigorously vortexed for 1 minute. The HSPs of the solvents are known from Barton.^[77] It was visually evaluated if HDI was either soluble or not soluble in the solvent. Hence, there is a three dimensional solubility radius where the centre (δ_D , δ_P , δ_H) was regarded as the resulting HSP. Using an excel sheet provided by the group of Hansen,^[164] the HSP of the compound was determined.

Table 6-6. Solvents and their respective HSPs used in the solubility tests.^[165]

Solvent	δ_D [MPa ^{1/2}]	δ_P [MPa ^{1/2}]	δ_H [MPa ^{1/2}]
1,2-Butandiol	16.6	10	21.5
1,3-Propylene glycole	16.8	9.4	23.3
1,4-Dioxane	17.5	1.8	9
1-Propanol	16	6.8	17.4
Acetone	15.5	10.4	7
Acetonitrile	15.3	18	6.1
Chlorobenzene	19	4.3	2
Chloroform	17.8	3.1	5.7
Cyclohexane	16.8	0	0.2
Diethyl ether	14.5	2.9	4.6
Dimethyl sulfoxide	18.4	16.4	10.2
Ethanol	15.8	8.8	19.4
Ethylene glycole	17	11	26
Ethyl acetate	15.8	5.3	7.2
Glycerol	17.4	12.1	29.3
Hexane	14.9	0	0
Methanol	14.7	12.3	22.3
N-Methyl-2-Pyrrolidone	18	12.3	7.2
N,N-Dimethyl formamide	17.4	13.7	11.3
Tetrahydrofuran	16.8	5.7	8
Toluene	18	1.4	2

6.6 Determination of cloud points

Cloud point curve analysis of the polyol mixtures with limited miscibility was carried out via in-line UV-vis spectrometry in a 250 mL flat flange reaction vessel that was heated via a thermal jacket and equipped with a mechanical stirrer. Temperature was controlled by a Julabo FN-25 refrigerated circulator. Temperature of the liquid mixtures was recorded by an Omega TC-08 thermocouple data logger. Samples ranging from 0 to 100 vol. % were evaluated. The temperature and UV-Vis probes were inserted directly into the sample liquid.

The sample was heated up till it became an optically clear mixture and was held at the temperature for 10 minutes to reach equilibrium state. This optically clear state was used as 100 % transmission reference for the analysis. Temperature was then decreased in 5 K steps and the aimed temperature was held for at least 10 minutes to minimize kinetic effects. The cloud point is defined as the temperature where the turbidity increases drastically.

Cloud points of the ternary mixture PPG/PEO/HDI were determined titrimetrically. Polyol mixtures with compositions ranging from 10 – 90 vol.% PEO600 content were prepared and HDI was added stepwise under stirring until the mixture becomes optically clear. The volume fractions (ϕ_{PPG2k} , ϕ_{PEO600} , ϕ_{HDI}) at the point of turbidity loss are regarded as the cloud point.

6.7 Binodal composition analysis by size exclusion chromatography

In comparison to the cloud points binodal compositions at distinct temperatures were determined by size exclusion chromatography. Phase separating 50:50 wt.% polyol mixtures were held at temperatures ranging from 25 – 160 °C for at least 22 hours under nitrogen until two clear phases are observed. Each phase is analysed by SEC and the respective weight percentage of the PEO600 and PPG2k is calculated by integration of the respective signal. Weight percentages are converted to volume percentages using the specific gravities ρ . (see Table 6-2 for ρ values)

6.8 Computational determination of phase diagrams

Binary polyol mixtures

The determined SPs were used to compute the phase diagrams of the compounds with limited miscibility. Flory-Huggins lattice theory can be applied to derive the free energy of mixing ΔG_{Mix} of polymer A and B.^[30] Here Coleman's and Painter's modified FH approach was used as it is given by Eq.(6-7).^[85] ϕ_i is the volume fraction of the polymers and χ is the FH interaction parameter. N_i the polymerization degree given by the fraction of the molar volume of the substance V_m divided by an arbitrarily chosen reference volume V_{ref} . In this study the molar volume of one propylene oxide unit according to Fedors ($V_{PO} = 52.4 \text{ cm}^3 \cdot \text{mol}^{-1}$) was set as V_{ref} . T is the absolute temperature in Kelvin and R is the molar gas constant.

$$g = \frac{\Delta G_{Mix}}{RT} \cdot \frac{V_{ref}}{V} = \frac{\phi_A}{N_A} \cdot \ln(\phi_A) + \frac{\phi_B}{N_B} \cdot \ln(\phi_B) + \chi_{A,B} \cdot \phi_A \cdot \phi_B \quad \text{Eq.(6-7)}$$

The FH interaction parameter for the binary system is based on the SPs δ_i as given by Eq.(6-8).

$$\chi_{A,B} = V_{ref} \cdot \frac{(\delta_A - \delta_B)^2}{R \cdot T} \quad \text{Eq.(6-8)}$$

For the calculation of the phase diagram the thermodynamic criteria for binodal conditions was used as given by Eq.(6-9).

$$\left(\frac{\partial \Delta G_{Mix}}{\partial \phi_i} \right)'_{P,T,n_j} = \left(\frac{\partial \Delta G_{Mix}}{\partial \phi_i} \right)''_{P,T,n_j} \quad \text{Eq.(6-9)}$$

Hence, Eq.(6-10) for both compounds and the volume fraction balances for phase 1 and 2 in Eq.(6-11) were used to define an objective function (OBJ) that had to be numerically solved. Additionally the shared tangent between the two phases (' and ') given in Eq.(6-12) was constructed used as condition for the binodal points.

$$\left(\frac{\partial \Delta G_{Mix}}{\partial \phi_A}\right)'_{P,T,n_j} - \left(\frac{\partial \Delta G_{Mix}}{\partial \phi_A}\right)''_{P,T,n_j} = 0; \text{ for } A \text{ and } B \quad \text{Eq.(6-10)}$$

$$\phi'_A + \phi'_B - 1 = 0; \text{ for phase ' and ''} \quad \text{Eq.(6-11)}$$

$$g(\phi'_A) - \phi'_A \cdot \left(\frac{\partial \Delta G_{Mix}}{\partial \phi_A}\right)^{\phi'_A}_{P,T,n_j} - g(\phi''_A) - \phi''_A \cdot \left(\frac{\partial \Delta G_{Mix}}{\partial \phi_A}\right)^{\phi''_A}_{P,T,n_j} = 0 \quad \text{Eq.(6-12)}$$

To avoid the trivial solution where each phase has the same composition, the penalty function $(\phi_A - \phi_B)^{-4}$ was applied to each operator.^[109] The equation matrix in Eq.(6-13) for determination of the binodal curve was numerically solved by MATLABs lsqnonlin solver till it reached a sum $\leq 10^{-10}$.

$$OBJ = \begin{bmatrix} Eq. (5 - 10) \cdot (\phi_A - \phi_B)^{-4} \\ Eq. (5 - 10) \cdot (\phi_A - \phi_B)^{-4} \\ Eq. (5 - 11) \cdot (\phi_A - \phi_B)^{-4} \\ Eq. (5 - 11) \cdot (\phi_A - \phi_B)^{-4} \\ Eq. (5 - 12) \cdot (\phi_A - \phi_B)^{-4} \end{bmatrix} \quad \text{Eq.(6-13)}$$

The binodal was calculated by a self-made MATLAB script (see Appendix IV-25) for a temperature scale from 20 to 160 °C.

Ternary mixtures

The computational method for the determination of the equilibrium phases of the reactive ternary mixtures is based on the FH approach for ternary mixtures consisting of a solvent and two polymers described by Hsu and Prausnitz.^[109] The Gibbs free energy for these systems is given by Eq.(6-14) where n_i is the amount of substance i , ϕ_i its volume fraction, χ_{ij} the respective binary interaction parameters and N_i is the ratio of the molar volume to that of the reference volume. Again the binary interaction parameters χ_{ij} are defined by Eq.(6-8).

$$\frac{\Delta G_{Mix}}{RT} = n_A \cdot \ln(\phi_A) + n_B \cdot \ln(\phi_B) + n_s \cdot \ln(\phi_s) + \left(\begin{array}{c} \chi_{A,B} \cdot \phi_A \cdot \phi_B + \chi_{A,s} \cdot \phi_A \cdot \phi_s + \\ \chi_{B,s} \cdot \phi_B \cdot \phi_s \end{array} \right) \cdot (N_A \cdot n_A + N_B \cdot n_B + N_s \cdot n_s) \quad \text{Eq.(6-14)}$$

The MATLAB script used the condition that the chemical potentials μ_i (Eq.(6-15)) are equal in the separate phases at the binodal.

$$\frac{\Delta \mu_A}{RT} = \ln(\phi_A) + \left[1 - \left(\frac{N_A}{N_B} \right) \right] \cdot \phi_B + (1 - N_A) \cdot \phi_s + N_A \cdot [\chi_A \cdot (\phi_B + \phi_s)^2 + \chi_B \cdot \phi_B^2 + \chi_s \cdot \phi_s^2] \quad \text{Eq.(6-15)}$$

with $\chi_A = 0.5 \cdot (\chi_{AS} + \chi_{AB} - \chi_{BS})$

The binodal curve was calculated by solving the non-linear equation (Eq.(6-16)) with fixed volume fractions of the solvent (HDI) till the sum reached $< 10^{-10}$. For this purpose, an algorithm has been implemented in MATLAB. It increases the HDI content at equidistant steps and computes the corresponding volume fractions of compound A and B. (see Appendix IV-26)

$$OBJ = \begin{bmatrix} \left(\frac{\Delta\mu_A'}{RT} - \frac{\Delta\mu_A''}{RT} \right)^2 \cdot (\phi_A' - \phi_A'')^{-4} \\ \left(\frac{\Delta\mu_B'}{RT} - \frac{\Delta\mu_B''}{RT} \right)^2 \cdot (\phi_B' - \phi_B'')^{-4} \\ \left(\frac{\Delta\mu_S'}{RT} - \frac{\Delta\mu_S''}{RT} \right)^2 \\ (1 - \phi_A - \phi_B - \phi_S)'^2 \\ (1 - \phi_A - \phi_B - \phi_S)''^2 \\ \left(\frac{\Delta\mu_S'}{RT} - \frac{\Delta\mu_S''}{RT} \right)^2 \end{bmatrix} \quad \text{Eq.(6-16)}$$

7 References

- [1] Author not mentioned, I.G. Farbenindustrie AG. in Frankfurt, Main, *Verfahren zur Herstellung von Polyurethanen bzw. Polyharnstoffen*, 1942, Patent No. 728981.
- [2] O. Bayer, *Angew. Chem.*, **1947**, 59, 9, 257–272.
- [3] D. Dieterich, *Chem. Unserer Zeit*, **1990**, 24, 3, 135–142.
- [4] G. Oertel, *Polyurethane Handbook*. Carl Hanser, **1993**.
- [5] D. K. Chattopadhyay, K. Raju, *Prog. Polym. Sci.*, **2007**, 32, 3, 352–418.
- [6] U. Meier-Westhues, *Polyurethane: Lacke, Kleb- und Dichtstoffe*. Vincentz Network, **2007**.
- [7] E. Delebecq, J.-P. Pascault, B. Boutevin, F. Ganachaud, *Chem. Rev.*, **2013**, 113, 1, 80–118.
- [8] P. Król, *Prog. Mater. Sci.*, **2007**, 52, 6, 915–1015.
- [9] I. Yilgor, E. Yilgor, *Polym. Rev.*, **2007**, 47, 4, 487–510.
- [10] E. Yilgör, İ. Yilgör, E. Yurtsever, *Polymer*, **2002**, 43, 24, 6551–6559.
- [11] I. Yilgör, E. Yilgör, G. L. Wilkes, *Polymer*, **2015**, 58, 0, A1 - A36.
- [12] M. Ionescu, *Chemistry and technology of polyols for polyurethanes*. Rapra Technology Ltd., Shawbury, Shrewsbury, Shropshire, SY4 4NR, U.K., **2005**.
- [13] Y. C. Chou, L. J. Lee, *Polym. Eng. Sci.*, **1994**, 34, 16, 1239–1249.
- [14] W. Li, A. J. Ryan, I. K. Meier, *Macromolecules*, **2002**, 35, 13, 5034–5042.
- [15] W. R. Willkomm, Z. S. Chen, C. W. Macosko, D. A. Gobran, E. L. Thomas, *Polym. Eng. Sci.*, **1988**, 28, 14, 888–900.
- [16] S. P. Ertem, E. Yilgor, C. Kosak, G. L. Wilkes, M. Zhang, I. Yilgor, *Polymer*, **2012**, 53, 21, 4614–4622.
- [17] C. H. Y. Chen, R. M. Briber, E. L. Thomas, M. Xu, W. J. MacKnight, *Polymer*, **1983**, 24, 10, 1333–1340.
- [18] S. Velankar, S. L. Cooper, *Macromolecules*, **2000**, 33, 2, 382–394.
- [19] J. Liu, D. Ma, Z. Li, *Eur. Polym. J.*, **2002**, 38, 4, 661–665.
- [20] R. Adhikari, P. A. Gunatillake, S. J. McCarthy, G. F. Meijs, *J. Appl. Polym. Sci.*, **2000**, 78, 5, 1071–1082.
- [21] D. P. Queiroz, de Pinho, Maria N., C. Dias, *Macromolecules*, **2003**, 36, 11, 4195–4200.
- [22] E. Yildirim, M. Yurtsever, G. L. Wilkes, I. Yilgör, *Polymer*, **2016**, 90, 204–214.

- [23]J. W. Cho, Y. C. Jung, Y.-C. Chung, B. C. Chun, *J. Appl. Polym. Sci.*, **2004**, *93*, 5, 2410–2415.
- [24]C.-t. Zhao, M. Norberta de Pinho, *Polymer*, **1999**, *40*, 22, 6089–6097.
- [25]D. P. Queiroz, M. C. Gonçalves, M. Norberta de Pinho, *J. Appl. Polym. Sci.*, **2007**, *103*, 1, 315–320.
- [26]D. P. Queiroz, M. Norberta de Pinho, *Desalination*, **2002**, *145*, 1–3, 379–383.
- [27]D. P. Queiroz, A. M. Botelho do Rego, M. Norberta de Pinho, *J. Membr. Sci.*, **2006**, *281*, 1–2, 239–244.
- [28]W. Bras, G. E. Derbyshire, D. Bogg, J. Cooke, M. J. Elwell, B. U. Komanschek, S. Naylor, A. J. Ryan, *Science*, **1995**, *267*, 5200, 996–999.
- [29]R. E. Camargo, C. W. Macosko, M. V. Tirrell, S. T. Wellinghoff, *Polym. Eng. Sci.*, **1982**, *22*, 11, 719–728.
- [30]P. J. Flory, *J. Chem. Phys.*, **1942**, *10*, 1, 51–61.
- [31]private communication with Covestro Deutschland AG.
- [32]J. Hildebrand, R. Scott, *The Solubility of Non-electrolytes*. Reinhold Publishing Corp., New York, **1949**.
- [33]C. Qian, S. J. Mumby, Eichinger, B. E., *Macromolecules*, **1991**, *24*, 7, 1655–1661.
- [34]R. Koningsveld, L. A. Kleintjens, *J. Polym. Sci., C Polym. Symp.*, **1977**, *61*, 1, 221–249.
- [35]R.-J. Roe, L. Lu, *J. Polym. Sci., Part B: Polym. Phys.*, **1985**, *23*, 5, 917–924.
- [36]H. Ulrich, *Chemistry and technology of isocyanates*. J. Wiley & Sons, Chichester, New York, **2001**.
- [37]S. G. Entelis, O. V. Nesterov, *Russ. Chem. Rev.*, **1966**, *35*, 12, 917.
- [38]A. M. Heintz, D. J. Duffy, S. L. Hsu, W. Suen, W. Chu, C. W. Paul, *Macromolecules*, **2003**, *36*, 8, 2695–2704.
- [39]G. Wegener, M. Brandt, L. Duda, J. Hofmann, B. Kleszczewski, D. Koch, R.-J. Kumpf, H. Orzesek, H.-G. Pirkl, C. Six, C. Steinlein, M. Weisbeck, *Appl. Catal., A*, **2001**, *221*, 1–2, 303–335.
- [40]K. C. Frisch, L. P. Rumao, *J. Macromol. Sci., Polym. Rev.*, **1970**, *5*, 1, 103–149.
- [41]W. J. Blank, Z. A. He, E. T. Hessell, *Prog. Org. Coat.*, **1999**, *35*, 1–4, 19–29.
- [42]R. van Maris, Y. Tamano, H. Yoshimura, K. M. Gay, *J. Cell. Plast.*, **2005**, *41*, 4, 305–322.

- [43]F. E. Bailey, J. V. Koleske, *Alkylene oxides and their polymers*. Dekker, New York, **1991**.
- [44]Deutsches Institut für Normung e. V., November 2007, DIN 53240-2:2007-11, *Bestimmung der Hydroxylzahl - Teil 2: Verfahren mit Katalysator*, Berlin. Beuth.
- [45]B. K. Kim, *Colloid Polym. Sci.*, **1996**, 274, 7, 599–611.
- [46]N. Sheikh, A. A. Katbab, H. Mirzadeh, *Int. J. Adhes. Adhes.*, **2000**, 20, 4, 299–304.
- [47]U. Šebenik, M. Krajnc, *Int. J. Adhes. Adhes.*, **2007**, 27, 7, 527–535.
- [48]S. Clauß, D. J. Dijkstra, J. Gabriel, O. Kläusler, M. Matner, W. Meckel, P. Niemz, *Int. J. Adhes. Adhes.*, **2011**, 31, 6, 513–523.
- [49]P. Cognard, *Handbook of Adhesives and Sealants: Basic Concepts and High Tech Bonding*. Elsevier, Amsterdam, **2005**.
- [50]Y. Cui, D. Chen, X. Wang, X. Tang, *Int. J. Adhes. Adhes.*, **2002**, 22, 4, 317–322.
- [51]T. C. Forschner, D. E. Gwyn, H. X. Xiao, B. Suthar, L. Sun, K. C. Frisch, *Adhes. Age*, **1999**, 42, 5, 20.
- [52]D. J. Duffy, A. M. Heintz, H. D. Stidham, S. L. Hsu, W. Suen, C. W. Paul, *Int. J. Adhes. Adhes.*, **2005**, 25, 1, 39–46.
- [53]D. J. Duffy, H. D. Stidham, S. L. Hsu, S. Sasaki, A. Takahara, T. Kajiyama, *J. Mater. Sci.*, **2002**, 37, 22, 4801–4809.
- [54]D. J. Duffy, A. M. Heintz, H. D. Stidham, S. L. Hsu, W. Suen, W. Chu, C. W. Paul, *J. Adhes.*, **2003**, 79, 11, 1091–1107.
- [55]Y. G. Jeong, T. Hashida, C. M. Nelson, S. L. Hsu, C. W. Paul, *Int. J. Adhes. Adhes.*, **2006**, 26, 8, 600–608.
- [56]P. J. Flory, *J. Am. Chem. Soc.*, **1936**, 58, 10, 1877–1885.
- [57]A. Singh, L. Weissbein, *J. Polym. Sci., Part A-1: Polym. Chem.*, **1966**, 4, 10, 2551–2561.
- [58]H. F. Mark, G. S. Whitby, *Collected papers of Wallace Hume Carothers on high polymeric substances*. Interscience Publishers Inc., **1940**.
- [59]M. J. O’Sickey, B. D. Lawrey, G. L. Wilkes, *J. Appl. Polym. Sci.*, **2002**, 84, 2, 229–243.
- [60]E. Yilgör, E. Burgaz, E. Yurtsever, İ. Yilgör, *Polymer*, **2000**, 41, 3, 849–857.
- [61]J. T. Garrett, J. S. Lin, J. Runt, *Macromolecules*, **2002**, 35, 1, 161–168.
- [62]I. Yilgor, E. Yilgor, I. G. Guler, T. C. Ward, G. L. Wilkes, *Polymer*, **2006**, 47, 11, 4105–4114.

- [63] A. Mishra, P. Maiti, *J. Appl. Polym. Sci.*, **2011**, *120*, 6, 3546–3555.
- [64] M. A. Hood, B. Wang, J. M. Sands, J. J. La Scala, F. L. Beyer, C. Y. Li, *Polymer*, **2010**, *51*, 10, 2191–2198.
- [65] Y. Li, W. Kang, J. O. Stoffer, B. Chu, *Macromolecules*, **1994**, *27*, 2, 612–614.
- [66] F. Li, J. Hou, W. Zhu, X. Zhang, M. Xu, X. Luo, D. Ma, B. K. Kim, *J. Appl. Polym. Sci.*, **1996**, *62*, 4, 631–638.
- [67] P. N. Lan, S. Corneillie, E. Schacht, M. Davies, A. Shard, *Biomaterials*, **1996**, *17*, 23, 2273–2280.
- [68] Z. S. Petrović, I. Javni, *J. Polym. Sci., Part B: Polym. Phys.*, **1989**, *27*, 3, 545–560.
- [69] S. Kim, D. Lee, *Macromol. Res.*, **2002**, *10*, 6, 365–368.
- [70] S. Das, D. F. Cox, G. L. Wilkes, D. B. Klinedinst, I. Yilgor, E. Yilgor, F. L. Beyer, *J. Macromol. Sci., Part B: Phys.*, **2007**, *46*, 5, 853–875.
- [71] E. Yilgör, E. Yurtsever, I. Yilgör, *Polymer*, **2002**, *43*, 24, 6561–6568.
- [72] L.-S. Teo, C.-Y. Chen, J.-F. Kuo, *Macromolecules*, **1997**, *30*, 6, 1793–1799.
- [73] W. Wang, W. Wang, X. Chen, X. Jing, Z. Su, *J. Polym. Sci., Part B: Polym. Phys.*, **2009**, *47*, 7, 685–695.
- [74] F.-S. Yen, L.-L. Lin, J.-L. Hong, *Macromolecules*, **1999**, *32*, 9, 3068–3079.
- [75] J. P. Sheth, D. B. Klinedinst, T. W. Pechar, G. L. Wilkes, E. Yilgor, I. Yilgor, *Macromolecules*, **2005**, *38*, 24, 10074–10079.
- [76] J. P. Sheth, D. B. Klinedinst, G. L. Wilkes, I. Yilgor, E. Yilgor, *Polymer*, **2005**, *46*, 18, 7317–7322.
- [77] A. F. M. Barton, *CRC handbook of solubility parameters and other cohesion parameters*. CRC Press, Boca Raton, **1991**.
- [78] C. M. Hansen, *Hansen solubility parameters: A user's handbook*. CRC Press, Boca Raton, **2007**.
- [79] D. Patterson, G. Delmas, *Off. Dig. Fed. Soc. Paint Technol*, **1962**, *34*, 450, 677–692.
- [80] C. M. Hansen, *Ind. Eng. Chem. Prod. Res. Dev.*, **1969**, *8*, 1, 2–11.
- [81] C. M. Hansen, *The three dimensional solubility parameter and solvent diffusion coefficient: Their importance in surface coating formulation*. Dissertation. Technische Hochschule Dänemarks, Copenhagen, **August 11**.
- [82] C. M. Hansen, *J. Paint Techn.*, **1967**, *39*, 505, 104–117.
- [83] C. M. Hansen, *J. Paint Techn.*, **1967**, *39*, 511, 505–510.

- [84]C. M. Hansen, K. Skaarup, *J. Paint Techn.*, **1967**, 39, 511, 511–514.
- [85]M. M. Coleman, J. F. Graf, P. C. Painter, *Specific interactions and the miscibility of polymer blends: Practical guides for predicting & designing miscible polymer mixtures*. Technomic Pub. Co., Lancaster, Pa., U.S.A., **1991**.
- [86]J. E. Mark, *Physical properties of polymer handbook*. Springer, New York, **2006**.
- [87]D. M. Koenhen, C. A. Smolders, *J. Appl. Polym. Sci.*, **1975**, 19, 4, 1163–1179.
- [88]K. L. Hoy, *J. Paint Techn.*, **1970**, 42, 541, 76–118.
- [89]P. A. Small, *J. Appl. Chem.*, **1953**, 3, 2, 71–80.
- [90]R. F. Fedors, *Polym. Eng. Sci.*, **1974**, 14, 2, 147–154.
- [91]D. W. van Krevelen, K. T. Nijenhuis (Eds.), *Properties of Polymers*. Elsevier, Amsterdam, **2009**.
- [92]E. Stefanis, C. Panayiotou, *Int. J. Thermophys.*, **2008**, 29, 2, 568–585.
- [93]E. Stefanis, L. Constantinou, C. Panayiotou, *Ind. Eng. Chem. Res.*, **2004**, 43, 19, 6253–6261.
- [94]A. Fredenslund, J. Gmehling, P. Rasmussen, *Vapor-liquid equilibria using UNIFAC: A group contribution method*. Elsevier Scientific Pub. Co., Amsterdam, **1977**.
- [95]A. Fredenslund, R. L. Jones, J. M. Prausnitz, *AIChE Journal*, **1975**, 21, 6, 1086–1099.
- [96]K. L. Hoy, *J. Coated Fabr.*, **1989**, 19, 1, 53–67.
- [97]K. L. Hoy, *The Hoy Tables of Solubility Parameters*. Union Carbide Solvents and Coatings Materials Division, **1967**.
- [98]A. L. Lydersen, R. A. Greenkorn, O. A. Hougen, *Generalized thermodynamic properties of pure fluids: Report No. 4*, University of Wisconsin. Engineering Experiment Station, **1955**.
- [99]A. L. Lydersen, R. A. Greenkorn, O. A. Hougen, *Estimation of Critical Properties of Organic Compounds by the Method of Group Contributions: Report No. 3*, University of Wisconsin. Engineering Experiment Station, **1955**.
- [100] M. L. Mavrovouniotis, *Ind. Eng. Chem. Res.*, **1990**, 29, 9, 1943–1953.
- [101] M. L. Huggins, *Ann. N. Y. Acad. Sci.*, **1942**, 43, 1, 1–32.
- [102] L. A. Utracki, C. A. Wilkie (Eds.), *Polymer blends handbook*. Springer, Dordrecht, **2014**.
- [103] J. Bicerano, *Prediction of Polymer Properties*. Marcel Dekker Inc, Hoboken, **2002**.

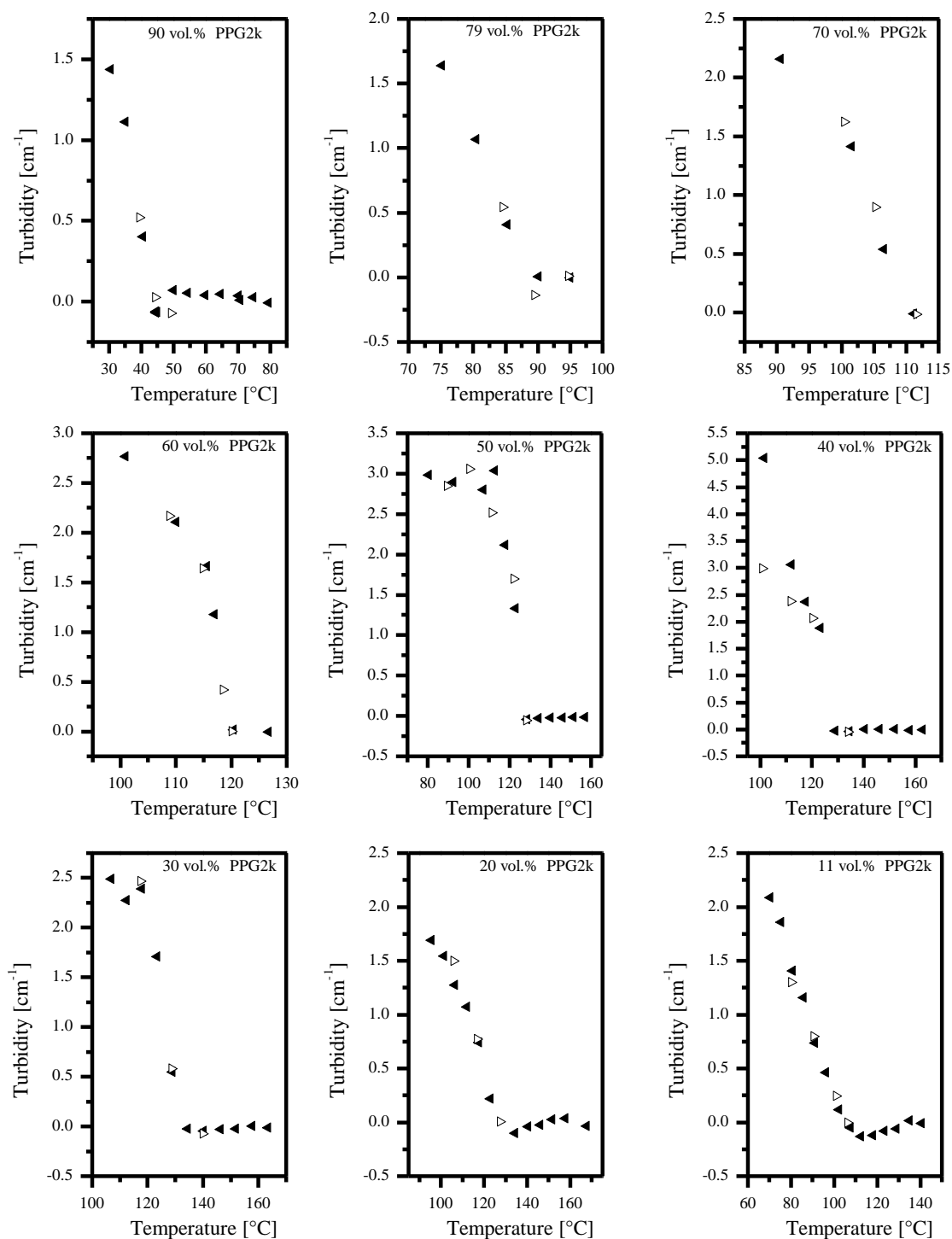
- [104] B. A. Wolf, *Macromol. Theory Simul.*, **2009**, *18*, 1, 30–41.
- [105] R. Koningsveld, L. A. Kleintjens, A. R. Shultz, *J. Polym. Sci., Part A-2*, **1970**, *8*, 8, 1261–1278.
- [106] Y. C. Bae, J. J. Shim, D. S. Soane, J. M. Prausnitz, *J. Appl. Polym. Sci.*, **1993**, *47*, 7, 1193–1206.
- [107] G. R. Strobl, *The physics of polymers: Concepts for understanding their structures and behavior*. Springer, Berlin, New York, **2007**.
- [108] F. S. Bates, *Science*, **1991**, *251*, 4996, 898–905.
- [109] C. C. Hsu, J. M. Prausnitz, *Macromolecules*, **1974**, *7*, 3, 320–324.
- [110] D. R. Cooper, C. Booth, *Polymer*, **1977**, *18*, 2, 164–170.
- [111] A. Friday, D. R. Cooper, C. Booth, *Polymer*, **1977**, *18*, 2, 171–174.
- [112] C. Booth, C. J. Pickles, *J. Polym. Sci., Polym. Phys. Ed.*, **1973**, *11*, 2, 249–264.
- [113] L. A. Utracki, R. Simha, *Polym. Int.*, **2004**, *53*, 3, 279–286.
- [114] G. A. Mannella, V. La Carrubba, V. Brucato, *Rev. Sci. Instrum.*, **2013**, *84*, 7, 75118.
- [115] R. Koningsveld, A. J. Staverman, *Kolloid Z. Z. Polym.*, *218*, 2, 114–124.
- [116] R. Koningsveld, A. J. Staverman, *J. Polym. Sci., Part A-2*, **1968**, *6*, 2, 349–366.
- [117] S. Pramanik, F. Ataollahi, B. Pinguan-Murphy, A. A. Oshkour, N. A. A. Osman, *Sci. Rep.*, **2015**, *5*, 9806 EP -.
- [118] F. M. B. Coutinho, L. C. Rezende, R. Quijada, *J. Polym. Sci., Part A: Polym. Chem.*, **1986**, *24*, 4, 727–735.
- [119] D. Kincal, S. Özkar, *J. Appl. Polym. Sci.*, **1997**, *66*, 10, 1979–1983.
- [120] H. Kothandaraman, A. S. Nasar, *J. Appl. Polym. Sci.*, **1993**, *50*, 9, 1611–1617.
- [121] C. Dubois, S. Désilets, A. Ait-Kadi, P. Tanguy, *J. Appl. Polym. Sci.*, **1995**, *58*, 4, 827–834.
- [122] K. C. Frisch, S. L. Reegen, B. Thir, *J. Polym. Sci., C Polym. Symp.*, **1967**, *16*, 4, 2191–2201.
- [123] H. G. Wissman, L. Rand, K. C. Frisch, *J. Appl. Polym. Sci.*, **1964**, *8*, 6, 2971–2978.
- [124] Q. Han, M. W. Urban, *J. Appl. Polym. Sci.*, **2002**, *86*, 9, 2322–2329.
- [125] L. Thiele, *Monatsh. Chem.*, **1992**, *123*, 10, 865–874.

- [126] T. N. M. Tuan Ismail, K. D. Poo Palam, Z. B. Abu Bakar, H. S. Soi, Y. S. Kian, H. Abu Hassan, C. Schiffman, A. Sendijarevic, V. Sendijarevic, I. Sendijarevic, *J. Appl. Polym. Sci.*, **2016**, *133*, 5, 42955.
- [127] M. L. Matuszak, K. C. Frisch, *J. Polym. Sci. Polym. Chem. Ed.*, **1973**, *11*, 3, 637–648.
- [128] A. D. McNaught, A. Wilkinson, *IUPAC. Compendium of Chemical Terminology, 2nd ed. (the "Gold Book")*. Blackwell Scientific Publications, Oxford, **1997**.
- [129] B. Schrader, D. Bougeard, *Infrared and Raman spectroscopy: Methods and applications*. VCH, Weinheim, New York, **1995**.
- [130] H. H. Li, *J. Phys. Chem. Ref. Data*, **1984**, *13*, 1, 103–150.
- [131] F. Comelli, S. Ottani, *J. Chem. Eng. Data*, **2004**, *49*, 4, 970–975.
- [132] J. Kiefer, K. Frank, M. F. Zehentbauer, P. H. Schuchmann, *Biosensors*, **2016**, *6*, 2.
- [133] J. Kiefer, K. Frank, H. P. Schuchmann, *Appl. Spectrosc.*, **2011**, *65*, 9, 1024–1028.
- [134] C. F. Bohren, D. R. Huffman, *Absorption and scattering of light by small particles*. Wiley, New York, **1983**.
- [135] M. Boulet-Audet, T. Buffeteau, S. Boudreault, N. Daugey, M. Pérolet, *J. Phys. Chem. B*, **2010**, *114*, 24, 8255–8261.
- [136] M. Miljkovic, B. Bird, M. Diem, *Analyst*, **2012**, *137*, 17, 3954–3964.
- [137] B. Mohlenhoff, M. Romeo, M. Diem, B. R. Wood, *Biophys. J.*, **2005**, *88*, 5, 3635–3640.
- [138] P. Bassan, H. J. Byrne, J. Lee, F. Bonnier, C. Clarke, P. Dumas, E. Gazi, M. D. Brown, N. W. Clarke, P. Gardner, *Analyst*, **2009**, *134*, 6, 1171–1175.
- [139] Y. Li, Z. Ren, M. Zhao, H. Yang, B. Chu, *Macromolecules*, **1993**, *26*, 4, 612–622.
- [140] Y. Camberlin, J. P. Pascault, *J. Polym. Sci., Part B: Polym. Phys.*, **1984**, *22*, 10, 1835–1844.
- [141] R. Hernandez, J. Weksler, A. Padsalgikar, T. Choi, E. Angelo, J. S. Lin, L.-C. Xu, C. A. Siedlecki, J. Runt, *Macromolecules*, **2008**, *41*, 24, 9767–9776.
- [142] B. Chu, T. Gao, Y. Li, J. Wang, C. R. Desper, C. A. Byrne, *Macromolecules*, **1992**, *25*, 21, 5724–5729.
- [143] C. B. Wang, S. L. Cooper, *Macromolecules*, **1983**, *16*, 5, 775–786.

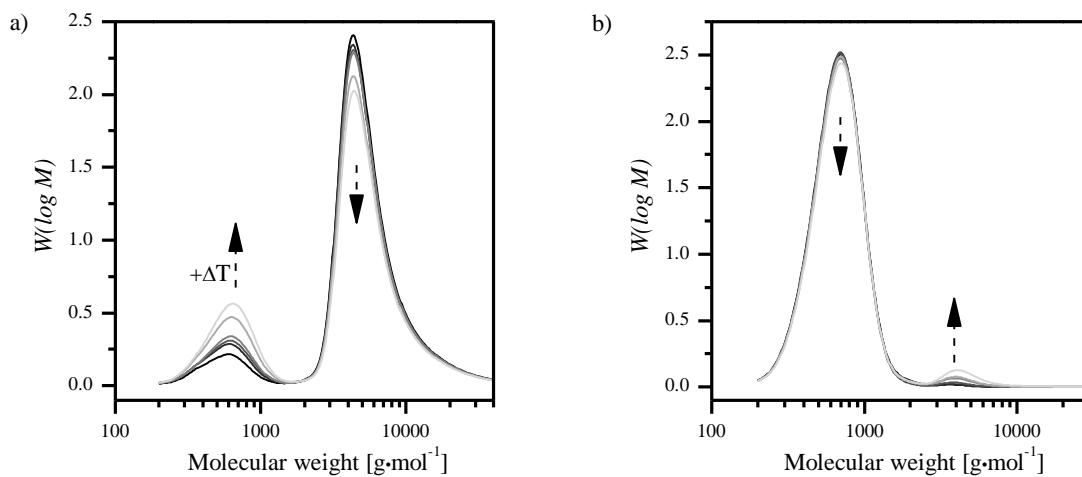
-
- [144] X. Li, W. Fu, Y. Wang, T. Chen, X. Liu, H. Lin, P. Sun, Q. Jin, D. Ding, *Polymer*, **2008**, *49*, 12, 2886–2897.
- [145] D. R. Paul, C. B. Bucknall, *Polymer blends: Formulation and Performance*. Wiley, New York, **2000**.
- [146] W. Brostow, R. Chiu, I. M. Kalogeras, A. Vassilikou-Dova, *Mater. Lett.*, **2008**, *62*, 17–18, 3152–3155.
- [147] T. G. Fox, P. J. Flory, *J. Appl. Phys.*, **1950**, *21*, 6, 581–591.
- [148] Ramamurthi, *Properties and behavior of polymers*. Wiley, Hoboken, N.J., **2011**.
- [149] A. Saiani, A. Novak, L. Rodier, G. Eeckhaut, J.-W. Leenslag, J. S. Higgins, *Macromolecules*, **2007**, *40*, 20, 7252–7262.
- [150] T. K. Chen, T. S. Shieh, J. Y. Chui, *Macromolecules*, **1998**, *31*, 4, 1312–1320.
- [151] P. Gabbott, *Principles and Applications of Thermal Analysis*. Blackwell Publishing Ltd, Oxford, **2008**.
- [152] G. Lagaly, O. Schulz, R. Zimehl, *Dispersionen und Emulsionen: Eine Einführung in die Kolloidik feinverteilter Stoffe einschließlich der Tonminerale*. Steinkopff; Imprint, Heidelberg, **1997**.
- [153] D. Filip, D. Macocinski, S. Vlad, *Eur. Polym. J.*, **2012**, *48*, 3, 464–471.
- [154] Q. Miao, Y. Jin, Y. Dong, Z. Cao, B. Zhang, *J. Polym. Res.*, **2010**, *17*, 6, 911–921.
- [155] I. Hevus, A. Kohut, A. Voronov, *Macromolecules*, **2010**, *43*, 18, 7488–7494.
- [156] P. van de Witte, P. J. Dijkstra, J. van den Berg, J. Feijen, *J. Membr. Sci.*, **1996**, *117*, 1, 1–31.
- [157] Covestro LLC, *Datasheet Acclaim 2200*, <http://www.polyurethanes.covestro.com/Handler/GenericForceDownload.ashx?itemID=9C51A2A0AAA14DF2BF7A6A39083052F7&lang=en>, Accessed 09.02.17.
- [158] Covestro AG, *Datasheet Desmophen L300*, <http://www.polyurethanes.covestro.com/Handler/GenericForceDownload.ashx?itemID=06FF3E23D9364D899FDABEC175D21127&lang=en>, Accessed 21.12.16.
- [159] Covestro AG, *Datasheet Desmophen 1111 BD*, http://www.csc-jaekle.de/fileadmin/MeBl/261/MeBl_261824_DE.pdf, Accessed 24.03.17.
- [160] Covestro AG, *Datasheet Desmophen 1262 BD*, www.csc-jaekle.de/fileadmin/MeBl/261/MeBl_261011_EN.pdf, Accessed 24.03.17.

- [161] Covestro LLC, *Datasheet Acclaim 4200*,
<http://www.polyurethanes.covestro.com/Handler/GenericForceDownload.ashx?itemID=03407F16A9E843DE83AF78AEC560E973&lang=de>, Accessed 24.03.17.
- [162] Deutsches Institut für Normung e. V., May 2007, DIN EN ISO 11909:2007-05,
Bindemittel für Beschichtungsstoffe – Isocyanatharze, Berlin. Beuth.
- [163] D.-Y. Hsu, C.-M. Chou, C.-Y. Chuang, P.-D. Hong, *ACS Macro Lett.*, **2015**, *4*,
12, 1341–1345.
- [164] C. M. Hansen, *HSP_Calculations.xlsx*, http://www.hansen-solubility.com/contents/HSP_Calculations.xlsx, Accessed 21.12.16.
- [165] A. F. M. Barton, *Chem. Rev.*, **1975**, *75*, 6, 731–753.

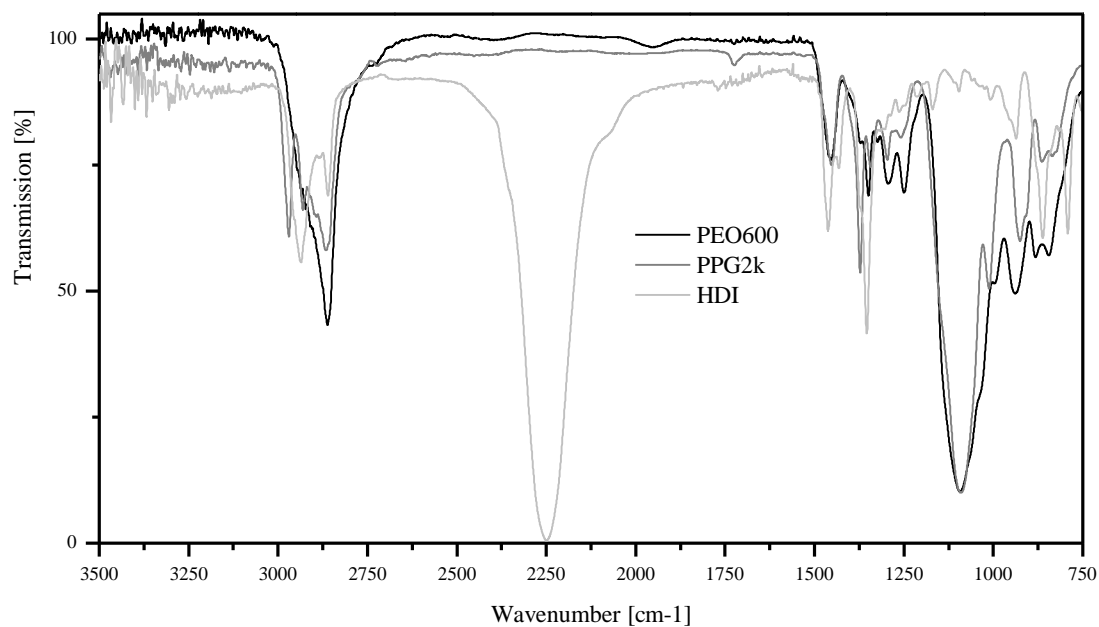
IV Appendix



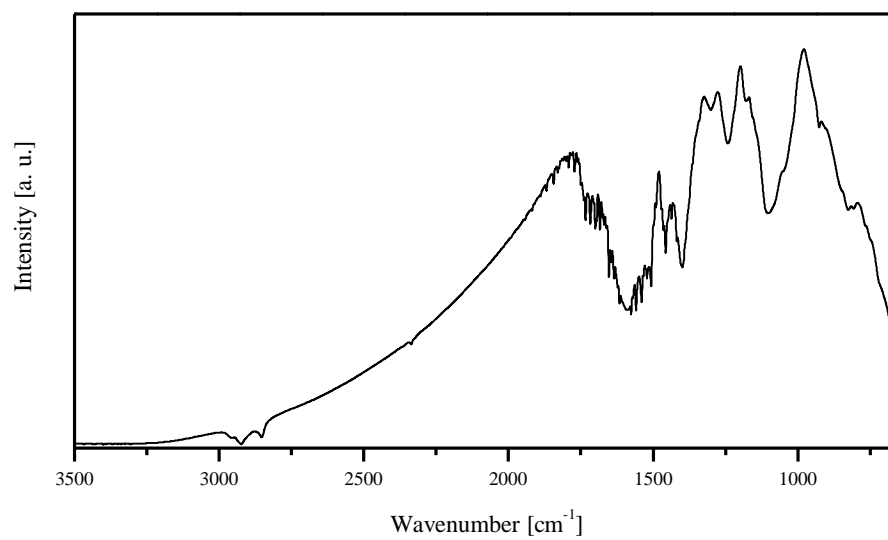
Appendix IV-1. Individual cloud point measurements of the PPG2k/PEO600 mixtures.



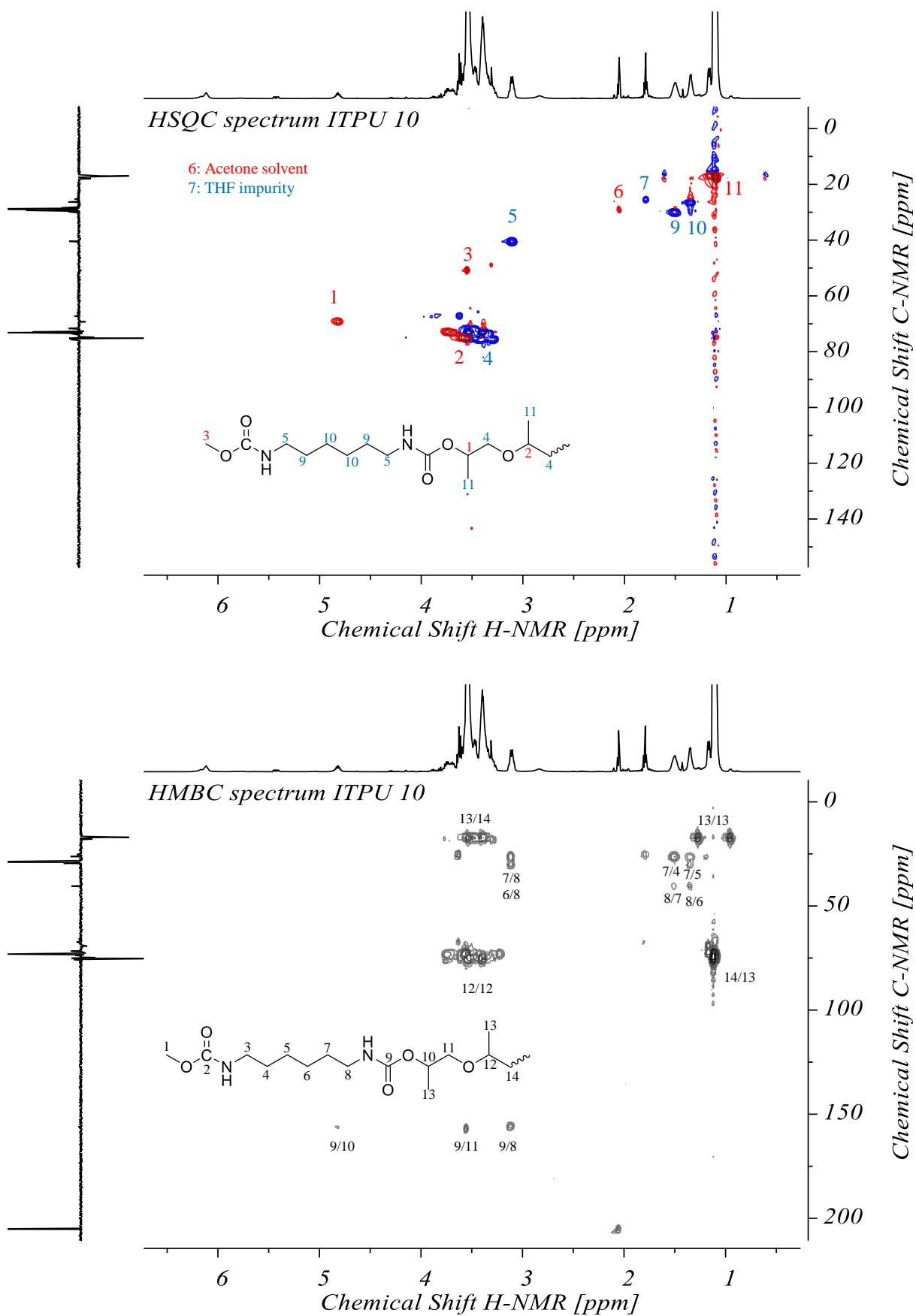
Appendix IV-2. Temperature dependent MWDs of the two phases in PPG4k/PEO600 mixtures. ($T= 50\text{ }^{\circ}\text{C}; 80\text{ }^{\circ}\text{C}; 100\text{ }^{\circ}\text{C}; 120\text{ }^{\circ}\text{C}; 130\text{ }^{\circ}\text{C}; 140\text{ }^{\circ}\text{C}$) a) PPG4k-rich phase and b) PEO600-rich phase



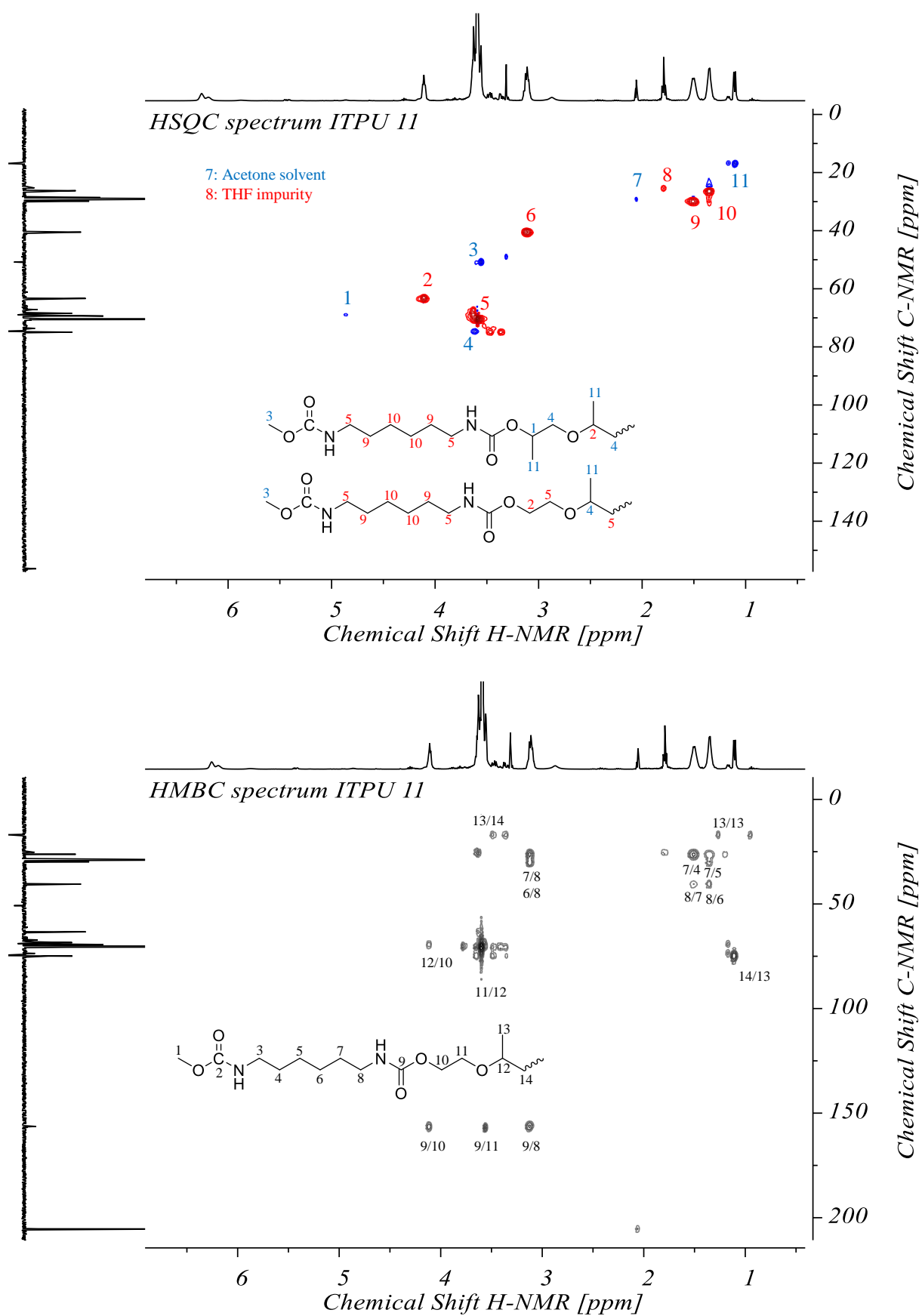
Appendix IV-3. FTIR spectra of PEO600, PPG2k and HDI.



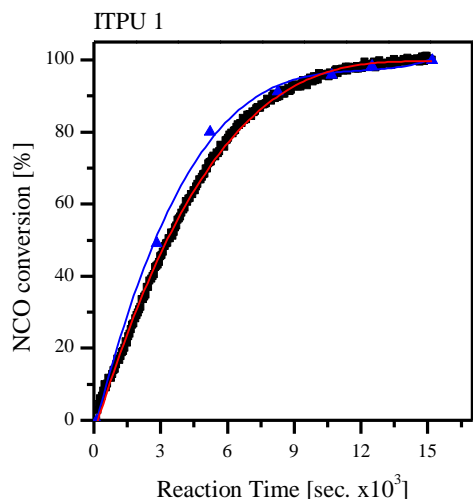
Appendix IV-4. FTIR background spectrum of the ZnSe probe in nitrogen atmosphere.



Appendix IV-5. HSQC and HMBC 2D-NMR spectra of ITPU 10.

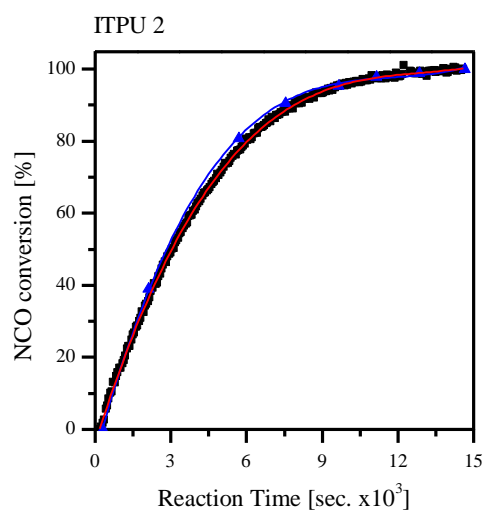


Appendix IV-6. HSQC and HMBC 2D-NMR spectra of ITPU 11.



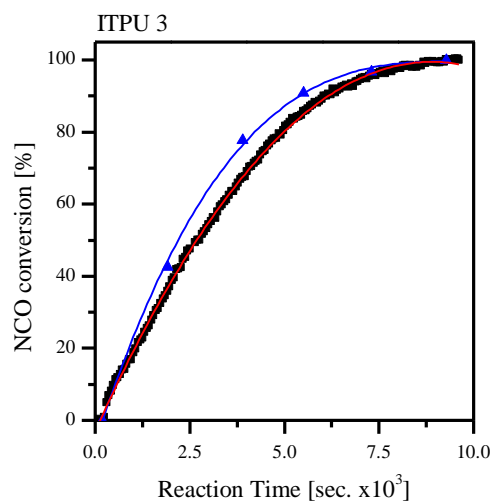
ITPU 1 FTIR			
Equation	$y = \text{Intercept} + B1*x^1 + B2*x^2 + B3*x^3$		
Adj. R-Square	0.99849		
		Value	Standard Error
NCO Conversion	Intercept	-3.77793	0.29725
	-- B1	0.02049	1.66047E-4
	-- B2	-1.35328E-6	2.50478E-8
	-- B3	2.97997E-11	1.0743E-12

ITPU 1 Titration			
Equation	$y = \text{Intercept} + B1*x^1 + B2*x^2 + B3*x^3$		
Adj. R-Square	0.99641		
		Value	Standard Error
NCO Conversion	Intercept	-3.26799	2.26289
	-- B1	0.02455	0.00138
	-- B2	-2.0317E-6	2.15003E-7
	-- B3	5.69216E-11	9.13726E-12



ITPU 2 FTIR			
Equation	$y = \text{Intercept} + B1*x^1 + B2*x^2 + B3*x^3$		
Adj. R-Square	0.99973		
		Value	Standard Error
NCO conversion	Intercept	-3.83564	0.12796
	-- B1	0.02239	7.43775E-5
	-- B2	-1.66384E-6	1.16499E-8
	-- B3	4.23439E-11	5.18828E-13

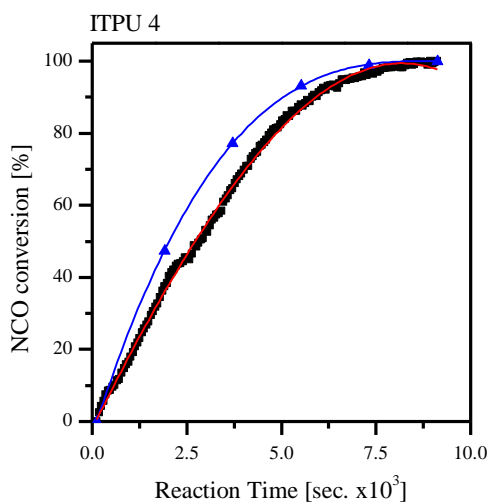
ITPU 2 Titration			
Equation	$y = \text{Intercept} + B1*x^1 + B2*x^2 + B3*x^3$		
Adj. R-Square	0.99943		
		Value	Standard Error
NCO Conversion	Intercept	-6.98061	0.94205
	-- B1	0.02571	6.40387E-4
	-- B2	-2.14312E-6	1.02735E-7
	-- B3	6.0681E-11	4.45873E-12



ITPU 3 FTIR			
Equation	$y = \text{Intercept} + B1*x^1 + B2*x^2 + B3*x^3$		
Adj. R-Square	0.99933		
		Value	Standard Error
NCO conversion	Intercept	-3.03521	0.26475
	-- B1	0.02343	2.34034E-4
	-- B2	-1.38303E-6	5.55345E-8
	-- B3	5.0583E-12	3.74373E-12

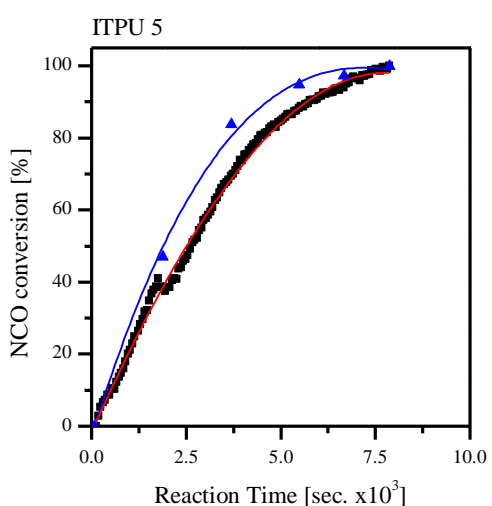
ITPU 3 Titration			
Equation	$y = \text{Intercept} + B1*x^1 + B2*x^2 + B3*x^3$		
Adj. R-Square	0.99807		
		Value	Standard Error
NCO Conversion	Intercept	-6.17288	1.92978
	-- B1	0.03231	0.00202
	-- B2	-3.28595E-6	5.24094E-7
	-- B3	1.11325E-10	3.62792E-11

Appendix IV-7. Fitted FTIR and NCO-titration based NCO conversions plus resulting parameters.



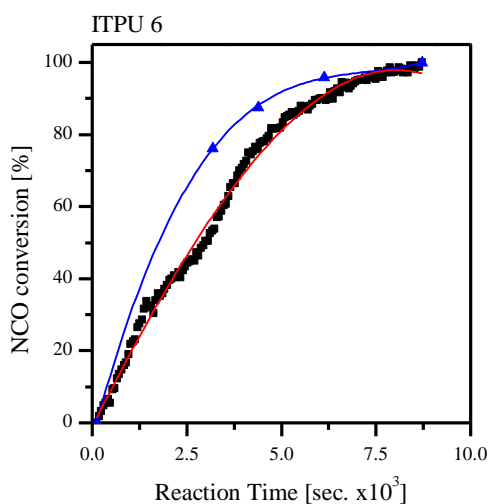
ITPU 4 Titration			
Equation	y = Intercept + B1*x^1 + B2*x^2 + B3*x^3		
Adj. R-Square	0.99994		
		Value	Standard Error
NCO conversion	Intercept	-3.96858	0.32926
	B1	0.03319	3.46611E-4
	B2	-3.49939E-6	9.23079E-8
	B3	1.21654E-10	6.56883E-12

ITPU 4 FTIR			
Equation	y = Intercept + B1*x^1 + B2*x^2 + B3*x^3		
Adj. R-Square	0.99846		
		Value	Standard Error
NCO conversion	Intercept	-2.00683	0.42181
	B1	0.02132	3.91697E-4
	B2	-6.69249E-7	9.80715E-8
	B3	-5.15215E-11	6.98688E-12



ITPU 5 FTIR			
Equation	y = Intercept + B1*x^1 + B2*x^2 + B3*x^3		
Adj. R-Square	0.99685		
		Value	Standard Error
NCO conversion	Intercept	-1.73753	0.63605
	B1	0.02366	6.79707E-4
	B2	-1.13008E-6	1.96281E-7
	B3	-3.36053E-11	1.61465E-11

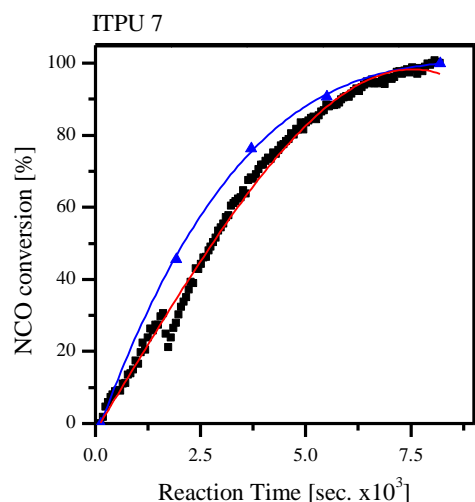
ITPU 5 Titration			
Equation	y = Intercept + B1*x^1 + B2*x^2 + B3*x^3		
Adj. R-Square	0.99178		
		Value	Standard Error
NCO Conversion	Intercept	-2.86658	3.73469
	-- B1	0.03444	0.00457
	-- B2	-3.64565E-6	1.41191E-6
	-- B3	1.16175E-10	1.16685E-10



ITPU 6 FTIR			
Equation	y = Intercept + B1*x^1 + B2*x^2 + B3*x^3		
Adj. R-Square	0.99468		
		Value	Standard Error
NCO conversion	Intercept	-1.12184	0.78747
	-- B1	0.02094	7.64662E-4
	-- B2	-6.13506E-7	2.00252E-7
	-- B3	-5.71036E-11	1.49254E-11

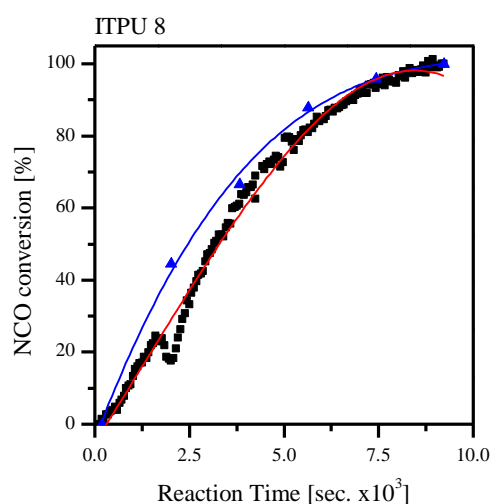
ITPU 6 Titration			
Equation	y = Intercept + B1*x^1 + B2*x^2 + B3*x^3		
Adj. R-Square	0.99974		
		Value	Standard Error
NCO Conversion	Intercept	-4.67655	0.72464
	-- B1	0.03986	9.3587E-4
	-- B2	-5.34243E-6	2.80557E-7
	-- B3	2.46466E-10	2.10402E-11

Appendix IV-8. Fitted FTIR and NCO-titration based NCO conversions plus resulting parameters.



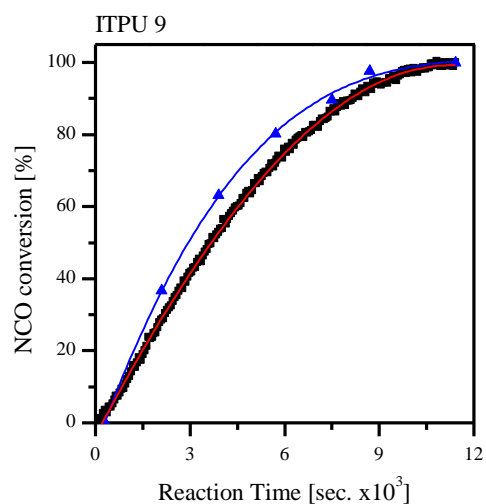
ITPU 7 FTIR			
Equation	$y = \text{Intercept} + B1*x^1 + B2*x^2 + B3*x^3$		
Adj. R-Square	0.99453		
		Value	Standard Error
NCO conversion	Intercept	-2.04765	0.85771
	-- B1	0.01907	8.83175E-4
	-- B2	2.38711E-7	2.45451E-7
	-- B3	-1.32968E-10	1.94204E-11

ITPU 7 Titration			
Equation	$y = \text{Intercept} + B1*x^1 + B2*x^2 + B3*x^3$		
Adj. R-Square	0.99881		
		Value	Standard Error
NCO Conversion	Intercept	-4.03244	1.53334
	-- B1	0.03243	0.00194
	-- B2	-3.41665E-6	5.99068E-7
	-- B3	1.22883E-10	4.76008E-11



ITPU 8 FTIR			
Equation	$y = \text{Intercept} + B1*x^1 + B2*x^2 + B3*x^3$		
Adj. R-Square	0.99148		
		Value	Standard Error
NCO conversion	Intercept	-5.15179	1.04717
	-- B1	0.01658	9.61898E-4
	-- B2	4.12146E-7	2.37685E-7
	-- B3	-1.09754E-10	1.67159E-11

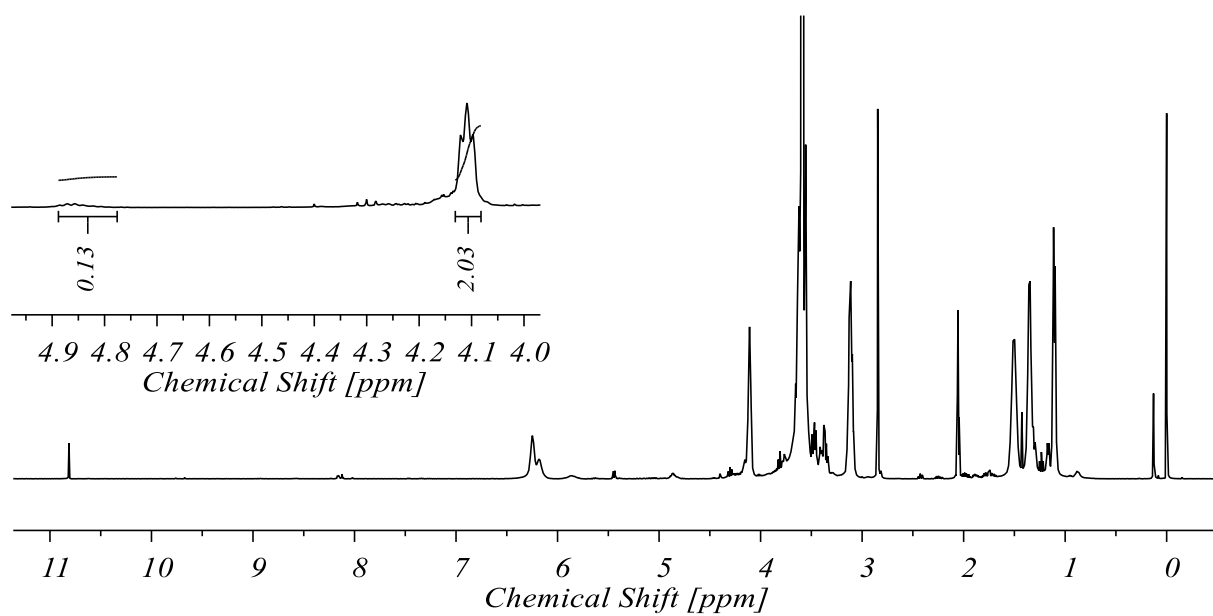
ITPU 8 Titration			
Equation	$y = \text{Intercept} + B1*x^1 + B2*x^2 + B3*x^3$		
Adj. R-Square	0.99414		
		Value	Standard Error
NCO Conversion	Intercept	-4.31185	3.28405
	-- B1	0.02781	0.00338
	-- B2	-2.51749E-6	8.79223E-7
	-- B3	7.91685E-11	6.14462E-11



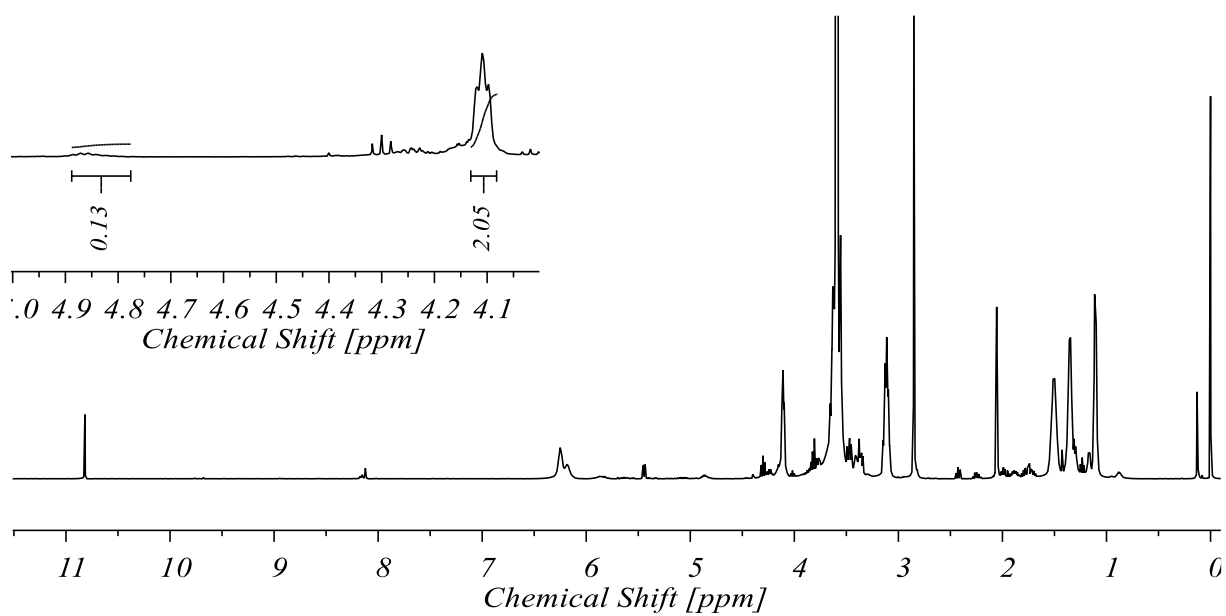
ITPU 9 FTIR			
Equation	$y = \text{Intercept} + B1*x^1 + B2*x^2 + B3*x^3$		
Adj. R-Square	0.99947		
		Value	Standard Error
NCO Conversion	Intercept	-3.70432	0.21857
	-- B1	0.01679	1.62789E-4
	-- B2	-5.51024E-7	3.26522E-8
	-- B3	-1.14106E-11	1.86121E-12

ITPU 9 Titration			
Equation	$y = \text{Intercept} + B1*x^1 + B2*x^2 + B3*x^3$		
Adj. R-Square	0.99816		
		Value	Standard Error
NCO Conversion	Intercept	-6.99731	1.83189
	-- B1	0.0245	0.00147
	-- B2	-1.88353E-6	2.98078E-7
	-- B3	4.91315E-11	1.65226E-11

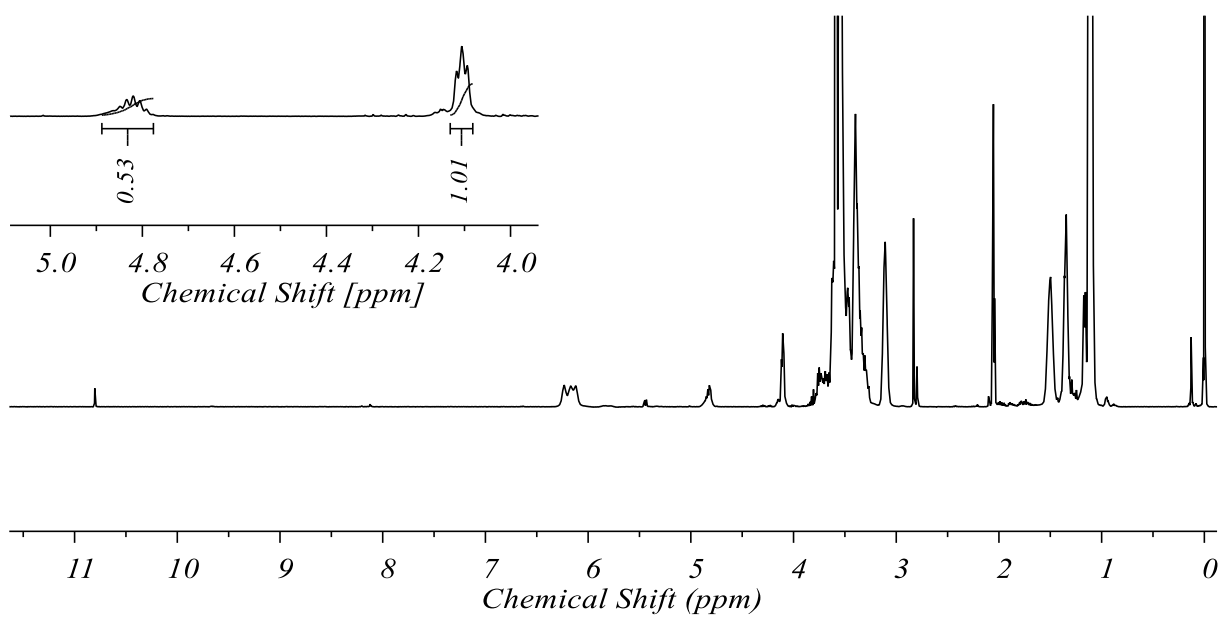
Appendix IV-9. Fitted FTIR and NCO-titration based NCO conversions plus resulting parameters.



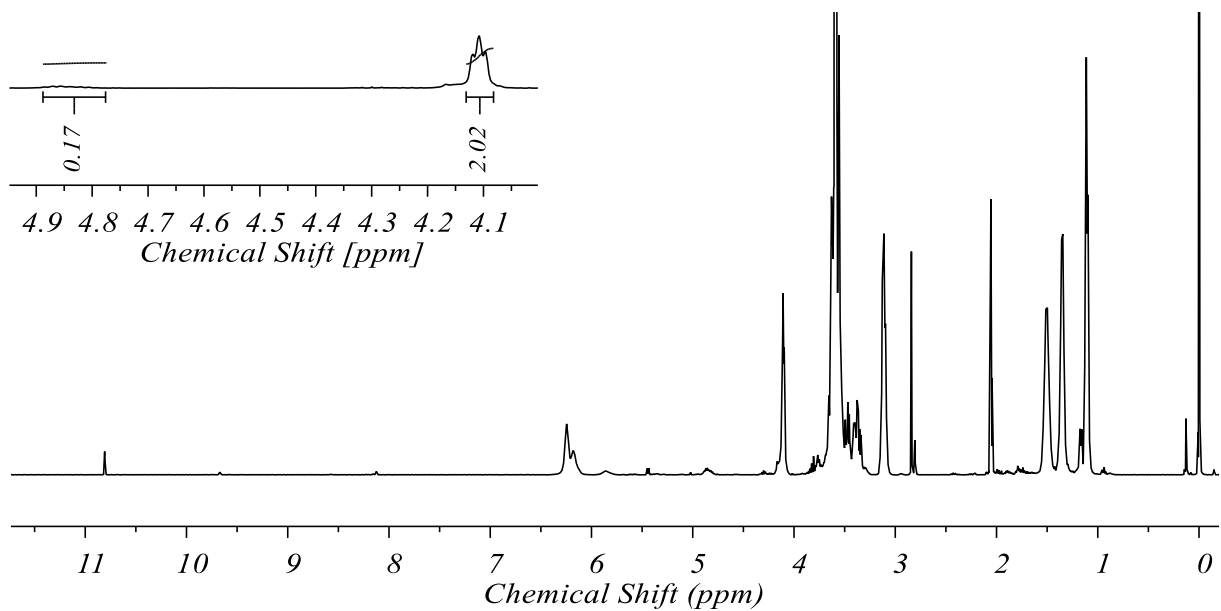
Appendix IV-10. $^1\text{H-NMR}$ spectrum of the upper sample from ITPU 1.



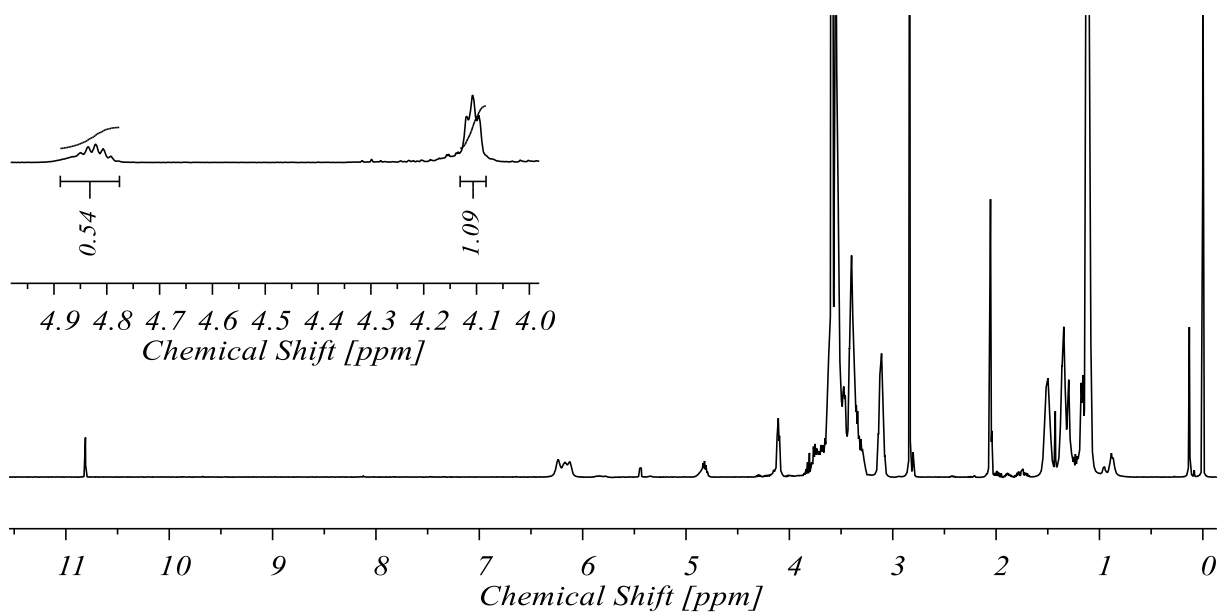
Appendix IV-11. $^1\text{H-NMR}$ spectrum of the lower sample from ITPU 1.



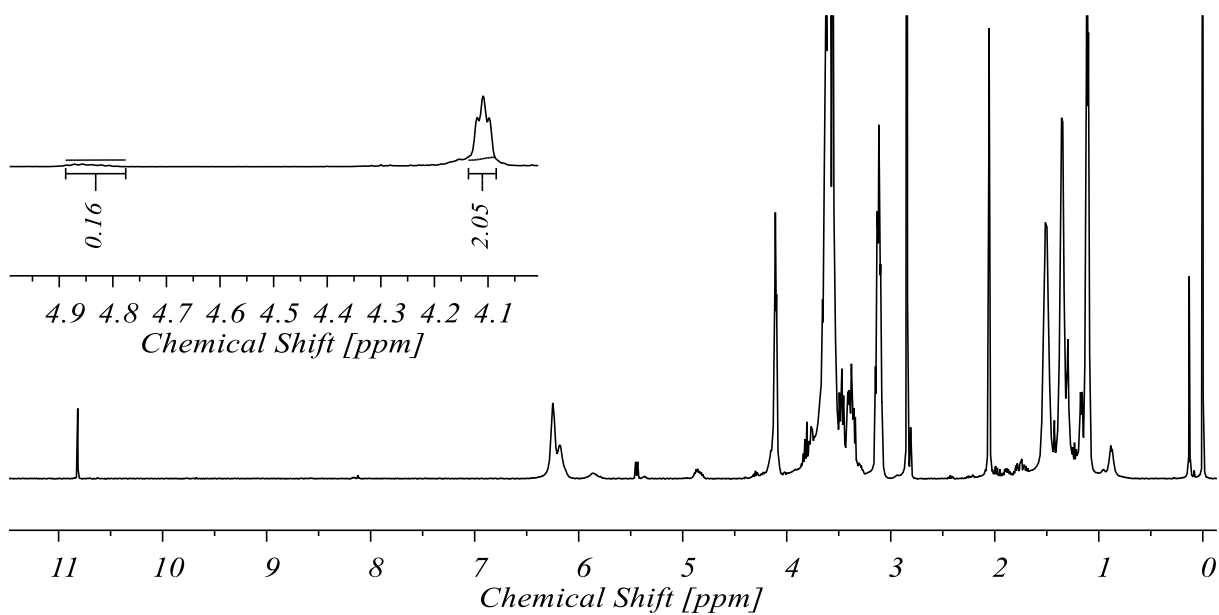
Appendix IV-12. ¹H-NMR spectrum of phase' from ITPU 3.



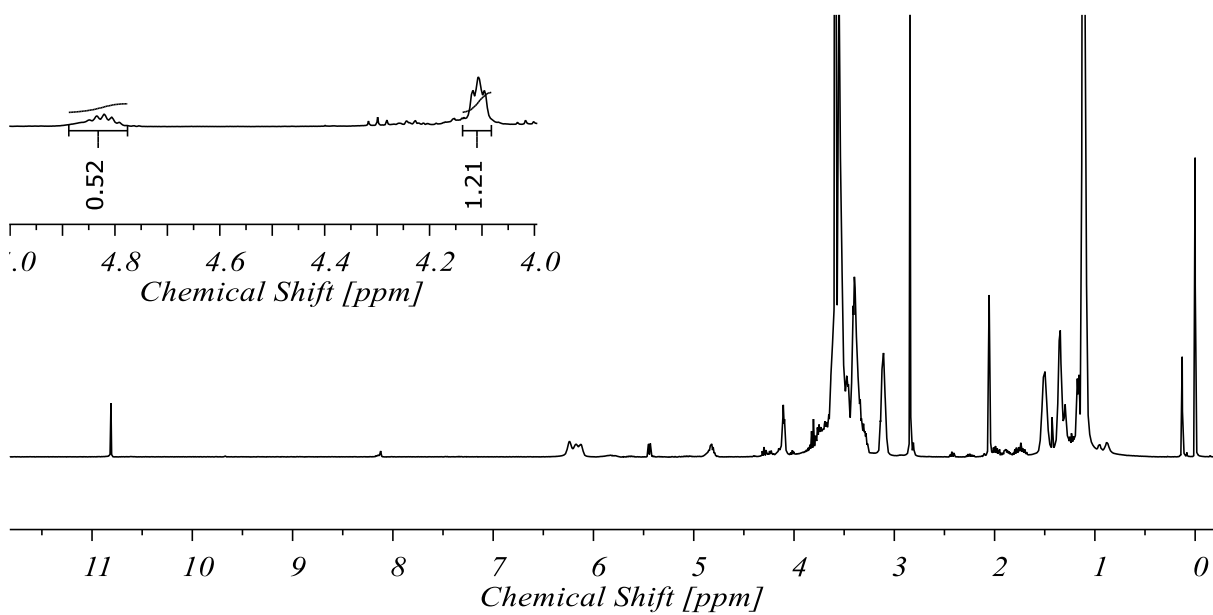
Appendix IV-13. ¹H-NMR spectrum of phase'' from ITPU 3.



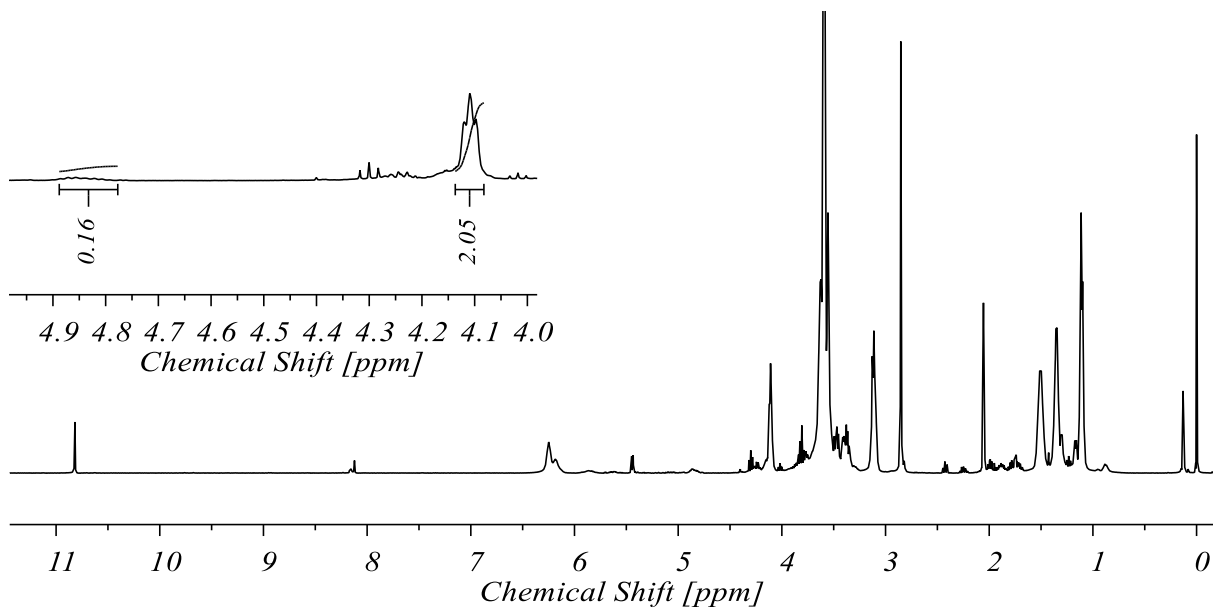
Appendix IV-14. ¹H-NMR spectrum of phase' from ITPU 4.



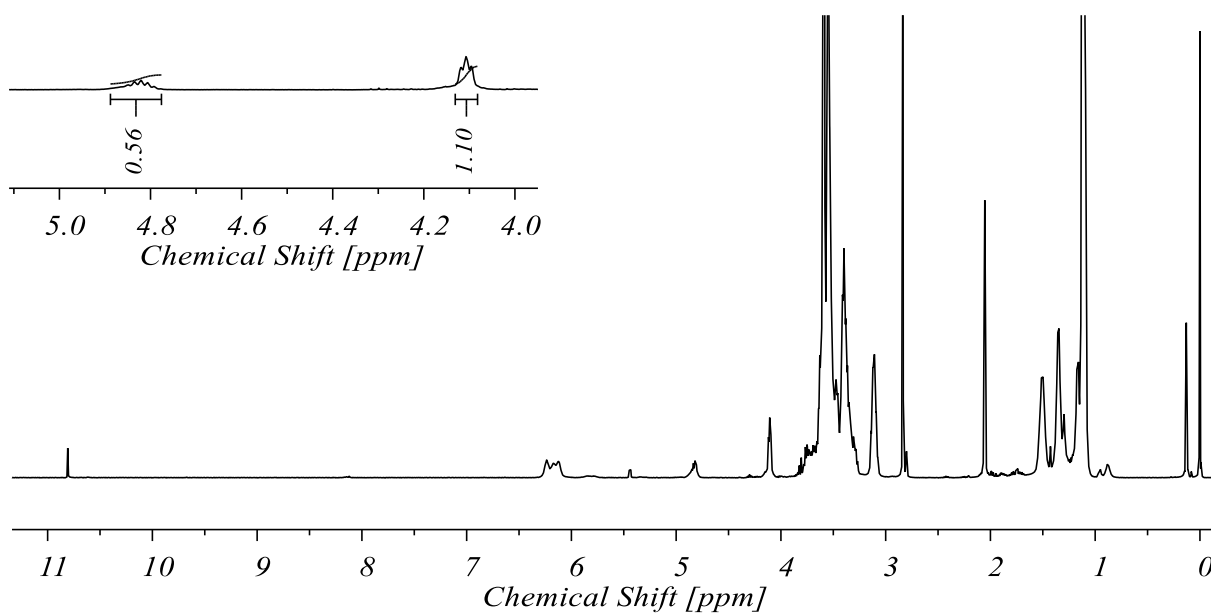
Appendix IV-15. ¹H-NMR spectrum of phase'' from ITPU 4.



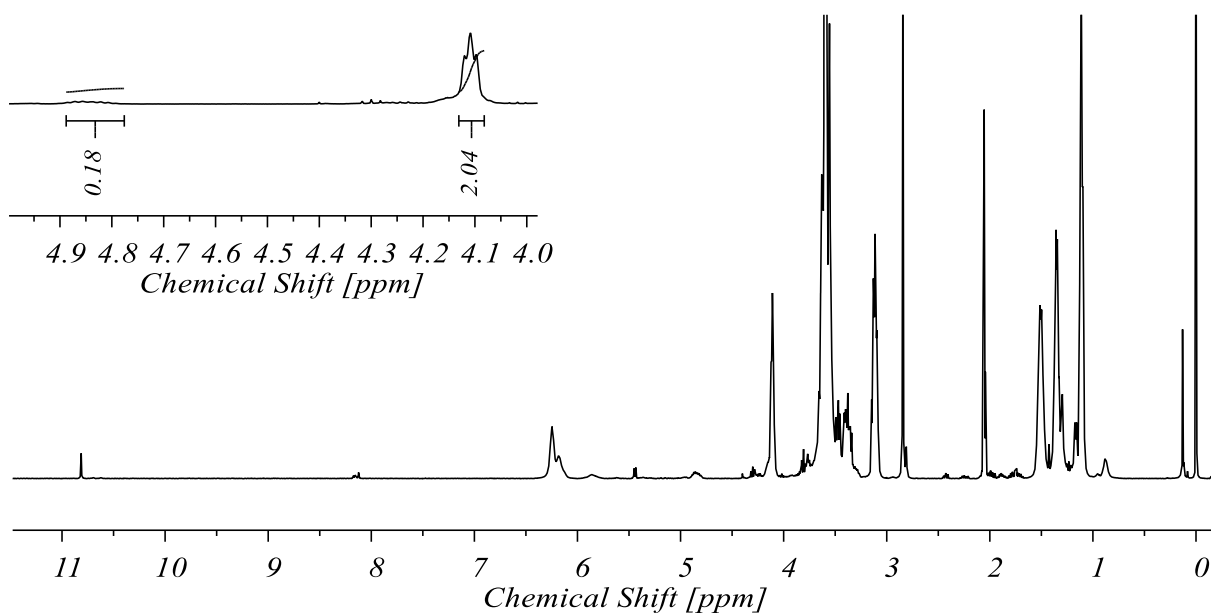
Appendix IV-16. $^1\text{H-NMR}$ spectrum of phase' from ITPU 5.



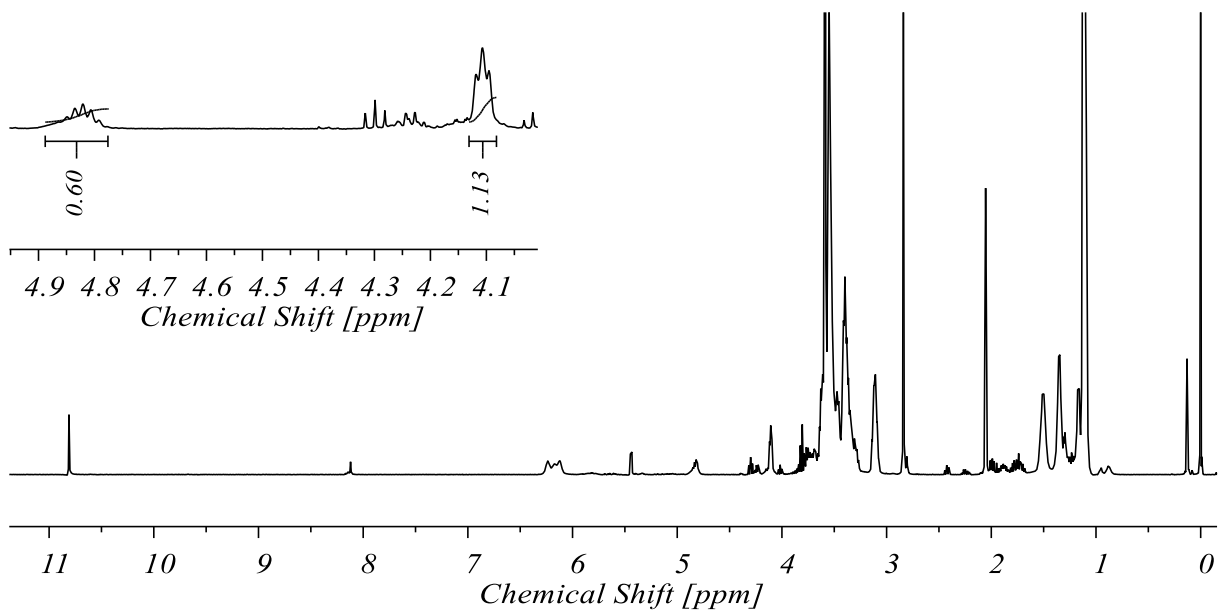
Appendix IV-17. $^1\text{H-NMR}$ spectrum of phase'' from ITPU 5.



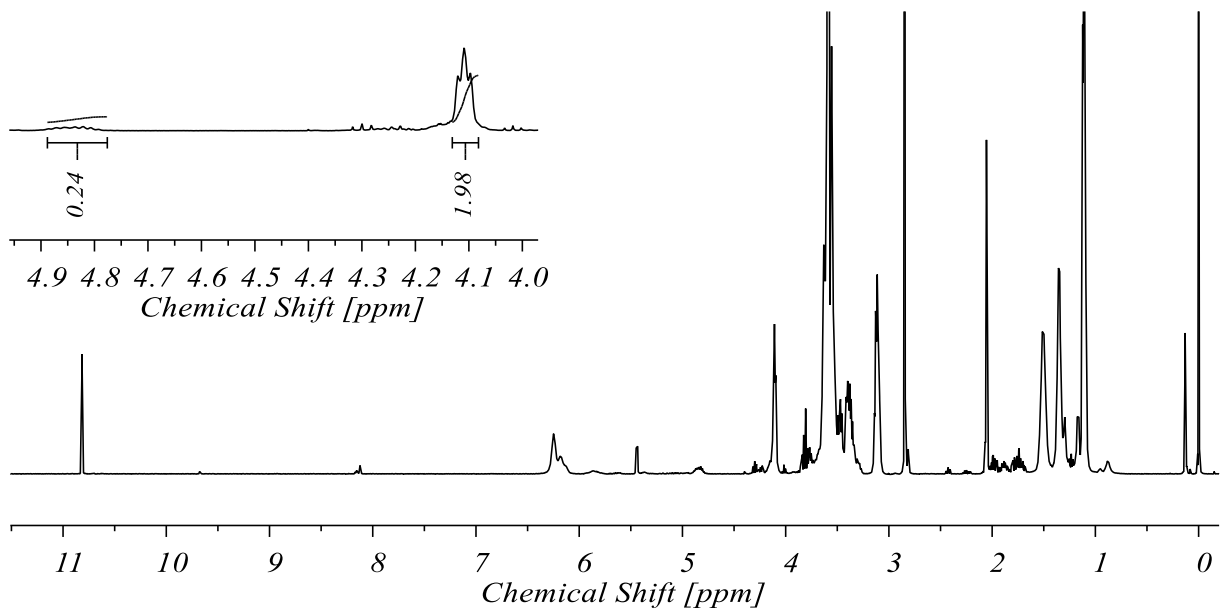
Appendix IV-18. $^1\text{H-NMR}$ spectrum of phase' from ITPU 6.



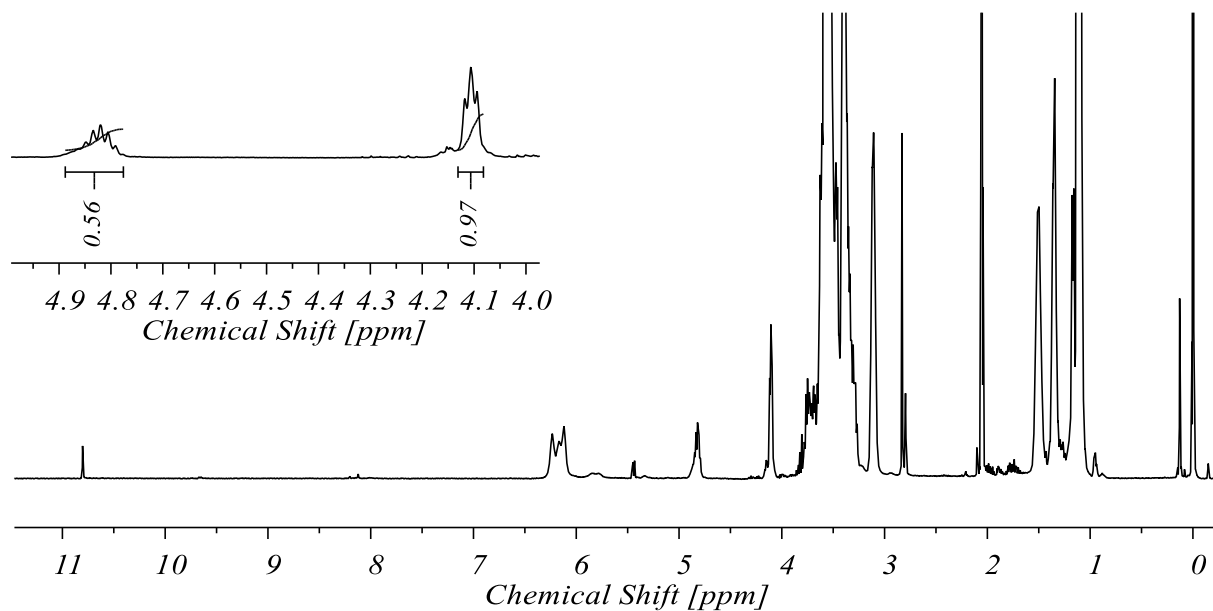
Appendix IV-19. $^1\text{H-NMR}$ spectrum of phase'' from ITPU 6.



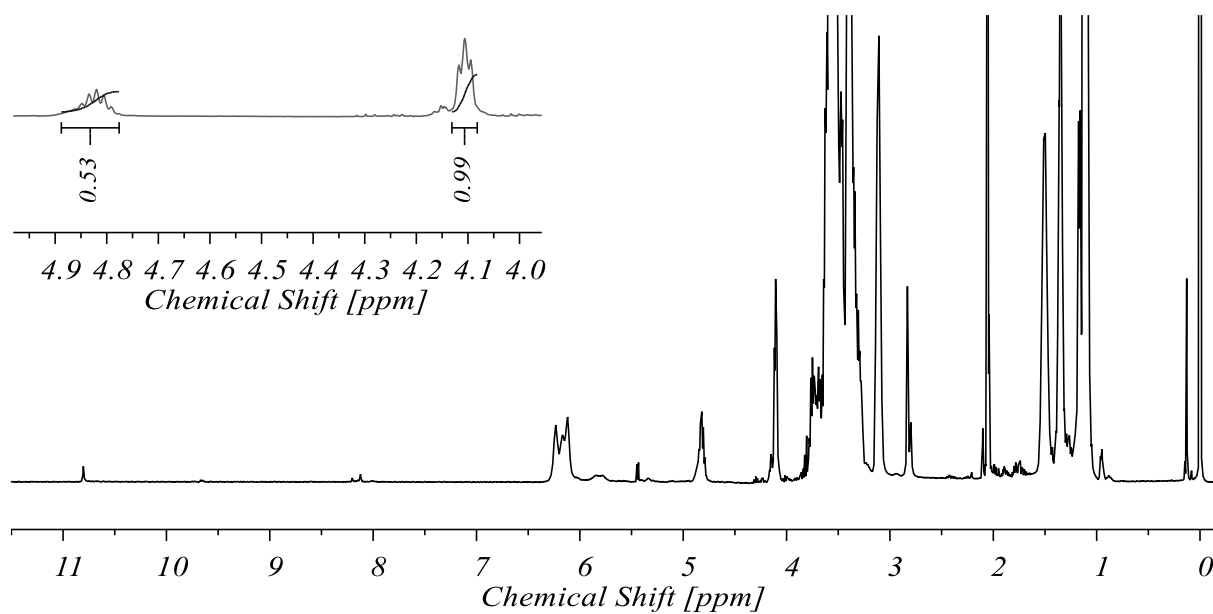
Appendix IV-20. $^1\text{H-NMR}$ spectrum of phase' from ITPU 7.



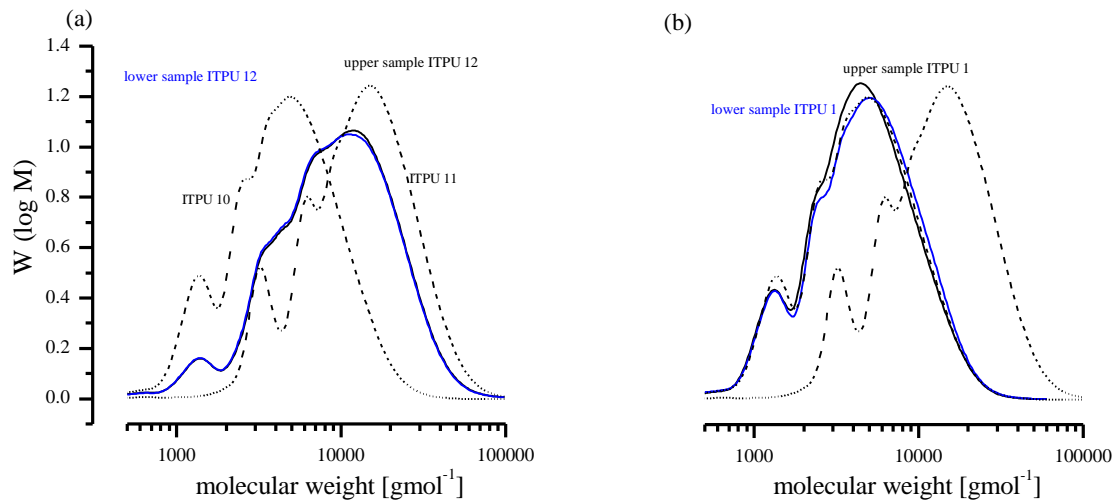
Appendix IV-21. $^1\text{H-NMR}$ spectrum of phase'' from ITPU 7.



Appendix IV-22. $^1\text{H-NMR}$ spectrum of the upper sample from ITPU 12.



Appendix IV-23. $^1\text{H-NMR}$ spectrum of the lower sample from ITPU 12.



Appendix IV-24. MWD of the upper and lower samples from ITPU 1 +12 after centrifugation.

Appendix IV-25. MATLAB code for the calculation of the binodal in binary systems.

Objective Function

```
function [OBJ] = funOBJ_final(phiPQ12)

%phiPQ12(1) = phiP1
%phiPQ12(2) = phiP2
%phiPQ12(3) = phiQ1
%phiPQ12(4) = phiQ2

%Load parameter from workspace

ivseg=evalin('base','vseg');
ichi = evalin('base','chi');
iRT=evalin('base','RT');
in12act = evalin('base','n12act');

%Calculation of  $\mu$  at phiPQ12

potPphi1 = log(phiPQ12(1)) / in12act(1) + 1/in12act(1) - 1/in12act(2) -
log(1-phiPQ12(1)) / in12act(2) + ichi() - 2*phiPQ12(1) * ichi();
potPphi2 = log(phiPQ12(2))/in12act(2)+1/in12act(2)-1/in12act(1)-log(1-
phiPQ12(2))/in12act(1)+ichi()-2*phiPQ12(2)*ichi();
potQphi1 = log(phiPQ12(3))/in12act(1)+1/in12act(1)-1/in12act(2)-log(1-
phiPQ12(3))/in12act(2)+ichi()-2*phiPQ12(3)*ichi();
potQphi2 = log(phiPQ12(4))/in12act(2)+1/in12act(2)-1/in12act(1)-log(1-
phiPQ12(4))/in12act(1)+ichi()-2*phiPQ12(4)*ichi();

%Calc. (G/RT)*Vr/V Flory Huggins
```

```

GmP1 = phiPQ12(1)/in12act(1)*log(phiPQ12(1))+(1-
phiPQ12(1))/in12act(2)*log((1-phiPQ12(1)))+(ichi*phiPQ12(1)*(1-
phiPQ12(1)));
GmQ1 = phiPQ12(3)/in12act(1)*log(phiPQ12(3))+(1-
phiPQ12(3))/in12act(2)*log((1-phiPQ12(3)))+(ichi*phiPQ12(3)*(1-
phiPQ12(3)));

% double tangent construction

dtcp1 = ((GmP1-potPphi1*phiPQ12(1)) - (GmQ1-
potQphi1*phiPQ12(3)))^2/(phiPQ12(1)-phiPQ12(3))^4;

%μ1 = μ1' and μ2 = μ2'

diffpotphi1 = (potPphi1-potQphi1)^2/(phiPQ12(1)-phiPQ12(3))^4;
diffpotphi2 = (potPphi2-potQphi2)^2/(phiPQ12(2)-phiPQ12(4))^4;

%volume balances

V1 = (1-phiPQ12(1)-phiPQ12(2))^2/(phiPQ12(1)-phiPQ12(3))^4;
V2 = (1-phiPQ12(3)-phiPQ12(4))^2/(phiPQ12(1)-phiPQ12(3))^4;

% Objective Funktion OBJ(phiP12,phiQ12)

OBJ = [ diffpotphi1;
        diffpotphi2;
        dtcp1;
        V1;
        V2];

end

```

Program routine

```

%Load Workspace
clear
clc

load binary.mat
clearvars dummy;
clearvars S;

%UI input
disp('Gewünschte Starttemperatur eingeben')
Tstart = input('T in °C eingeben: ');
disp('Gewünschte Endtemperatur eingeben')
Tend = input('T in °C eingeben: ');
disp('Wähle Substanz A aus')
disp(substances)
act1 = input('Reihennummer der Substanz A: ');
disp('Wähle Substanz B aus')
act2 = input('Reihennummer der Substanz B: ');

ActTemp = Tstart;
iMax = Tend-Tstart;

%disp('Dateiname des Ergebnisreports')

```

Appendix

```
%Prep of result table

Name = input('Dateiname des Ergebnisreports:', 's');
fileformat = '.xlsx';
Info =
{act12name(1, :), act12name(2, :); hilde12act(1), hilde12act(2); Vm12act(1), Vm12act(2)};
filename = strcat(Name, fileformat);
labels1 = {'Substances'; 'Hildebrand Par.'; 'molar Volume'};
labels2 = {'Temperatur[°C]', 'phi1P Binodal', 'phi2P BinodalP', 'phi1Q Binodal', 'phi2Q Binodal', 'Residuum'};
xlswrite(filename, labels2, 'Ergebnisse', 'A6:F6');
xlswrite(filename, labels1, 'Ergebnisse', 'A1:A4');
xlswrite(filename, Info, 'Ergebnisse', 'B1:C3');
xlswrite(filename, a12, 'Ergebnisse', 'B4');
%acts =

%Update variables and parameters

act12name = [substances(act1(), :); substances(act2(), :)];
Vm12act = [Vm12data(act1()); Vm12data(act2())];
vseg = 5.24e-5; %vseg mol. vol. of PO acc. to Fedors!
n12act = [Vm12act(1)/vseg(); Vm12act(2)/vseg()];
hilde12act = [hilde12data(act1()); hilde12data(act2())];
RT = R()*(273.15+Tstart);
chi = vseg()*1e6*(hilde12act(1)-hilde12act(2))^2/RT();

% minimisation of OBJ function

for i = 0:iMax

whilecount = 0
ActTemp = Tstart + i;
RT = R()*(273.15+ActTemp);
chi = vseg()*1e6*(hilde12act(1)-hilde12act(2))^2/RT();

x0 = [(0.5 - 0) * rand() + 0; (0.5 - 1) * rand() + 1; (0.5 - 1) * rand() + 1; (0.5 - 0) * rand() + 0]; % Starting guess
Resvec = funOBJ_final(x0);
Res = sum(Resvec);

    while Res > 1e-10

        whilecount = whilecount + 1

x0 = [(0.5 - 0) * rand() + 0;
(0.5 - 1) * rand() + 1;
(0.5 - 1) * rand() + 1;
(0.5 - 0) * rand() + 0]; % Starting guess

ub=ones(1,4);
lb=0*ones(1,4);

options = optimset('MaxFunEvals',10000,'MaxIter',10000,'TolFun',1e-20);%
Tol fun step << Residuum ist scheinbar vorraussetzung das es funktioniert.
[x,resnorm,residual,exitflag] = lsqnonlin(@funOBJ_final,x0,lb,ub,options);

Resvec = funOBJ_final(x);
Res = sum(Resvec);
```

```

        if whilecount== 500
            break
        end

    end

end

PhiP1 = x(1);
PhiP2 = x(2);
PhiQ1 = x(3);
PhiQ2 = x(4);
Res;
dummy(i+1,:) = [ActTemp,PhiP1,PhiP2,PhiQ1,PhiQ2,Res];

end

S.(Name) = dummy;
save(strcat('D:\C. Wenning\Documents\Unterlagen Promotion\MATLAB\Via
Phi_Binary Phase Calculation_Final OK\',Name, '.mat'), '-struct', 'S') %
EDITED

xlswrite(filename,dummy,'Ergebnisse','A7');

save binary.mat;

```

Appendix IV-26. MATLAB code for the calculation of the binodal in ternary systems.

Objective Function

```

function [obj ] = funOBJTer(phiPQ12s)

%phiPQ12(1) = phiP1
%phiPQ12(2) = phiP2
%phiPQ12(3) = phiPs
%phiPQ12(4) = phiQ1
%phiPQ12(5) = phiQ2
%phiPQ12(6) = phiQs

iRT=evalin('base','RT');
ix12s = evalin('base','x12s');
im12s = evalin('base','m12sact');

%Calc.  $\mu/RT$ 

potP1 = (log(phiPQ12s(1))+(1-(im12s(1)/im12s(2)))*phiPQ12s(2)+(1-
im12s(1))*phiPQ12s(3)+im12s(1)*(ix12s(1)*(phiPQ12s(2)+phiPQ12s(3))^2+ix12s(
2)*phiPQ12s(2)^2+ix12s(3)*phiPQ12s(3)^2))/iRT;
potP2 = (log(phiPQ12s(2))+(1-(im12s(2)/im12s(1)))*phiPQ12s(1)+(1-
im12s(2))*phiPQ12s(3)+im12s(2)*(ix12s(2)*(phiPQ12s(1)+phiPQ12s(3))^2+ix12s(
1)*phiPQ12s(1)^2+ix12s(3)*phiPQ12s(3)^2))/iRT;
potPs = (log(phiPQ12s(3))+(1-(1/im12s(1)))*phiPQ12s(1)+(1-
(1/im12s(2)))*phiPQ12s(2)+ix12s(3)*(phiPQ12s(1)+phiPQ12s(2))^2+ix12s(1)*phi
PQ12s(1)^2+ix12s(2)*phiPQ12s(2)^2))/iRT;

```

Appendix

```
potQ1 = (log(phiPQ12s(4))+(1-(im12s(1)/im12s(2)))*phiPQ12s(5)+(1-
im12s(1))*phiPQ12s(6)+im12s(1)*(ix12s(1)*(phiPQ12s(5)+phiPQ12s(6))^2+ix12s(
2)*phiPQ12s(5)^2+ix12s(3)*phiPQ12s(6)^2)/iRT;
potQ2 = (log(phiPQ12s(5))+(1-(im12s(2)/im12s(1)))*phiPQ12s(4)+(1-
im12s(2))*phiPQ12s(6)+im12s(2)*(ix12s(2)*(phiPQ12s(4)+phiPQ12s(6))^2+ix12s(
1)*phiPQ12s(4)^2+ix12s(3)*phiPQ12s(6)^2)/iRT;
potQs = (log(phiPQ12s(6))+(1-(1/im12s(1)))*phiPQ12s(4)+(1-
(1/im12s(2)))*phiPQ12s(5)+ix12s(3)*(phiPQ12s(4)+phiPQ12s(5))^2+ix12s(1)*phi
PQ12s(4)^2+ix12s(2)*phiPQ12s(5)^2)/iRT;

potP12s = [potP1;potP2;potPs];
potQ12s = [potQ1;potQ2;potQs];
potPQ12s = [potP12s;potQ12s];

%μ = μ'

diffpotphi1 = (potP1-potQ1)^2/(phiPQ12s(1)-phiPQ12s(4))^4;
diffpotphi2 = (potP2-potQ2)^2/(phiPQ12s(2)-phiPQ12s(5))^4;
diffpotphis = (potPs-potQs)^2;

%volume balances

V1 = (1-phiPQ12s(1)-phiPQ12s(2)-phiPQ12s(3))^2;
V2 = (1-phiPQ12s(4)-phiPQ12s(5)-phiPQ12s(6))^2;

%Objective Funktion OBJ(phiP12,phiQ12)

obj = [ diffpotphi1;
        diffpotphi2;
        diffpotphis;
        V1;
        V2;
        diffpotphis];

end
```

Program routine

```
%Load Workspace
clear Workspace
clc

load ternary.mat

clear dummy;
clear S;

%User input parameter choice
disp('Gewünschte Temperatur eingeben')
T= input('T in °C eingeben: ');
disp('Gewünschte Startkonzentration eingeben')
sstart = input('Volumenanteil Lösemittel 0,x: ');
disp('Gewünschte Konzentrationsintervalle eingeben')
sintervall = input('Intervall Lösemittel 0,x: ');
disp('Wähle Substanz A aus')
disp(substances)
```

```

act1 = input('Reihennummer der Substanz A: ');
disp('Wähle Substanz B aus')
act2 = input('Reihennummer der Substanz B: ');
disp('Wähle Substant s aus')
acts = input('Reihennummer der Substanz s: ');
Acts = sstart;
sMax = (1-sstart)/sintervall;

%Update variables

act12sname = [substances(act1(),:); substances(act2(),:);
substances(acts(),:)];
Vm12sact = [Vm12sdata(act1());Vm12sdata(act2());Vm12sdata(acts())];
vseg = Vm12sact(3);
m12sact = [Vm12sact(1)/Vm12sact(3); Vm12sact(2)/Vm12sact(3);
Vm12sact(3)/Vm12sact(3)];
hilde12sact =
[hilde12sdata(act1());hilde12sdata(act2());hilde12sdata(acts())];
RT = R()*(273.15+T);

%Prep of results table

Name = input('Dateiname des Ergebnisreports: ','s');
fileformat = '.xlsx';
Info =
{act12sname(1,:),act12sname(2,:),act12sname(3,:);hilde12sact(1),hilde12sact
(2),hilde12sact(3);Vm12sact(1),Vm12sact(2),Vm12sact(3)};
filename = strcat(Name,fileformat);
labels1 = {'Substances';'Hildebrand Par.';'molar Volume';'Parameter a'};
labels2 = {'Temperatur[°C]','phi1P Binodal','phi2P Binodal','phisP
Binodal','phi1Q Binodal','phi2Q Binodal','phisQ Binodal','Residuum'};
xlswrite(filename,labels2,'Ergebnisse','A5:H5');
xlswrite(filename,labels1,'Ergebnisse','A1:A4');
xlswrite(filename,Info,'Ergebnisse','B1:D3');

x12sbin = [vseg*1e6*(hilde12sact(1)-hilde12sact(2))^2/RT(); %x12
           vseg*1e6*(hilde12sact(1)-hilde12sact(3))^2/RT(); %x1s
           vseg*1e6*(hilde12sact(2)-hilde12sact(3))^2/RT()]; %x2s

% Calc. of FH interaction parameter acc. to Hsu und Prausnitz

x12s = [0.5*(x12sbin(1)+x12sbin(2)-x12sbin(3)); %x1
        0.5*(x12sbin(1)+x12sbin(3)-x12sbin(2)); %x2
        0.5*(x12sbin(2)+x12sbin(3)-x12sbin(1))]; %xs

% minimisation of OBJ

for i = 0:sMax-1

Acts = sstart + i*sintervall;
RT = R()*(273.15+T);

x0 = [(0.5-0)* rand();% Starting guess
      (0.5-1) * rand()+1;
      Acts;
      (0.5-1) * rand()+1;
      (0.5-0)* rand();
      Acts];

```

Appendix

```
Resvec = funOBJTer(x0);
Res = sum(Resvec);

Whilecount = 0;

ub=ones(1,6);
lb=0*ones(1,6);

    while Res > 1e-10

        Whilecount = Whilecount + 1;

x0 = [(0.5-0)* rand();% Starting guess
      (0.5-1) * rand()+1;
      Acts;
      (0.5-1) * rand()+1;
      (0.5-0)* rand();
      Acts+0.001];% Starting guess

options = optimset('MaxFunEvals',10000,'MaxIter',10000,'TolFun', 1e-20);
[x,resnorm,residual,exitflag] = lsqnonlin(@funOBJTer,x0,lb,ub,options);
Resvec = funOBJTer(x);
Res = sum(Resvec);

        if Whilecount == 100
            break
        end

    end

PhiP1 = x(1);
PhiP2 = x(2);
PhiPs = x(3);
PhiQ1 = x(4);
PhiQ2 = x(5);
PhiQs = x(6);

Res;

dummy(i+1,:) = [T,PhiP1,PhiP2,PhiPs,PhiQ1,PhiQ2,PhiQs,Res];

end

S.(Name) = dummy;
save(strcat('D:\C. Wenning\Documents\Unterlagen Promotion\MATLAB\Ternary
Phases Calculation\',Name, '.mat'), '-struct', 'S') % EDITED

xlswrite(filename,dummy,'Ergebnisse','A7');
```

V *Figures*

Figure 3-1. Structural unit of polyurethanes.....	5
Figure 3-2. Resonance structures of the isocyanate group.	5
Figure 3-3. Addition of an alcohol to an isocyanate group. ^[37]	6
Figure 3-4. Structures of 1,6 hexamethylene diisocyanate (HDI) and isophorone diisocyanate.	6
Figure 3-5. The reaction of isocyanates with water molecules towards carbon dioxide and urea.	7
Figure 3-6. Addition of an isocyanate and an urethane group to an allophanate.	7
Figure 3-7. Chemical structure of DBTDL (left) and DABCO (right).	8
Figure 3-8. Monomers and general synthesis route for common polyether polyols.	9
Figure 3-9. Schulz-Flory distribution at an index of 1.5.	11
Figure 3-10. Schematically illustration of the structure of a linear PU chain containing hard and soft segments.....	12
Figure 3-11. H-bonding between hard segment and (left)hard segment, (middle) PEO and (right) PDMS.	13
Figure 3-12. Illustration of a polymeric chain (grey) arranged in a lattice of solvent molecules (black).....	20
Figure 3-13. Schematically illustration of a phase diagram of a binary polymer blend of A and B.....	22
Figure 4-1. Free energy of mixing of the PPG series with PEO600 derived from the SPs based on Fedors' (a) and Hoy's GCT (b).	25
Figure 4-2. Temperature dependent turbidity analysis performed on a 50:50 vol.% PPG2k/PEO600 polyol mixture.....	26
Figure 4-3. Temperature dependent MWDs of the two phases in PPG2k/PEO600 mixtures..	28
Figure 4-4. Theoretical and experimental phase diagram of PPG2k/PEO600 (a) and PPG4k/PEO600 (b) mixtures.....	28
Figure 4-5. Predicted free energies of mixing using the SPs of HDI based on Fedors and Hoy.	30
Figure 4-6. Results from the HSP determination by experimental solubility test of HDI.	32
Figure 4-7. Predicted free energies of mixing using the SPs of HDI based on Stefanis and solubility tests.	32
Figure 4-8. Predicted ternary phase diagrams based on the different solubility parameters for HDI.	34
Figure 4-9. Theoretical and experimental ternary phase diagram of PPG2k/PEO600/HDI. ...	35
Figure 4-10. FTIR spectrum of the reaction mixture ITPU 10.....	40
Figure 4-11. Comparison of FTIR measurement and NCO%-content titration in ITPU 10 formation.....	41
Figure 4-12. Second-order plot of the polymerisation kinetics.	43
Figure 4-13. ¹ H-NMR spectrum of the resulting ITPU comprising 50/50 mol.% PEO600 and PPG2k.	44
Figure 4-14. Conversion of the primary and secondary OH groups from PEO and PPG determined by ¹ H-NMR.....	45

Figure 4-15. Illustration of the competing second order kinetics.	46
Figure 4-16. Second order plots of the kinetic data from the NCO%-content titration during all polymerisations.	47
Figure 4-17. Collection of the results from the reaction monitoring of the bi-soft segment polymerisations with Φ_{PEO600} ranging from 10 to 90 vol.%.....	50
Figure 4-18. Collection of the results from the reaction monitoring of the bi-soft segment polymerisations with Φ_{PEO600} ranging from 10 to 90 vol.%.....	51
Figure 4-19. FTIR spectra at the time right before and in the drop of the NCO conversion of ITPU 7.	54
Figure 4-20. Turbidity versus NCO conversion based on the NCO%-content titration (a) and FTIR analysis (b).....	57
Figure 4-21. Schematically simplified illustration of the hypothetical binodal (grey curve) in the ternary phase diagram.	59
Figure 4-22. Effect of increasing PPG molecular weight on the glass transitions of mixed soft segment PPG/PEO600 ITPUs.	61
Figure 4-23. DSC thermograms of different PPG2k/PEO600 ITPUs.	63
Figure 4-24. Molecular weight distributions of the synthesised ITPU products listed in Table 3-9.....	66
Figure 4-25. Schematically illustration of the experimental approach to analyse the separate phases.	67
Figure 4-26. Illustration of the estimation procedure of the molar fractions of PEO600 with respect to PPG2k in the separate phases.	68
Figure 4-27. Determined volume and molar fractions of PEO600 soft segments in the isolated phases from the ITPUs after centrifugation.	69
Figure 4-28. MWDs of the samples from upper (phase') and lower (phase'') phase after centrifugation of ITPU 3(—), 4(—), 5(—), 6(—), and 7(—).	71
Figure 4-29. Micrographs of emulsions (a) ITPU 1 ($\Phi_{\text{PPG2k}} = 10$ vol.%), (b) ITPU 5 ($\Phi_{\text{PPG2k}} = 50$ vol.%) and (c) ITPU 12 ($\Phi_{\text{PPG2k}} = 79$ vol.%).	73
Figure 4-30. Schematic illustration of the phase evolution during the reaction progress including optical micrographs of the products.	75
Figure 6-1. Schematic partitioning of the polyether polyol structure for the calculation of the SP.	91

VI Tables

Table 3-1. Relative reactivities of isocyanates with hydrogen active compounds.	6
Table 3-2. Relative catalytic reactivity of DBTDL and DABCO.	8
Table 3-3. Group contributions from Fedors' theory.	17
Table 3-4. Group contribution of Hoy used in this thesis.	18
Table 3-5. Set of formulae in Hoy's GCT for the calculation of the SP of low-molecular compounds and amorphous polymers.	18
Table 3-6. Extract of first-order contributions of Stefanis' GCT.....	19
Table 4-1. Resulting SPs of the polyether polyols based on Fedors' and Hoy' GCT.	24
Table 4-2. Calculation of the SP of HDI based on Fedors and Hoy.	30
Table 4-3. Calculation of the SP of HDI based on Stefanis.	31
Table 4-4. Hansen SP of HDI determined by solubility tests.....	31
Table 4-5. List of characteristic IR vibrations in the prepared polyurethanes. ^[9,117]	40
Table 4-6. SEC results for the PPG2k/PEO600 ITPUs.	65
Table 6-1. Information about the used chemicals.	83
Table 6-2. Characteristics of the linear difunctional polyether polyols.	84
Table 6-3. Experimental details in the synthesis of PPG/PEO600 bi-soft segment ITPUs.	88
Table 6-4. Notation and composition of the PPG2k/PEO600 bi-soft segment ITPUs.....	89
Table 6-5. Derived group contributions for typical chemical units of polyether polyols on basis of Fedors' ^[90] dataset.	91
Table 6-6. Solvents and their respective HSPs used in the solubility tests.	92



Ich versichere, dass ich die von mir vorgelegte Dissertation selbständig angefertigt, die benutzten Quellen und Hilfsmittel vollständig angegeben und die Stellen der Arbeit – einschließlich Tabellen, Karten und Abbildungen –, die anderen Werken im Wortlaut oder dem Sinn nach entnommen sind, in jedem Einzelfall als Entlehnung kenntlich gemacht habe; dass diese Dissertation noch keiner anderen Fakultät oder Universität zur Prüfung vorgelegen hat; dass sie – abgesehen von unten angegebenen Teilpublikationen – noch nicht veröffentlicht worden ist, sowie, dass ich eine solche Veröffentlichung vor Abschluss des Promotionsverfahrens nicht vornehmen werde. Die Bestimmungen der Promotionsordnung sind mir bekannt. Die von mir vorgelegte Dissertation ist von Prof. Dr. Annette M. Schmidt betreut worden.

(Unterschrift) Vorname / Nachname

Teilpublikation:

C. Wenning, S. Barbe, D. Achten, A. M. Schmidt, M. C. Leimenstoll, *Macromol. Chem. Phys.* 2017, 1700544.